NASA Contractor Report 165726

VOL. I

WAKES AND PERFORMANCE OF LIGHT AIRCRAFT PROPELLERS

by

JEFFREY ALAN ZIMMER

MASSACHUSETTS INSTITUTE OF TECHNOLOGY

June 1980

(NASA-CR-165726) WAKES AND PERFORMANCE OF LIGHT AIRCRAFT PROPELLERS, VOLUME 1 Interim Report (Massachusetts Inst. of Tech.) 192 p

N81-75186

Unclas
00/07 42416

Contract NAS1-15154

REPRODUCED BY
NATIONAL TECHNICAL
INFORMATION SERVICE
U.S. DEPARTMENT OF COMMERCE
SPRINGFIELD, VA. 22161

WAKES AND PERFORMANCE

OF LIGHT AIRCRAFT PROPELLERS

by

JEFFREY ALAN ZIMMER, Hertz Fellow

ABSTRACT

Three quarter-scale light aircraft propellers are tested under a variety of operating conditions. Wake surveys are made at three axial locations with both a three-hole pressure probe and a single-sensor rotating hot wire. Thrust and torque are also measured. The test results are compared to a lifting line theory, which is deemed adequate for practical design purposes.

A theory of rotating hot wires is also formulated for the case of an ideal sensor rotated to four positions. Closed-form solutions are given for the three velocity components in terms of the four hot wire readings. An efficient numerical procedure is then developed that deals with non-ideal sensors and redundant data containing errors.

NOTICE

THIS DOCUMENT HAS BEEN REPRODUCED FROM THE BEST COPY FURNISHED US BY THE SPONSORING AGENCY. ALTHOUGH IT IS RECOGNIZED THAT CERTAIN PORTIONS ARE ILLEGIBLE, IT IS BEING RELEASED IN THE INTEREST OF MAKING AVAILABLE AS MUCH INFORMATION AS POSSIBLE.

ACKNOWLEDGEMENTS

The author thanks the following people:

Professors K. U. Ingard and S. H. Crandall, for their encouragement and good advice; Dr. George Succi, the Organizer; Dr. David Munro, for inspiring conversations about propeller theory; Professor E. E. Larrabee, for his comments and good-natured assistance; Roger Osgood, Charles MacMillan and Lisa Richardson, who helped run the experiments; Mr. Frank Durgin, Mr. Al Shaw, Mr. Fred Merlis, Mr. Don Weiner, and Mr. Paul Bauer, for their technical expertise and generosity with equipment.

The author also recognizes Mr. Joseph Marksteiner, Mr. John Stanley, Mr. Thorwald Christensen and Mr. Robert Parks for their contributions to the project. Without the skills and advice of these extraordinary craftsmen, none of the experimental apparatus could have been constructed.

The author received excellent personal financial support from the Fannie and John Hertz Foundation. The project itself was supported by contract NAS1-15154 granted from NASA Langley Research Center and co-sponsored by the Environmental Protection Agency.

TABLE OF CONTENTS

		Page
Abstract		2
Acknowledgments		3
List of Tables		7
List of Figures		8
Chapter 1:	INTRODUCTION	9
1.1	Project Objectives	9
1.2	Aerodynamic Propeller Test Program .	10
Chapter 2:	LITERATURE SURVEY	13
2.1	Aerodynamic Measurements.	13
2.2	Theoretical Work of the Past . . .	18
2.3	Earlier Work With Rotating Hot Wires	27
Chapter 3:	THEORY	31
3.1	Propeller Theory	31
3.2	Scaling Considerations	33
3.3	Relation Between Theory And Measurements . . .	35

TABLE OF CONTENTS

(continued)

		Page
Chapter 4:	COBRA PROBE WAKE SURVEYS	38
4.1	Description of the Test Facility .	38
4.2	Theory of the Cobra Probe. . . .	40
4.3	Calibration Procedure	42
4.4	Experimental Procedure.	44
4.5	Data Reduction	46
Chapter 5:	HOT WIRE WAKE SURVEYS	49
5.1	Introductory Remarks	49
5.2	Theory of Four-Wire "Composite Probe"	54
5.3	Numerical Scheme for "Composite Probe"	62
5.4	Calibration and Associated Geometry	66
5.5	Experimental Procedure.	70
5.6	Data Reduction	72
Chapter 6:	PERFORMANCE MEASUREMENTS	76
Chapter 7:	DISCUSSION OF THE RESULTS	80
7.1	Introduction to the Data Collection	80
7.2	Wake Surveys	84
7.3	Performance Measurements	96

TABLE OF CONTENTS

(continued)

		Page
Chapter 8:	CONCLUSION	99
8.1	Assessment of Theory	99
8.2	Comments on the Experiments. . . .	100
Appendix A:	Miscellaneous Calculations	105
Appendix B:	Cobra Probe Calibration	113
Appendix C:	Hot Wire Calibration	124
Appendix D:	Computer Programs	133
Appendix E:	Error Analysis	172
References	. . . . .	189
Tables	. . . . .	193
Figures	. . . . .	206

LIST OF TABLES

		Page
I	Formulae for the Propeller Theory	194
II	Reynolds Numbers for Model Propellers	196
III	Estimated Errors in Swirl Velocity in Wake, Hot Wire Data	197
IV	Estimated Errors in Swirl Velocity Outside Wake, Hot Wire Data	198
V	Thrust and Torque Errors	199
VI	Free Stream Tangential Velocities	200
VII	Definitions of Quantities in Reduced Data	201
VIII	Annotated Index to Wake Surveys	203
IX	Index to Performance Measurements	205

LIST OF FIGURES

		Page
1	Probes	207
2	Vortex structure	208
3	Wind tunnel test facility	209
4	Nacelles	210
5	Situation of probes in wake	211
6	The "composite probe"	212
7	Geometric solution of ideal hot wire equations	213
8	Multiple solutions with four and three wires	214
9	Coordinate systems for the hot wire	215
10	Unit vectors for gradient calculation	216
11	Slipstream geometry	216
12	Thrust and torque flexures	217
13	Strain gauge bridges	218
14-49	Cobra probe wake surveys	219 - 254
50-79	Hot wire wake surveys	255 - 284
80-139	Performance data	285 - 344

Chapter 1

INTRODUCTION

1.1 Project Objectives

The work reported in this thesis forms part of a larger project, whose goal is to design and test a light aircraft propeller that produces less noise than conventional propellers, but has similar operating characteristics. Such a propeller could be installed on existing planes as a retrofit option. Dr. George Succi of M.I.T. has developed an acoustic theory to predict the sound field of a propeller. A very important input to this theory is the aerodynamic blade loading, which we estimate with a lifting line theory described by Larrabee [1]*, and later reworked by Munro [2].

Succi's work indicates that the radial loading distribution of a propeller has much to do with the amount of noise it produces. A propeller whose loading is concentrated at the inboard sections will be quieter than a propeller that produces the same thrust, but has heavily loaded outboard sections. While this gives us a means of achieving our end, we must temper our enthusiasm with practical considerations. There exists for propellers

*square brackets [] denote references at end of paper.

an optimal radial load distribution, analogous to the elliptic span loading for wings, that maximizes the efficiency for a given total thrust (or torque). However, our acoustically-designed blades will in general have non-optimal loading. We wish to decrease the noise as much as possible and still have an economically acceptable propeller.

A test program is deemed necessary to guide our efforts. Our tests fall into two very broad categories: 1) acoustic measurements, and 2) aerodynamic measurements. The latter tests are the subject of this thesis, and may be further divided into two types: a) wake surveys, and b) performance measurements.

1.2 Aerodynamic Propeller Test Program

M.I.T. does not own a wind tunnel large enough to test full-scale prototype propellers. Our models are one-quarter-scale, and turn at four times the full-scale RPM to accomplish Mach number scaling. The Reynolds numbers, however, are four times smaller in the model than they are at full scale. Fortunately, low Reynolds number effects become noticeable only in the low RPM range of the models, which is of little interest acoustically because the sound levels are so low.

Our test program centers around three propellers made

at the Institute. The first model, the Cessna, is a miniature copy of the 1C160 two-bladed propeller used on the Cessna Skyhawk airplane. The Cessna has RAF6 series airfoil sections. Another propeller, the Bruiser, has large inner chords to shift the loading inboard. It has NACA 64 series sections out to the 70% radius, and 16 series airfoils from the 80% radius to the tip. Between the 70% and 80% radii, a transition between the airfoil types occurs. The Bruiser is rather heavily loaded, and thus provides a more severe test of the lifting line theory, which assumes light loading. The Windsong propeller has a load distribution similar to that of the Bruiser, except the magnitude of the loading is reduced to furnish a total thrust close to that of the Cessna. The blade tip radius measured from the propeller axis, R, is R = 0.2413 m for the Cessna, R = 0.2381 m for the Bruiser, and R = 0.2381 m for the Windsong.

We turn these propellers at either 7,000 or 10,000 RPM. Some of the 10,000 RPM measurements are made with the blades set at a reduced angle. We can mount any one of three nacelles on the motor stand that drives the propellers. The minimum nacelle is the smallest possible body that can enclose the motor. The symmetric nacelle is a large body of revolution. The asymmetric nacelle simulates the nose of a single propeller light airplane. The reader will find a more thorough description of the

test facility at the beginning of Chapter 2.

The main feature of this thesis is a rather large collection of aerodynamic data for our three propellers. Three main types of experiments compose the collection: cobra probe wake surveys (two-dimensional flow measurements), rotating hot wire surveys (three-dimensional flow measurements), and performance measurements (thrust and torque). The three experimental techniques are discussed at length in Chapters 4, 5, and 6, respectively. A number of appendices contain pertinent details. In the following chapter, we present an historical survey of aerodynamic propeller measurements and theories.

Chapter 2

LITERATURE SURVEY

A fairly extensive search of the literature reveals that a great deal of work has been done with airplane propellers. The author does not attempt to be exhaustive here, but merely reviews some of the more interesting and relevant papers that the last 60 years have produced. The first part of our survey deals with earlier investigations of propeller flow fields and performance. We then trace the development of the various propeller theories, and finally look at past work with single-sensor rotating hot wire probes.

2.1 Aerodynamic Propeller Measurements

In this section we glance at quite a number of experimental propeller studies. Both performance and wake measurements appear frequently in the literature before 1955. Almost all of this work, in the United States, at least, received support from the NACA.

One of the earliest and most ambitious projects concerning propellers was carried out by Durand and Lesley at Stanford in the early 1920's [3]. Over a period of three years, no fewer than 146 propellers were made, most having two blades, with assorted tip shapes, chord distributions, airfoil sections, etc. Every propeller was

tested over a wide range of RPM. Thrust and torque were tabulated in the form of efficiency and dimensionless power coefficients. The main object of the study was to determine what design factors governed efficiency. Durand's large body of data also provided theorists with much food for thought. The early investigators had various ingenious mechanical arrangements for measuring thrust and torque. Some placed an entire full-sized airplane, propeller and all, on a balance to make static performance tests. Strain gauge arrangements such as the one we used apparently didn't become popular until the 1950's.

In 1924, a certain J. W. Crowley, Jr. reported his "Investigation of Slipstream Velocity" in NACA Report 194 [4]. This is the earliest wake survey found by the author, and differs from all the others in that it was made with the airplane in flight. Measurements of total pressure and swirl angle were made at seven axial stations. Rather than calibrate a single pressure probe and move it through the wake, Crowley built a wake rake supporting a number of fixed individual probes. This was the norm with pressure probe surveys.

Some work done with a "counter-propeller" by Lesley in the early 1930's [5] receives mention for two reasons. First, the "counter-propeller" reported was a rather

curious object. The extra "propeller" consisted of four large stator blades, which increased the efficiency by 2% according to Lesley. The usual counter-propeller had two sets of blades that both rotated in opposite directions. Second, Lesley made wake measurements with a "cylindrical yaw probe," as opposed to the more typical "yaw head." The first instrument is shown in Fig. 1. Swirl measurements obtained from a cylindrical probe were probably better than those obtained from other three hole pressure probes. Lesley did not present his swirl data in the form of "faired curves" like so many of his contemporaries, whose swirl data tended to be a little scattered. The "cylindrical yaw probe" will be mentioned again in Section 8.2.

A very extensive set of wake surveys was made by Reid in 1946 [6], who employed a rake of 11 yaw probes. Eight 2.8 foot diameter model propellers, having 3 and 4 blades, were studied at various advance ratios and blade angle settings. Measurements of swirl angle and total pressure were made for eighty different cases. Interestingly, none of the data compared well with predictions made by Glauert's propeller theory. This happened because they used the 1935 version of Glauert's article [7], which contains a few errors.

By far, the most beautiful piece of work found by the

author is "A Survey of the Flow at the Plane of the Propeller of a Twin-Engine Airplane," done by J.C. Roberts and P.F. Yaggy in 1950[8]. It is unique among the works reviewed in that all three velocity components were measured with a pressure probe. The propellers were removed, and the plane was mounted in the 40- by 80- foot wind tunnel at NASA-AMES. A rake of eight 5-hole pitot-static probes was swept through one disc plane to measure the flow in great detail. The data was presented in an elegant fashion, with polar plots of the flow angles.

Another unusual project was Leland Salters' study of the axial development of the wake of a stationary pair of large counter-rotating propellers [9]. The wake spread "qualitatively like an unheated jet." Salters also noted: "The slipstream was found to writhe, twist, and distort with or without sidewinds or gusts...quite often the boundaries would retain one shape for a period of 5 to 20 seconds and then shift to another shape..."

Several papers dealt with yawed propellers. Some Italian investigators of the late 1930's [10] built a very complicated mechanical balance that could be rotated 360° about its vertical axis. It was used to study the effect of the propeller slipstream on the airplane tail [11]. Pendley [12] found that a yaw angle as small as one degree

seriously upset the correspondence between the thrust measured directly and that computed from a total pressure wake survey, partly because the slipstream boundary shifted toward one side of the shaft. McLemore and Cannon [13] made performance measurements on a four-bladed propeller at yaw angles from zero to 180 degrees. Predictions based on a modified stip theory gave poor results at angles greater than 15 degrees.

Experimental work on propellers after 1955 is exceedingly rare, most efforts being directed toward the jet engine. One exception is some work done in France in 1973. Daniel Favier [14] presents some three-dimensional propeller wake measurements made with a rotating hot film probe. These are the only three-dimensional air propeller measurements found by the author. The probe is commercial (DISA 55A88), and has two nickel wedge films whose directional characteristics resemble those of pressure ports rather than hot wires. Only one of the sensors is used, and the probe is rotated to four positions at each of the 37 radial locations. With a simple but approximate procedure [15], limited to small flow angles, the time-averaged velocity components are deduced from the four hot film readings. The investigators also use smoke visualizations to measure vortex sheet spacing and swirl angle. A theory due to Valensi [16] does a good job of predicting the vortex spacing. There is also good

agreement between the hot film and smoke measurements regarding the swirl angle. Oddly, the theory does a poor job of predicting the actual velocities found with the hot film. It underestimates both the swirl and axial components by a factor of about three.

2.2 Theoretical Work of the Past

We next look at some of the theoretical work that has been done on airplane propellers. We divide these papers into three categories: 1) articles bearing directly upon our project, 2) other works concerning the minimum induced loss propeller, 3) papers that deal with arbitrary blade loading.

2.2.1 Articles Directly Concerned with the Project

The theory used by us has its origins in a paper by A. Betz [17]. The author knows of this paper through Larrabee [1], Glauert [7], and Goldstein [18]. A minimum induced loss propeller deposits the minimum amount of kinetic energy into its wake for a given thrust, viscous losses ignored. Betz shows that if such a propeller has "light loading" (i.e. the wake contracts very little), then the flow field in its infinite wake is the same as the potential flow around a set of rigid, helical sheets that moves axially backward with the so-called "displacement" velocity. The hypothetical sheets coincide

with the vortex sheets shed by the blades, but the vortex sheets themselves are not rigid even though they look that way. Each helical element of a sheet may possess both axial and rotational velocities. The Betz criterion is that the "displacement" velocity, which we would perceive as the axial velocity if we were unaware of the rotation, remains constant on the sheet.

The jump in velocity potential across the vortex sheets (or the rigid sheets) at a particular radius determines the circulation about the blade at that radius. One may thus find the optimum circulation distribution by solving an associated potential flow problem. In an addendum to Betz's paper, Prandtl gives an approximate solution for the velocity field by forming an analogy with two-dimensional flow over a row of semi-infinite plates. The result of the combined efforts of Betz and Prandtl is an expression for the optimum radial distribution of circulation along a propeller blade.

Prandtl's addendum, however, serves a useful purpose by itself. Many theorists apply elementary momentum and energy principles to the slipstream in order to relate the disc loading to conditions in the ultimate wake. This becomes very awkward unless an infinite number of blades is assumed. In the case of a real propeller, one can use Prandtl's plate flow solution, in the form of a "vortex

sheet spacing factor," to estimate the actual velocities at the blades from circumferentially-averaged quantities. Often, people use this procedure with non-optimal loading, when the "vortex sheet spacing factor" no longer strictly applies.

Glauert combines Prandtl's factor, momentum and energy relations in the slipstream, and two-dimensional airfoil theory to create his "vortex theory," which assumes that each airfoil section along the blade acts independently of all the other sections. He deals with both arbitrary and minimum induced loss loading. Larrabee [1] corrects some algebraic errors in Glauert's article, and summarizes the "vortex theory" in a computationally convenient fashion.

Larrabee's algorithm for a light aircraft propeller with arbitrary loading yields the total thrust, torque, and the axial and tangential components of induced velocity as a function of radius, for known RPM, forward speed, and blade geometry. The algorithm works as follows. Divide the blades into a number of radial sections, each of which has known two dimensional airfoil characteristics. At a particular radius, guess the helix angle of the vortex sheet, which is somewhat greater than the angle indicated by the advance ratio because of the (unknown) induced velocity. Use the two-dimensional

airfoil section characteristics to find the lift and drag (per unit span) of the section. Insert the values for lift and drag into the relations for swirl and axial momentum balance and solve for the induced velocity, which gives another value for the helix angle. Compare this second value to the one we started with, and iterate until the two angles agree. Once the helix angles, and hence the attack angles, are found for all the sections, sum the lift and drag forces along the blade to find the total thrust and torque of the propeller. Incidentally, Prandtl's factor enters into the momentum balance relations. Munro [2] uses many of Larrabee's ideas, but he derives a correction factor for the circulation about the blade elements, thus obviating the iteration scheme. Munro's theory is discussed in Chapter 3.

2.2.2 Minimum Induced Loss Propellers

Much effort has been directed towards minimum induced loss propellers for obvious practical reasons. Recall that Prandtl, in his addendum to Betz' paper, offers an approximate solution for the flow about rigid helical sheets. Goldstein [18] solves this potential flow problem exactly, and finds the optimum radial circulation distribution. His result, which involves an infinite series of Bessel functions, agrees suprisingly well with the distribution of Betz and Prandtl, at least for small

advance ratios. In accordance with the light loading assumption, the helix angle does not include the effect of induced velocity. Goldstein finds the relations between the thrust, torque, advance ratio, and the "displacement" velocity. These relations, along with the induced velocities at the blades which he also calculates, are the tools needed to design an actual propeller blade that will have the desired circulation.

Having figured out how to make an efficient propeller with light loading (small wake contraction), the theorists next attack the heavily loaded case. A number of people, including Glauert [7] Theodorsen [19], Poliakhov [20], and Losch [21], state that the condition for minimum induced loss for a heavily loaded propeller differs little from the Betz criterion. They claim the only difference is that the pitch of the rigid screw increases because of the finite "displacement" velocity. To the author's knowledge, no one has furnished a rigorous proof of this. Glauert puts forth a fairly convincing, but simplistic argument.

The Betz-Helmbold theory, as described by Losch [2], deals with the case of an infinite number of blades, the main idea being to relate the flow in the ultimate wake to the flow in the disc plane. Prandtl, in the same paper, provides a somewhat less cumbersome approximate

version of this theory. Kramer [22], through a rudimentary transformation of variables, then extends Prandtl's work to the case of a finite number of blades, and uses it to transform the Goldstein circulation distribution in the infinite wake into a new distribution at the disc. None of these investigators deals with the problem of actual blade design.

Theodorsen [19] determines the optimum circulation distribution in the ultimate wake experimentally by constructing electrical models of the potential flow about helical sheets, and deduces the circulation in the disc plane by assuming that all annuli in the wake contract proportionally. He next uses a Biot-Savart type calculation to compute the axial component of induced velocity in the disc plane, which is required for design purposes. Theodorsen's estimates of the wake contraction seem rather small in the author's opinion. He claims that the total contraction for typical propellers under ordinary operating conditions is on the order of 1% of the propeller radius. A simple momentum calculation, in which the slipstream is modelled as a jet, shows that the 1% figure corresponds to unusually low thrust.

Poliakhov [20] probably comes closer than anyone else to an exact solution of the problem. He begins by solving the old Betz problem for light loading because, "the

method proposed by Betz himself is not very clear and at times raises some doubt as to its rigor." The optimum circulation distribution for a "moderately loaded" propeller is found by performing an elaborate variational calculation in the disc plane. The solution, which pertains to a finite number of blades, has the advantage that the induced velocities in the disc plane fall out of the analysis almost automatically.

Interestingly, Betz [23] re-examines the minimum induced loss problem for the case of stator blades fitted behind the propeller. As the number of stator blades increases, the peak of the optimum circulation distribution moves inboard. There also exists an optimum length for stator blades.

A nice contribution to the general minimum induced loss problem has been made by Munro [24], whose discovery we now describe. Suppose a fixed surface S lies immersed in an inviscid, incompressible fluid. The only vorticity in the space lies on S. Given the total linear and angular momenta of the flow, what is the distribution of vorticity on S that minimizes the total kinetic energy in the flow? It turns out that the potential flow field created by this optimal distribution is exactly that of a rigid, impermeable surface, which coincides with S, and undergoes both translation and rotation. Thus, if we

choose S to be the helical surface swept out by a propeller, we immediately arrive at the Betz criterion. One need only solve the indicated potential flow problem as Goldstein did. Munro does not make any "light loading" assumptions in the proof of his theorem. However, one cannot apply his result without knowing the shape of the surface S, which we do not really know it the propeller is heavily loaded.

2.2.3 Papers Dealing With Arbitrary Loading

We conclude this section by mentioning a few theorists who have not restricted themselves to minimum induced loss propellers. In an early and fascinating paper, G. de Bothezat [25] discusses propellers from a very general point of view. He gathers all of the various working states of a propeller, including braking, free wheeling, etc., into a cycle, by studying the "specific function," which is essentially the blade element efficiency. He correctly describes, names, and predicts analytically the "vortex ring state." Unfortunately, the theory assumes an infinite number of blades, and de Bothezat fails to connect his work with two-dimensional airfoil theory. Hence, he advocates experiments to determine the nature of the flow in the disc plane.

A few years later, Bienen [26] extends the work of Betz and Prandtl to arrive at a simple, but basically

correct method for analyzing a lightly loaded propeller with an arbitrary circulation distribution. It strongly resembles Glauert's approach, and uses Larrabee's technique of finding the true angle of attack at each section by comparing a momentum balance with the two dimensional section characteristics.

An ingenious method due to H. Reissner [27] accounts for finite blade number in a direct fashion. He assumes helical vortex sheets, and takes advantage of the resulting symmetry with a peculiar spiral coordinate system. He models the vortex sheets as jumps in velocity potential, which can have arbitrary radial dependence, and solves for the velocity field in terms of Bessel series. Unfortunately, if one wishes to design an optimum propeller with this method, by specifying the torque and forward speed, one must solve a very formidable set of integral equations. The theory is applied more readily to propellers with known circulation or else known blade geometry.

We have mentioned the technique of integrating along vortex lines in the slipstream to find the induced velocities. One of the most important pioneers in this area is Moriya [28], who carefully describes the application of the Biot-Savart law to propellers, and deals in a rational manner with the singular integrands

that occur where each line springs from the blade. Moriya summarizes his calculations in a series of charts, from which the induced velocities may be found for a known arbitrary circulation distribution. The theory applies only to light loading, because the vortex lines are helical.

A much later investigator, Hough [29], uses Biot-Savart's law to calculate the complete, three-dimensional, fluctuating flow field in the disc plane. He assumes a constant radial circulation distribution along the lightly loaded blades, so that the trailing vortex system consists only of helical tip vortices and a hub vortex, but the basic procedure applies equally well to other types of loading.

2.3 Earlier Work With Rotating Hot Wires

In this section, we review several papers that pertain to the rotating hot wire technique. With the exception of the work by Favier and Pellerin (already reviewed in Section 2.1), efforts involving rotating hot wires have been directed either toward turbomachinery or the turbulence problem. The author's search for relevant literature was largely guided by a very extensive bibliography of thermal anemometry, prepared by Peter Freymuth of the University of Colorado in 1978 [30].

In 1958, Fujita and Kovasznay [31] succeeded in measuring three components of the Reynolds stress tensor ($\overline{u^2}$, $\overline{v^2}$, $\overline{uv}$) by orienting a single sensor hot wire to 36 different angular positions. The wire was not slanted, and always remained in one plane. Since the large number of rotations provided more than the necessary amount of information, a least squares technique was used to obtain the three components from 36 anemometer voltages, which were time-averaged after linearization. The investigators reported excellent agreement between their theory and the experiment.

Whitfield, et al [32], rotated a single slanted wire to map the three-dimensional, ensemble-averaged flow field behind a turbine engine rotor. The wire made an angle of 54.7 degrees with the axis of rotation of the probe. At each of 23 radial stations, the wire was twisted to three mutually perpendicular directions. While the wire remained at a particular orientation, the time history of the linearized anemometer voltage was tape recorded, together with pulses that synchronized the voltage with the angular position of the rotor. All of the waveforms thus obtained were then educted over an integral number of rotor revolutions. The wires were assumed to have ideal directional characteristics, and this permitted an analytical solution of the set of three nonlinear equations relating the velocity vector to the voltages.

There was one such set for each measurement point. The author will show later that these analytical solutions, while convenient, are extremely sensitive to measurement errors.

Schmidt and Okiishi [33] used Whitfield's basic experimental procedure to study the flow field between blade rows of a compressor. However, ideal wire directional characteristics were not assumed. Rather, a second order algebraic function, having ten empirical constants, was least squares fitted to the hot wire calibration data. At each point in the flow, a set of six nonlinear equations was solved with the Newton-Raphson method. Although there were only three measurements and three unknowns, a particularly inconvenient choice of angular coordinates necessitated three additional equations to relate all the various angles. Lakshminarayana and Davino [34] later used this exact same procedure to investigate guidevane and stator blade wakes.

The most beautiful feature of a rotating wire is its ability to gather redundant data, and thus greatly improve the reliability of the experiment, with a minimum of effort. Only the first of the four groups mentioned above took advantage of this feature. The author will later show that three hot wires do not completely specify the velocity vector; the inversion of the nonlinear hot wire

equations is not unique. From the standpoint of ambiguity, mutually orthogonal wires are the worst choice of geometry. The one advantage of this arrangement is that, if ideal wire characteristics are assumed, the equations may be inverted analytically. Whitfield, et al, sacrificed uniqueness and redundance, but at least they obtained a simplified data reduction procedure. The later investigators use calibration functions that preclude analytical inversion, and yet they still adopt the orthogonal geometry with its ambiguity. One wonders at this curious evolution of technique.

Chapter 3

THEORY

3.1 Propeller Theory

The propeller theory used in this thesis is the work of David Munro [2], and has much in common with the work of Prof. Larrabee [1]. It has four main restrictions. First, the solidity of the propeller, defined as the ratio of the projected area of the blades to the propeller disc area, must be small. Second, the ratio of the forward speed to the tip speed (advance ratio) is also assumed small. Third, compressibility limits the analysis in two ways. The blade section properties depend on the relative Mach number, which is as high as 0.7 at the tip in our experiments. This dependence is modelled in an approximate fashion by a Glauert correction, which breaks down completely at Mach 1.0. Furthermore, the flow field in the immediate vicinity of the blade is compressible, but Munro observes that this is not an important effect if the forward mach number does not exceed about 0.2. Finally, it is assumed that the vortex sheets, which are inherently unstable, do not roll up until they are far downstream. If the propeller is lightly loaded, the sheets are weak and may indeed persist awhile. In fact, the theory cannot deal with a heavily loaded propeller even if the sheets never roll up. Heavy loading implies

large wake contraction, whereas the theory models the flow with a pair of helical vortex sheets.

The blades are divided into a number of radial sections (usually about ten), whose two-dimensional airfoil characteristics are known. As in the lifting line theory of wings, Munro estimates the induced velocity at each section to correct for the finite length of the lifting surface. By choosing clever paths of integration around the helical vortex lines that compose the sheets, he finds approximate closed-form expressions for the circumferentially-averaged induced velocities in terms of the radial circulation. Interestingly, the induced velocities at a given radius depend only upon the circulation at that radius. He performs this calculation in the infinite wake. Since a helical geometry is assumed, symmetry dictates that the induced velocities in the disk plane must be half the velocities at infinity. Munro then uses Prandtl's "vortex sheet spacing factor" to relate the induced velocities at the blade to his circumferential averages. The expressions in Table I (please see) are taken directly from his doctoral thesis [2].

The lift and drag coefficients refer to the direction of motion, which is along the helical path specified by the forward velocity, angular velocity, and radius r.

Once we have performed the calculations at a number of radii, we simply add up the lift and drag forces to find the total thrust and torque of the propeller. The reader will notice that the theoretical curves for the wake surveys contain 31 points, whereas we have section data at only ten or eleven radii. The additional points are obtained by linearly interpolating the section characteristics.

Munro's theory, like most propeller theories, applies when the propeller operates in unobstructed flow. For many of our tests, however, we attach one of the large nacelles to the test stand, and this decreases the inflow velocities by some fraction $\delta(r)$. We have calculated $\delta(r)$ for the case when there is no propeller, and simply replace V by $V\,\delta(r)$ everywhere in Table I when a large nacelle blocks the wake. With the asymmetric nacelle, the fraction depends on the circumferential coordinate θ as well as the radius, in which case we replace V by $V\langle \delta(r,\theta)\rangle_\theta$. Admittedly, these simple substitutions seem crude, but they work surprisingly well for the performance predictions. No wake measurements are made with the asymmetric nacelle.

3.2 Scaling Considerations

We have mentioned that our quarter-scale model propellers achieve Mach number scaling, but not Reynolds

number scaling. In this respect, the Cessna differs from the other two models. The airfoil section characteristics for the Cessna are computed using a Reynolds number of 3.65×10^5, which actually corresponds to the 80% radius on the model propeller at 10,000 RPM [35]. Table II contains a list of Reynolds numbers, based on chord, for the three models. The Bruiser and the Windsong, on the other hand, are conceived as full-scale prototype propellers, and we design them using experimental section data for a Reynolds number of about 1×10^6. We use these same section data in predicting the behavior of the quarter-scale models.

The wind tunnel facility imposes another scaling restriction. The full-scale forward speed at the design condition is about 62 m/s, but the tunnel has a top speed of 30 m/s. Hence, at 10,000 RPM, the Mach numbers are full scale (the quarter-scale model turns at four times the full-scale RPM), but the advance ratio is too low. Thus, the model propeller is proportionately more heavily loaded than the real propeller. We reduce the blade angles in some of the tests to bring the intensity of loading down to an appropriate level, but , of course, we then lose geometric similarity. Therefore, all our tests are off design in some sense or another. While this is unfortunate, in that we can never study the propellers at their operating points, it doesn't prevent us from assessing the theory, which supposedly can handle off

design conditions.

The wake surveys are made at 10,000 and 7,000 RPM. The significance of the latter speed is that it is the lowest rotation rate that causes enough sound for good acoustic measurements.

3.3 Relation Between Theory and Measurements

Several quantities predicted by the theory may be measured conveniently. At a particular rate of rotation and forward velocity (tunnel speed), the gross behavior of a propeller is characterized by the torque exerted by the shaft that turns it, and the thrust it produces. The induced velocities in the wake give more detailed information, but their interpretation requires some thought.

The theory says nothing about the way the wake develops. It only predicts velocities right in the disc plane and in the fully developed wake at infinity. We cannot make flow measurements at either of these locations. Suppose, however, that we ignore viscous forces, which are important only in the vortex sheets, and pretend the wake flow is incompressible and has no losses. We now say that vorticity is conserved in the wake as well as mass, and that vortex lines move with the fluid. The circulation, if expressed as a function of the mass flow,

is independent of axial location even when a nacelle sits behind the propeller. See Figure 2. If the mass flow through the circular loop C equals that through C', then the circulations about the two loops are equal. Hence, a good way of checking the theory is to predict the distribution of circulation versus mass flow, and then compare this with the same distribution computed directly from experimental data. As we'll see later, this mapping procedure works well.

A more conventional way to interpret wake data, used by Peter Dunbeck [36], is to estimate the axial velocity in the infinite wake by measuring the circumferentially-averaged total pressure p in the undeveloped wake, i.e.

$$V_{AXIAL}(\infty) = \sqrt{\frac{2p}{\rho}} \qquad (1)$$

where p is measured relative to the atmosphere and ρ equals the air density. The reasoning is that the static pressure buildup immediately behind the propeller gets converted into kinetic energy downstream when the pressure is atmospheric across the wake. This argument neglects the swirl and radial components of velocity because they are comparatively small and complicate matters. Radii at the measurement station are related to those at the blade by assuming that all annuli contract proportionally.

When we use (1) at different radial stations in the wake, we essentially apply the energy equation independently to separate, semi-infinite annular regions. If we force this set of concentric tubes around some object that blocks the flow, the radial component of velocity is no longer negligible. We could apply a Bernoulli integral along a spiral path between vortex sheets out to infinity, and hence find the ultimate velocity, but this time we have no mapping to connect radii at the measurement station to radii at the propeller disc. The total pressure is therefore not a particularly useful quantity when the propeller operates in front of a large nacelle.

We can make one more interesting measurement. If we get as close to the propeller as we dare with a hot wire, we are almost in the disc -- close enough that a comparison between theory and experiment in this region could be informative.

In summary, we have four types of experiments to make. In a performance measurement, thrust and torque are measured as a function of RPM at a constant tunnel speed. We can find the circulation in the wake as a function of mass flow. Finally, we measure the axial velocity just behind the propeller and also "at infinity" using the total pressure when appropriate.

Chapter 4

COBRA PROBE WAKE SURVEYS

The following sections describe the cobra probe wake survey technique. A simple theory of cobra probe behavior, whose main purpose is to guide the calibration procedure, begins the chapter. We then outline this procedure, and present the results in the form of empirical calibration functions. The experimental and data reduction procedures for a wake survey are explained. A note on the wind tunnel test facility, in which all the experiments for this thesis were performed, begins the chapter.

4.1 Description of the Test Facility

All of the measurements reported in this thesis were made in the 5' x 7' Acoustic Tunnel in Building 33, M.I.T. This tunnel has a closed circuit. The large jet enters an anechoic room, as shown in Figure 3. The jet has an RMS turbulence level of approximately 1%, and the velocity across the mouth is uniform to within less than 1% [37]. We measure wind speed with a large pilot-static probe A, that communicates with a slant tube alcohol manometer outside the tunnel. Our usual "wind speed" is actually 2 1/2 inches of alcohol (500 pascals) dynamic pressure. A thermometer and a barometer enable us to convert the

dynamic pressure into velocity using the correct air density. We take temperature readings as often as possible during the tests. Hence, the true wind speed varies slightly between tests, but it is generally around 29.5 m/s.

The propeller stand B, C is mounted rigidly to the building. The streamlined post B supports an assembly of flexures that carry a D.C. aircraft starter motor within the nacelle C. The flexures are instrumented with strain gauges to measure the propeller thrust and torque. We monitor the shaft RPM with an optical trigger. Three nacelles (Figure 4) may be mounted on the stand. The minimum nacelle is the smallest possible structure that will enclose the motor without producing excessive drag. The symmetric nacelle has a radius given by

$$r/R = 0.449(x/R)^{1/8} + 0.156(x/R) - 0.0361(x/R)^2,$$

where R = propeller radius, x = distance from nose. The disc plane is 0.0321 meters in front of the nose. The asymmetric nacelle has the same afterbody as the smmetric nacelle, but its forebody resembles the front end of a single engine airplane. The flowfield in the absence of the propeller has been computed for the latter two nacelles. All three bodies have small motor cooling inlets at the nose. The magnitudes of the inlet velocities are not known, but the vacuum pump that drives

the cooling flow is quite weak.

A motorized traversing mechanism D sits well outside the propeller slipstream, and carries either a three-hole pressure probe or a single-sensor hot wire (not shown) along a radial path through the wake. A microswitch E opens a circuit at 0.0635 cm path intervals.

4.2 Theory of the Cobra Probe

The cobra probe (Figure 1) is a three-hole pitot-static pressure probe. One can develop a simple model for its behavior by assuming that the dynamic pressure at a port depends only upon the velocity component normal to the port, and that Bernoulli's formula applies. Provided that $\vec{v}$ lies in the plane containing the centers of all three ports, one may deduce analytical expressions for the static pressure, the magnitude of $\vec{v}$, and the flow angle (θ, Figure 1) in terms of the three port pressures p_l, p_c and p_r. Essentially, this amounts to solving three nonlinear algebraic equations in three unknowns.

Consider the center hole. If the static pressure of the flow at the probe location is p_s, the flow angle is θ, and the magnitude of the velocity is v, then our assumption is that the total pressure at the hole will be

$$p_c = p_s + \tfrac{1}{2}\rho(v\cos\theta)^2$$

During the actual experiments, the probe was referenced to the tunnel stagnation pressure (usually 2 1/2 in. alcohol or 500 pascals). From the standpoint of our analysis, this means we should subtract the reference pressure, p_o, from the right hand side of the above equation. We may write equations for p_c and p_r that are exactly analogous to the one for p_c; they merely account for the angles of the different probe faces. Thus, our set of equations is

$$p_c = p_s + \tfrac{1}{2}\rho v^2\cos^2\theta - p_o \qquad (2)$$

$$p_L = p_s + \tfrac{1}{2}\rho v^2\cos^2(\theta + \tfrac{\pi}{4}) - p_o \qquad (3)$$

$$p_R = p_s + \tfrac{1}{2}\rho v^2\cos^2(\theta - \tfrac{\pi}{4}) - p_o . \qquad (4)$$

After applying some common trigonometric identities to the above system, we find that it is actually linear in the three unknowns $p_s - p_o + 1/4\,\rho\,v^2$, $1/4\,\rho\,v^2\sin 2\theta$, $1/4\,\rho v^2\cos 2\theta$ with knowns p_l, p_c, and p_r. Incidentally, if the face angles of the probe were not $\pi/4$ we could not make this linear conversion. One may easily invert the converted system and rearrange to find

$$\tan 2\theta = \left[\frac{p_R - p_L}{2p_c - p_L - p_R}\right] \qquad (5)$$

$$\frac{1}{2}\rho V^2 = (2p_c - p_L - p_R)[1 + \tan^2 2\theta]^{1/2} \qquad (6)$$

$$p_s = p_o + \frac{p_L + p_R}{2} - \frac{1}{4}\rho V^2 \qquad (7)$$

It is nice that (6) also is independent of p_o.

Formula (6) gives the magnitude of the velocity at the point of measurement. We estimate the axial component in the fully developed wake, $v_{ax}(\infty)$, by setting

$$v_{ax}(\infty) = \sqrt{\frac{2(p_c + p_o)}{\rho}} \qquad (8)$$

The significance of this quantity has already been discussed in Section 3.2.

4.3 Calibration Procedure

Equations (5) through (7) of the previous section cannot perfectly represent the behavior of the probe, as they are derived from crude assumptions and not from the true flow field. The hope is that when they are compared to the actual probe characteristics, the result will be a one-to-one correspondence allowing one to convert p_l, p_c, p_r into the actual velocity and pressure at the measuring station. This correspondence takes the form of a set of calibration curves. These are generated by placing the probe in a low-turbulence jet and recording its output versus flow angle θ at each of several tunnel speeds. Three strain gauge transducers measure the port pressures.

In the present case the calibration has an angular range of θ from -6° to 20° and a speed range of $1/2\,\rho\,v^2$ from 370 to 1950 pascals.

Empirical functions consisting of straight line segments accurately represent the calibration curves. We summarize the results here. Appendix B contains the relevant details. The flow angle θ depends on the three port pressures in the following way:

$$\theta = A\theta_T + B$$

$$\theta_T \equiv \frac{1}{2}\arctan\left[\frac{p_R - p_L}{2p_c - p_L - p_R}\right] \tag{9}$$

where

$$A = 1.20 \qquad B = -1.03 \text{ degrees}.$$

The local speed v satisfies the rule:

$$\frac{1}{2}\rho v_T^2 \equiv \begin{cases} A\left(\frac{1}{2}\rho v^2\right) + B\,, & \theta_T \leq 0.8 \text{ degrees} \\ A\left(\frac{1}{2}\rho v^2\right) + B + (\theta_T - 0.8)\left[C\sqrt[7]{\frac{1}{2}\rho v^2} + D\right], & \theta_T > 0.8 \text{ degrees} \end{cases} \tag{10}$$

$$\frac{1}{2}\rho v_T^2 \equiv (2p_c - p_L - p_R)\left[1 + \tan^2 2\theta\right]^{1/2},$$

where

$$A = 1.48, -B = 20.9 \text{ pascals},$$

$$C = 41.1 \text{ (pascals)}^{6/7}/\text{degree},$$

D = -88.0 pascals/degree.

The calibration for static pressure p_s obeys a third empirical law quite similar to the one for v:

$$p_s = p_{ST} + f(\theta, v)$$

$$f(\theta, v) \equiv \begin{cases} A + B(\frac{1}{2}\rho v^2), & \theta_T \leq 6 \text{ degrees} \\ A + B(\frac{1}{2}\rho v^2) + (\theta_T - 6.0)[C\sqrt{\frac{1}{2}\rho v^2} + D], & \theta_T > 6 \text{ degrees} \end{cases} \quad (11)$$

$$p_{ST} \equiv p_o + \frac{p_L + p_R}{2} - \frac{1}{4}\rho v^2 ,$$

where

A = -2.06 pascals, B = 0.287,

C = 12.37 $(\text{pascals})^{6/7}$/degree,

D = -25.0 pascals/degree,

p_o = wind tunnel stagnation pressure in pascals.

The above functions are convenient in that they summarize a large amount of calibration data. The expression (9) represents the angular behavior to within 0.50^o. The velocity function (10) and the pressure function (11) represent the data to within about 2% and 5%, respectively. The data reduction computer program does not use them, however, as will be explained.

4.4 Experimental Procedure

In this section we review in detail the experimental procedure that is used for the pressure probe wake

surveys. The basic facility, illustrated in Figure 3, has already been described. We mount the cobra probe on the traverse D using an assortment of clamps and rods to position it so that its head moves along a vertical line drawn radially from the propeller axis. We show an enlarged view of the probe's situation in Figure 5. The strain gauge pressure transducers are sensitive to changes in temperature, and therefore remain outside the tunnel. They communicate with the probe via tubes several meters in length. As in the calibration, the stagnation pressure tap (p_o) of the tunnel manometer is connected to the back ends of all three transducers as a reference. The main piece of equipment outside the tunnel is a digital oscilloscope with both core and disc memories. A wake survey with the cobra probe is made as follows.

The voltage outputs from the center and left port transducers are connected to the two channels of the oscilloscope. We interpose simple capacitive filters between the transducers and the 'scope to achieve time averaging, although the probe and the tubes already accomplish most of the averaging. The microswitch E triggers the scope to accept data at 0.0635 cm (1/40 inch) intervals of traverse distance. The probe is initially positioned so that it almost touches the nacelle, and as it moves up the oscilloscope records the filtered transducer voltages on two of its four memory

quarters. We then return the traverse to its starting position and run it up again, only this time the center and right port filtered transducer voltages are recorded on the other two memory quarters. For most of the surveys the two center port traces lie right on top of each other, attesting to the repeatability of the measurements.

After the data is reviewed and deemed satisfactory, it is transferred to a mini floppy disc for permanent storage. Also, we copy the contents of the disc onto a magnetic tape for computer processing.

4.5 Data Reduction

The cobra probe is calibrated under "ideal" conditions. The tunnel speed is very steady, and the probe axis makes an angle of $90^{o} \pm 1/2^{o}$ with the flow direction. (Angles other than 90^{o} correspond to non-zero radial velocities in the wake.) During the actual propeller experiments the probe experiences somewhat different conditions. We know the wake contracts, but we can only hope the radial velocities are small because the probe cannot measure them. The finite number of blades introduces unsteadiness, but the probe can't measure this either; the frequency response of the instrument is much too low. As we'll see later, both unsteadiness and radial velocities distort the cobra probe measurements.

We attempt to mitigate these difficulties by forcing the probe to read known free stream conditions at some setpoint just outside the wake. In the free stream, $1/2\ \rho v^2 = 500$ pascals, $\theta = 0^o$ and $p_s = 0$ (measured relative to the atmosphere). The calibration curves uniquely determine p_l, p_c and p_r for these conditions. Call these special pressures the free stream values p_{lo}, p_{co}, and p_{ro}. Define zero adjusts $z_l = p_{lo} - p_l'$, $z_c = p_{co} - p_c'$, $z_r = p_{ro} - p_r'$, where the primed pressures are the values observed at the set point. The zero adjusts are added to the pressure readings for all radial positions in the survey. The probe now gives a reasonable reading outside the wake. The readings, of course, become increasingly susceptible to error as we move inboard away from the set point, because the effects that necessitate the zero adjust procedure change with radial location. This is an unavoidable consequence of using a cobra probe in a propeller wake.

The corrected port pressures, through the calibration curves, determine the flow angle, the local speed, and the static pressure at each radial station. The FORTRAN program PREDUCE accepts the port pressures and converts them into the desired quantities. PREDUCE does not solve the set of equations (9) to (11) directly. Rather, it reads a modified set of calibration curves from a separate file in the form of arrays, stores them,

and applies a procedure that combines searching and linear interpolation to find θ, v, and p_s at each survey station. The modification of the calibration curves involves shifting the data points so that they occur at regular intervals of θ_T. The reader is referred to Appendix B for a step by step account of the technique used by PREDUCE. PREDUCE does not require any fitted functions such as (9), (10) or (11) to operate, and is quite adaptable to other three hole probes because it reads calibration data from a separate file. Appendix D contains the commented source code for PREDUCE, along with a bit more discussion.

Chapter 5

HOT WIRE SURVEYS

5.1 Introductory Remarks

The cobra probe measurements were made shortly after the author joined the project. At that time, no other instrument was available. The cobra probe, and other similar three-hole yaw probes, are the "classical" propeller wake survey instruments. They are rugged, easy to use, and require only one calibration provided they do not receive damage through mistreatment. They do, however, suffer from two very serious inadequacies. Their behavior in unsteady flow is, at best, mysterious, and they lose their utility if the flow is three-dimensional.

The flow field of a propeller is unsteady when observed from a fixed frame because of the finite number of blades. Our probe has a frequency response on the order of 1 Hz, whereas the blade passage frequency of 10,000 RPM is 330 Hz. The ports of the cobra probe communicate with pressure transducers via long ducts, which can harbor standing waves and may damp pressure fluctuations through viscous losses. Iberall [38] finds that the transmission characteristics of these duct-port systems are not only very complicated, but are extremely sensitive to the geometry, which we cannot accurately

measure. Also, the flow situation at the port is asymmetric about the plane C-C in Figure 1. Since the diaphragm of a transducer must move a finite distance to register any pressure, an oscillating flow must exist at the port in the presence of unsteady pressure. The asymmetry of the port causes the flow resistance to depend on the direction of flow. The average pressures on either side of plane C-C must therefore differ by some unknown amount. Weyer [39] has studied this effect experimentally and reports that the pressure difference depends on the geometry of the port, the amplitude of the fluctuations, and also the time dependence of the fluctuations. Weyer finds pressure differences as large as 8% with a square wave pressure oscillation whose peak to peak amplitude is 50% of the mean. In short, the port-duct-transducer combination filters the time-dependent pressure in some poorly understood fashion. The mere presence of averaging errors does not irk the author nearly so much as the fact that he cannot assess them. Furthermore, even in the absence of such errors, the probe will give an RMS average velocity, not the true mean required by our momentum theory.

Three-hole probes are often used in propeller wake studies under the assumption that the radial velocities (wake contraction) are too small to affect the probe readings. In many cases, including several of the surveys

reported here, this assumption is correct. It is obviously incorrect if the propeller operates in front of a large body. Our symmetric nacelle has a slope of roughly 15^{o} with respect to the shaft axis one-half a propeller radius behind the disc plane. The uncertainties arising from two factors -- the radial velocities and the unsteady flow -- motivated the author to design a better wake experiment with a rotating hot wire.

The hot wire, with its associated electronics, has a frequency reponse of about 2000 Hz, as found by a simple square wave test. Hence, the instruments do little in the way of averaging. We low-pass filter the amemometer signal <u>after</u> it is linearized. Hence, the filtered voltage is proportional to the quantity $\langle |\vec{V}| f \rangle_t$. The function f represents the directional characteristics of the hot wire. Since it is nonlinear with flow angle, directional averaging errors are still present. However, these errors are quite small, as shown in Appendix E. The directional averaging affects the filtered voltage by less than 1%, so we come very close to obtaining the true mean velocity.

The following five sections describe the hot wire wake survey technique. Before delving into the details, let us motivate the choice of probe geometry and experimental arrangement by outlining our requirements:

1) We want all three components of the time-averaged velocity.

2) Probe must be reasonably durable and easily repaired by us.

3) Probe must not require overly elaborate calibrations, because of the likelihood of breakage.

4) We would like measurements as detailed as possible (many radial stations).

Five-hole pressure probes either give poor time averages (if the pressure transducers are connected to the ports with ducts), or are extremely fragile (if miniature tranducers are located in the ports). All multiple-hole pressure probes require very elaborate calibrations. Requirements 2) and 3) also rule out multiple hot wire probes. We may, however, rotate a single hot wire to obtain the three components of $\vec{v}$ if we're only interested in the time average.

A rotating, slanted hot wire probe is shown in Figure 1. The circular locking plate A is fixed to the bushing B which attaches to the traversing mechanism in the tunnel. All other parts of the instrument rotate as a unit. The locking plate has several small holes, spaced 90^{o} apart.

The pin C snaps into these holes under the influence of the spring D. The head of the probe E is a separate piece that mounts onto the shaft with a threaded joint and a locking nut F. The head carries two brass needles that hold the 1 mil diameter tungsten wire. Actually two heads exist (referred to later as probes #1 and #2), so the experiments may continue if one head gets broken. The hollow shaft contains two wires G connected to the needles. The entire probe, including the wire heads, was made by the author.

The probe is connected to a linearized constant temperature anemometer, an instrument that holds the wire at a fixed temperature by modulating the wire current. The instrument's output is a voltage that varies linearly with the "effective cooling velocity," which is here taken to be $|\vec{v}|\, f(\frac{\vec{v}}{|\vec{v}|}, \hat{w})$. The vector $\vec{v}$ represents the flow velocity and f is a geometric factor that depends on the direction of $\vec{v}$ relative to the wire, whose orientation is defined by the unit vector $\hat{w}$. At a particular point in the flow, the probe is twisted about the axis to change $\hat{w}$ and hence f. The voltages obtained for different rotations are related through coordinate transformations. The number of rotations needed is nominally three since $\vec{v}$ has three components. We actually use four rotations spaced 90^{o} apart, for reasons that will be discussed later.

Usually one rotates the wire as it traverses the wake. That is, the wire is taken through all of its rotations before moving to the next station. Another method is to traverse the wake several times in succession, each time with the wire in a different position. The first method is sounder than the second in that the readings from the wire at its different rotations are all taken under the same experimental conditions. The second method essentially requires that we duplicate the experiment as many times as there are wire rotations. However, we choose the second method because it is much more efficient. The wire is rotated only between traverses rather than at every radial station. For a given amount of time in the laboratory, we can obtain a much more detailed picture of the flow. As far as the problem of repeating the experiment is concerned, the main obstacle is the sensitivity of the hot wire to changes in ambient temperature. This difficulty turns out to be much less serious than one might think, as will be shown. Our first task is to study the behavior of a "composite probe," made of four identical slanted hot wires rotated about the probe axis in 90^{o} intervals.

5.2 Theory of Four-Wire "Composite Probe"

We shall begin our study of the rotating hot wire by first proposing a simple model. While this model is not

really accurate enough to use in the experiments, it will do much to further our understanding of the measurement technique. Figure 6 illustrates all four rotations of the probe simultaneously. This "composite probe" may be thought of as a four-wire probe with no interference between sensors. Assume that a hot wire is cooled only by the component of velocity normal to the wire, which is equivalent to saying that the wire is infinitely long. If the angles made by the wires with the velocity vector $\vec{v}$ are θ_i, then the effective cooling velocities are taken as

$$V_i = |\vec{v}| \sin\theta_i = |\vec{v} \times \hat{w}_i| \ , \quad i = 1,4 \ .$$

Rewriting these equations in terms of the wire slant angle θ_o and the components of $\vec{v}$ yields

$$V_1^2 = v_2^2 + (v_3 \cos\theta_o - v_1 \sin\theta_o)^2 \qquad (12)$$

$$V_2^2 = v_1^2 + (v_2 \sin\theta_o - v_3 \cos\theta_o)^2 \qquad (13)$$

$$V_3^2 = v_2^2 + (v_3 \cos\theta_o + v_1 \sin\theta_o)^2 \qquad (14)$$

$$V_4^2 = v_1^2 + (v_2 \sin\theta_o + v_3 \cos\theta_o)^2 \qquad (15)$$

where $v = v_1\hat{i} + v_2\hat{j} + v_3\hat{k}$. Geometrically, (12) through (15) represent four cylinders with radii V_i and axial directions $\hat{w}_i$. All the cylinder axes pass through the origin. A solution to this set of equations is a point in velocity space that lies on all four cylinders.

Although the set is redundant, it nonetheless yields at least two solutions for $\vec{v}$. For certain special directions of $\vec{v}$ we obtain four or even six solutions. Uniqueness of solutions is most easily studied through geometry. By manipulating the equations one may cast the problem into all sorts of geometrical forms, some of which are easier to visualize than the intersection of multiple cylinders. One particularly nice form, obtained by adding and subtracting pairs of equations, is

$$\frac{V_1^2 + V_3^2}{2} = v_1^2 \sin^2\theta_o + v_2^2 + v_3^2 \cos^2\theta_o \qquad (16)$$

$$\frac{V_2^2 + V_4^2}{2} = v_1^2 + v_2^2 \sin^2\theta_o + v_3^2 \cos^2\theta_o \qquad (17)$$

$$V_2^2 - V_4^2 = -4 v_2 v_3 \sin\theta_o \cos\theta_o \qquad (18)$$

$$V_1^2 - V_3^2 = -4 v_1 v_3 \sin\theta_o \cos\theta_o \qquad (19)$$

Equations (16) and (17) represent ellipsoids, and (18) and (19) are degenerate hyperboloids. We get a usetul alternate equation by combining (18) and (19).

$$v_2(V_1^2 - V_3^2) = v_1(V_2^2 - V_4^2) \qquad (20)$$

This is a plane containing the third axis. It $v_\perp \neq 0$, we may find v from V_i geometrically using (16), (17), (19) and (20) as follows.

1) Cut the ellipsoid (16) with the plane (20) to

create an ellipse (Figure 7, upper left).

2) Pierce the two sheets of the hyperboloid (19) with the ellipse. This gives either two or four intersection points (Figure 7, upper right).

3) Cut the ellipsoid (17) with the plane (20) to form another ellipse (Figure 7, lower left). This ellipse intersects the ellipse of step 1) at four points.

4) Pierce the hyperboloid with the second ellipse to form two or four more intersection points. If a solution exists, two of these points will coincide with two of the points found in step 3).

The complete picture for a typical case is projected onto the 1-3 plane in the lower right illustration of Figure 7. Note that if $v_1 = 0$, the ellipses intersect in the 2-3 plane, and we use the hyperboloid (18) to select the two solutions.

Our four wires usually can tell us the velocity to within overall sign. Choosing the appropriate sign poses no problem in a propeller wake, where the general direction of the flow is known. Two special cases of interest yield more than two solutions. If $v_1 = \pm v_2$, the two ellipses of Figure 7 coalesce. Each sheet of the

hyperboloid is pierced twice by the ellipse, giving us four solutions. Two of the solutions point in the wrong general direction. The remaining two, however, will not necessarily be very different. At some ratio $r = v_1/v_3$, the hyperboloid becomes tangent to the ellipse, leading to only two solutions. However, if v_1 is close to, but does not equal $\pm rv_3$, we will have difficulty in choosing the appropriate $\hat{\mathbf{v}}$. The ratio r depends purely on the wire slant angle θ_o, viz.

$$r = \frac{\cos\theta_o}{\sqrt{1+\sin^2\theta_o}} \tag{21}$$

For $\theta_o = 35^o$, $r = 0.71$. Thus if $v_1 = \pm v_2$, the probe will give ambiguous results when $\hat{\mathbf{v}}$ makes an angle with the probe axis near 27^o. When $v_1 = \pm v_2$, equations (12) and (13) become the same, as do (14) and (15). We graph the two independent equations at the top of Figure 8 for a specific case. The ellipses intersect at four points.

The second special case of nonunique solutions occurs when the four effective velocities V_i are identical. This time we get six solutions, parallel to the $\pm\hat{i}$, $\pm\hat{j}$, and $\pm\hat{k}$ axes. Fortunately, all these vectors differ enough in direction that the choice should be obvious. Note that all the non-unique solutions have their origin in the symmetry of the "composite" probe. We may thus rid ourselves of these unwanted solutions by changing just one of the four rotation angles. While this would

considerably complicate our geometrical study of the probe behavior, it would not have any effect on the numerical procedure that we finally adopt to reduce the hot wire data.

We present analytical solutions to the set (12) through (15):

$$v_3^2 = \frac{(V_2^2 - V_4^2)^2 - (V_1^2 - V_3^2)^2}{8\sin^2\theta_o(V_1^2 + V_3^2 - V_2^2 - V_4^2)} \qquad (22)$$

$$v_1^2 = \beta_1 \pm \sqrt{\beta_1^2 - 4\alpha\gamma_1} \qquad (23) \qquad v_2^2 = \beta_2 \pm \sqrt{\beta_2^2 - 4\alpha\gamma_2} \qquad (24)$$

$$\alpha = 2(1 - \sin^4\theta_o)$$

$$\beta_1 = [(V_2^2 + V_4^2) - \sin^2\theta_o(V_1^2 + V_3^2)]$$

$$\beta_2 = [(V_1^2 + V_3^2) - \sin^2\theta_o(V_2^2 + V_4^2)]$$

$$\gamma_1 = \cos^2\theta_o(V_3^2 - V_1^2)^2 / 8\sin^2\theta_o$$

$$\gamma_2 = \cos^2\theta_o(V_4^2 - V_2^2)^2 / 8\sin^2\theta_o$$

If $v_1 \neq \pm v_2$, the easiest way to find $\vec{v}$ is with (22), (18), and (19). If $v_1 = \pm v_2$, the denominator of (22) vanishes, so one can use (23) or (24) along with (18), (19), or (20). Note that if $v_1 \neq \pm v_2$, (23) and (24) still work, but they give four solutions, only two of which satisfy the complete set of equations. The spurious values may be identified by substituting back into the set (12) and (15).

These analytical solutions have two main drawbacks.

First, hot wires do not really obey the directional law

$$V = |\vec{v} \times \hat{w}| ,$$

although the probes used in this work come fairly close. Second and more importantly, the closed form solutions, especially (22), are very susceptible to errors in the effective velocities, which are measured quantities. Notice that all of the solutions involve differences between squares of V_i. This is a dangerous arrangement, especially when we anticipate rather small flow angles and hence similar values for the V_i. A curious result of our redundant formulation is that, in the event of inaccurate effective velocities, we obtain different estimates of $\vec{v}$ depending on whether we use (22), (23), or (24). An example shows this.

EXAMPLE:

$$\vec{v} = \hat{i} + 2\hat{j} - 8\hat{k}$$

Use (12) to (15) to find the four V_i's, and then change V_1 by +4%, V_2 by -3%, V_3 by +2%, and V_4 by -4%. With these perturbed values, the various formulas yield the following results:

$$(22): \quad v_3 = -3.44$$

$$(23),(19),(20): \quad \vec{v} = 1.66\hat{i} + 2.63\hat{j} - 5.73\hat{k}$$

$$(24),(18),(20): \quad \vec{v} = 1.10\hat{i} + 1.74\hat{j} - 8.64\hat{k}$$

While the largest measurement error introduced is 4%, the smallest error in any of the velocity components is 8%. One can obtain a crude estimate of v_3 when the other components are relatively small by averaging the effective velocities and dividing by sin 55°. This procedure, when applied to the above example, gives $v_3 = -8.24$. The fact that this simple estimate comes closer to the real value than any of the formulas suggests that tyhe formulas don't provide the best possible $\vec{v}$ in the presence of errors. This observation leads to the development of a much more general numerical scheme for recovering $\vec{v}$ from a set of effective velocities.

We conclude this section with a few observations concerning 3-wire probes. The cylinder representation is most convenient for this purpose. Suppose we have three mutually perpendicular wires. In the center of Figure 8, we view such an arrangement with the 1-3 plane at eye level, and show the "bent circles" that result when two cylinders intersect. Clearly, the third cylinder along the 2-axis will intersect the "bent circles" at <u>eight</u> points! For one very special case, only four solutions exist. We conclude that, from the standpoint of unique determination of the velocity, mutually perpendicular wires constitute the worst possible choice of geometry for three wires. We can improve the situation somewhat by choosing non-orthogonal wire orientations, but in general

we will still have at least four solutions to contend with (Figure 8, bottom). Two solutions (the usual case with four wires) will be obtained only for certain special directions of $\vec{v}$.

5.3 Numerical Scheme for "Composite Probe"

Suppose our hot wire has an effective cooling velocity given by $\mathcal{U} = |\vec{v}|\, f(\hat{w}, \vec{v}/|\vec{v}|)$ where $\hat{w}$ represents the direction of the wire filament, and f is a geometrical direction factor as mentioned previously. If we rotate the wire to four different positions at a given point in the flow, we have a set of four equations, viz.

$$\mathcal{U}_i = |\vec{v}|\, f(\hat{w}_i, \frac{\vec{v}}{|\vec{v}|}) \;, \quad i = 1,4 \qquad (25)$$

Since $\vec{v}$ has only three dimensions, no $\vec{v}$ can satisfy all of the equations if the $\mathcal{U}_i$ have errors. The best we can do is minimize some function that indicates a mismatch between $\vec{v}$ and the $\mathcal{U}_i$. The most obvious choice for such a function is a sum of squares of errors, defined by

$$Q(\vec{v}) = \sum_{i=1}^{4} \left(|\vec{v}|\, f(\hat{w}_i, \frac{\vec{v}}{|\vec{v}|}) - \mathcal{U}_i\right)^2 \qquad (26)$$

Our computational challenge, then, is to find the vector $\vec{v}$ that minimizes Q. Note that (25) still represents four cylinders, but they are not true cylinders because of the non-ideal directional behavior. When we

minimize Q, we find the vector $\vec{v}$ that is closest to all four distorted cylinders in a least squares sense. Various schemes exist for problems of this type. The author has found that for this particular case, the best method is an iteration that utilizes an analytical expression for $-\vec{\nabla}Q$ to determine the next guess for $\vec{v}$.

Iteration Procedure

1) Guess $\vec{v}$. Also decide upon some initial step size a, an accuracy parameter ϵ , and step size adjustment parameters R_{max}, R_{min}.

2) Compute $-\vec{\nabla}Q$.

3) Set $\vec{v}_{new} = \vec{v} - a\dfrac{\vec{\nabla}Q}{|\vec{\nabla}Q|}$

4) If $|\vec{v}_{new} - \vec{v}| < |\vec{v}_{new}|\epsilon$, stop.

5) Compute $-\vec{\nabla}Q_{new}$, and find $Z = \left|\frac{1}{2}\left(\dfrac{\vec{\nabla}Q_{NEW}}{|\vec{\nabla}Q_{NEW}|} - \dfrac{\vec{\nabla}Q}{|\vec{\nabla}Q|}\right)\right|$. Set $a \leftarrow a/R$, where $R = Z(R_{max} - R_{min}) + R_{min}$.

6) Set $\vec{v} \longleftarrow \vec{v}_{new}$, $\vec{\nabla}Q \longleftarrow \vec{\nabla}Q_{new}$, and return to 3).

The novel feature of the plan is step 5). The quantity Z essentially measures the dissimilarity in direction between the new gradient and the old gradient. If $\vec{\nabla}Q_{new}$ and $\vec{\nabla}Q_{old}$ point in exactly the same direction, Z = 0. If $\vec{\nabla}Q_{new}$ and $\vec{\nabla}Q_{old}$ are antiparallel, Z = 1. A feeling for the significance of Z may be gained by

considering a valley with depth $h = h(x,y)$ whose lowest point we wish to find. Here $\vec{\nabla}h$ has two dimensions rather than three. If Z approaches unity, we have jumped to the other side of the valley. A very small Z indicates we're creeping along slowly. The idea is to decrease the step size if we're jumping, and increase it if we're creeping. The parameters R_{max} and R_{min} must lie within the ranges

$$R_{max} > 1 \qquad 0 < R_{min} < 1,$$

and are empirically adjusted until the program operates well.

The reader may question the choice of the accuracy criterion of step 4). After all, we have $\vec{\nabla}Q$, so why not iterate until $|\vec{\nabla}Q| < \delta$, where $\delta \ll 1$? The reason is that the author could not answer this very important question: Given that $|\vec{\nabla}Q| = \delta$, how close are we to a stationery point of Q? There undoubtedly exists an answer to this, but it is quite complicated. The most reliable accuracy test, at least in theory, is one that computes Q at many locations on a sphere of radius δ surrounding the point $\vec{v}$ in velocity space. If Q everywhere on the sphere exceeds $Q(\vec{v})$, we may rest assured that we are within a distance δ of a minimum. The author tried to use this procedure and found it to be an expensive nuisance. The main trouble with it is that the variations in Q close to a minimum are so small that vitually the entire program must

be made double precision. Step 4) resulted from the following train of thought.

Suppose we pick a fairly large step size and a small ϵ. Presumably, the iterated vector $\vec{v}$ will overshoot the target point a few times as the step size decreases. While $\vec{v}$ bounces around, the gradient undergoes radical changes in direction, and we "home in" on the minimum. The final answer for $\vec{v}$ will not be too much farther from the minimum point than a distance $|\epsilon\vec{v}|$.

The author has no analytical proof of this argument, which seems intuitively plausible. However, the computer program has been extensively tested with perturbed effective velocities in the spirit of the example given earlier. It is known that for sufficiently small ϵ and large step size, the output of the program is consistent regardless of what trial vector starts the iteration. Furthermore, ϵ is chosen such that a factor of ten decrease in ϵ does not change the output significantly.

As a final comment, we note that steps 3), 4), and 5) of our computational scheme must work in Cartesian coordinates. This complicates things considerably, because the hot wire directional factor, f, is most conveniently described in terms of a spherical coordinate system that rotates with the probe.

5.4 Calibration and Associated Geometry

We next present some of the more important details of the hot wire work. Included are the probe geometry, and the basic results of the wire and anemometer calibrations.

Refer to Figure 9. The upper right drawing shows the so-called probe frame, where $\hat{k}$ is in the direction of the probe axis (Figure 6). The probe frame is related to the room frame $\hat{i}_R$, $\hat{j}_R$, $\hat{k}_R$ (Figure 9, upper left) through rotation about the $\hat{i}$ axis. The angle β is either 8^o or 12^o, depending on the nacelle used and the axial location of the survey. The unit vector $\hat{k}_R$ points upstream, and is parallel to the propeller axis. The propeller is right-handed, so $\hat{i}_R$ points in the direction of negative swirl velocity. The unit vector $\hat{j}_R$ points in the outward radial direction.

The spherical coordinates $|\vec{v}|$, Λ, and Φ specify the negative of the velocity vector. We regard Q as a function of these three variables. In Figure 9, lower left, we show the wire coordinates $|\vec{v}|$, θ, and φ with respect to the rotating auxiliary frame $\hat{i}'$, $\hat{j}'$, $\hat{k}'$. The angles θ and φ enter the direction factor f. The lower right drawing of Figure 9 defines the relationship between the probe and auxiliary frames for wire rotation number 1. For rotations 2, 3, and 4, the long needle intersects the $-\hat{i}$, $-\hat{j}$, and $+\hat{i}$ axes respectively, while the short needle

stays colinear with the $\hat{k}$ axis. Note that the numbering of the rotations differs here from the original numbering in Figure 6.

Since we want the gradient $\vec{\nabla}Q$ as a function of $|\vec{v}|$, Λ, and Φ, we need to express the angles θ and φ in terms of these coordinates. This expression differs for each rotation. One can find the four required transformations by working out the one for the first rotation, and then rotating $\vec{v}$ (rather than the auxiliary frame) about the $\hat{k}$ axis. This yields

$$\cos\theta_i = \sin\theta_o \cos\Lambda + \cos\theta_o \sin\Lambda \sin\Phi_i \qquad (27)$$

$$\sin\varphi_i = \sin\Lambda \cos\Phi_i / \sin\theta_i$$

$$\Phi_i = \Phi - (i-1)\frac{\pi}{2} \qquad i = 1, 4$$

In the range of validity of the directional calibrations, these formulas are neither singular nor multivalued.

The directional factor f that is fitted to the calibration data has the form

$$f(\theta, \varphi) = \sin\theta(a + b\varphi^2) . \qquad (28)$$

The parabolic correction in φ accounts for the fact that the needles destroy the rotational symmetry of the probe about its wire. The function Q we wish to minimize thus

becomes

$$Q(|\vec{v}|,\Lambda,\Phi) = \sum_{i=1}^{4} (|\vec{v}|\sin\theta_i(a+b\varphi_i^2) - \mathcal{U}_i)^2 \qquad (29)$$

where θ_i, φ_i are considered functions of Λ, Φ through (27). The computer program HOTWIREV requires $\vec{\nabla}Q$ in Cartesian coordinates, an involved bit of mathematics found in Appendix A. Figure 10 illustrates the spherical unit vectors needed for the gradient. The appendix also includes the particular expressions used to convert between the various coordinate systems.

Only two probes, designated Probe #1 and Probe #2, are used in the experiments. They are nominally identical, and their dimensions appear in Figure 1. The tungsten wires have a diameter of one mil. The probes obey the empirical law $\mathcal{U}$ = effective cooling velocity $= |\vec{v}|\sin\theta \cdot(a + b\varphi^2)$ over the calibration range $15^\circ < \theta < 95^\circ$, $-40^\circ < \varphi < 40^\circ$, 25 m/s $< |\vec{v}| <$ 45 m/s. As part of the directional calibration, we choose values for the wire slant angle θ_o that make the sine curves fit the calibration data. These values do not quite agree with those measured directly with the aid of a photo enlarger. The actual angles are $\theta_w = 39^\circ$ and $\theta_w = 34^\circ$ for probes #1 and #2, respectively. Since the slant angles measured by calibration describe the probe behavior, these angles, and not the actual ones, enter the numerical work. The wire constants are a = 0.736, b = 0.1621 rad^{-2}, $\theta_o = 37^\circ$ for

probe #1, and a = 0.786, b= 0.1136 rad^{-2}, θ_o = 35° for probe #2. The constant a differs from unity because all calibrations are referenced to the linearized anemometer output voltage with the wire in "normal" position. See Figure 9, lower right. "Normal" position occurs when the flow velocity vector is parallel to the $\hat{i}$ axis. The directional calibrations are found to be virtually independent of wind speed, and are made at a speed of 32 m/s in two open jet, low-turbulence wind tunnels at M.I.T.: the 12" x 12" wind tunnel in the Aeroclastic Laboratory, and a somewhat larger tunnel in the Acoustics and Vibration Laboratory. Appendix C contains the relevant details.

Speed calibrations are also required to determine the relation between the linearized anemometer voltage V and the effective velocity $\mathcal{U}$. These are not done separately, but rather as part of the propeller experiments. We perform them with the wire in "normal" position. At a particular temperature and flow direction, V does indeed vary linearly with velocity, as illustrated by Figure C-4 of Appendix C. However, both the constant of proportionality and the offset voltage depend upon temperature. The experiments are done in a closed circuit tunnel, where the temperature rises by as much as 10°F during a single traverse through the wake. Since we cannot calibrate during a traverse, we need to make some

assumptions regarding the behavior of the instruments between calibrations.

The third section of Appendix A is a simple analysis, based on King's law, of the effect of ambient temperature changes on V. A linear temperature correction for the constant of proportionality appears adequate. The analysis also predicts negligible changes in the offset voltage, whereas, in fact, we observe quite substantial offset drift during the experiments. The drift is most likely an artifact of the electronics, which we assume to be ideal in the appendix. For now, we simply take a linear relation for the anemometer behavior. We'll find later that this relation works quite well.

$$V = (A + at) + (B + bt)\mathcal{U} \qquad (30)$$

The set of four speed constants A, a, B, b differs slightly for each survey, and is determined through speed calibrations in which we vary the termperature.

5.5 Experimental Procedure

The experimental procedure for a hot wire survey resembles that for a cobra probe survey. We show an enlarged view of the hot wire probe's situation in Figure 5. A wake survey with the single-sensor rotating hot wire is made as follows.

The linearized Flow Corporation anemometer is connected both to the digital memory oscilloscope and to an FM tape deck. A simple capacitive filter is interposed between the oscilloscope and the hot wire output to achieve time averaging. The microswitch on the motorized traverse triggers the 'scope as with the cobra probe. The wire is initially positioned as close to the nacelle as possible, and as it moves up the 'scope records the time-averaged linearizer voltage for radial stations spaced 0.0635 cm apart. At the same time, the tape recorder, operating at a speed of 15 ips, records the time dependent history of the voltage during the traverse on one of its four tracks. The other tracks contain the microswitch pulse, the signal from a 1/8" B&K microphone, and a voice identifying the information. The pulse keeps track of the radial position of the traverse. The microphone allows us to check any anomalies in the acoustic signal against the corresponding hot wire output. A survey comprises four traverses, each time with the wire rotated to one of its four positions.

At the beginning and end of each traverse we record the tunnel temperature. We also make speed calibrations before and after the survey, as follows. With the wire in "normal" position (Section 5.4), we run the tunnel at three speeds, nominally 22.5, 26.0, and 29.5 m/s. At each speed we write down the tunnel temperature and the

linearized voltage. The tunnel heats up as we run it. Typically, the temperatures at 22.5 and 29.5 m/s differ by 5°F. The temperature change for the entire survey, defined as the difference between the temperature at the beginning of the first speed calibration and the temperature at the end of the second calibration, is usually about 10°F.

The four quarters of the oscilloscope memory contain the voltages from all of the rotations. We transfer this information to the mini floppy disc memory of the scope for storage, and later to magnetic tape for computer processing.

5.6 Data Reduction

In this section, we discuss in detail the data reduction for a hot wire wake survey. This occurs in essentially three stages. First, we deduce the speed constants from the speed calibrations. Then we feed the raw data to the VAX11/780 at M.I.T.'s Joint Computer Facility. Finally, two FORTRAN programs HOTWIREV and HOTPROC convert the linearized anemometer voltages into velocities and other relevant quantities.

Recall that the two speed calibrations for a survey yield six triads of wind speed, voltage, and temperature. This is more than enough information to determine the four

speed constants. We use the triads at the 22.5 and 29.5 m/s wind speeds to form a set of four linear equations in the unknowns A, a, B, b. After solving the set, we use the two remaining triads at 26.0 m/s to check for consistency. These checks indicate that the anemometer equation $V = (A + at) + (B + bt)\omega$ is accurate to about 1%.

We need to know the temperature as a function of radius for each traverse in order to use the anemometer equation. At present, however, there is no way to read the tunnel temperature from outside, and we choose not to enter the tunnel while the propeller spins. The temperatures at the beginning and end of each traverse are known, and the traversing mechanism moves the probe through the slipstream at a constant rate. We simply assume that the temperature varies linearly with radius between the two endpoint values.

The magnetic tape, in ANSI standard format, holds four files for each survey, one for each wire position. The files contain time-averaged voltages in an integer format that conserves space. The appropriate files are read directly onto the research disc at the computer facility.

In addition to the voltages, HOTWIREV requires some other information, including a number of constants and

also the operating parameters R_{max}, R_{min}, and ϵ of Section 5.3. These parameters influence the efficiency of the program. HOTWIREV facilitates their adjustment by "remembering" all of the input. It does this by writing the input onto auxiliary files. The operator may repeat a run with different operating parameters without retelling the machine all the other information. The adjustment of the operating parameters is not extremely critical, however. The author retained one set of parameters for all the hot wire data reduction, and these were found after only a couple of tries.

HOTWIREV has a particularly easy time with our data because the points are so close together. The velocity differs very little from one point to the next. The first point that HOTWIREV works on is the farthest outboard radial station in the survey, which lies outside the slipstream. Hence, the initial guess for velocity that we give the program is just the free stream velocity. HOTWIREV supplies its own guesses after this first point. After it finds the velocity vector at a station, it uses this vector as the first guess in the iteration for the next station.

The output of HOTWIREV consists of a single file containing the velocity vectors at all the radial locations, expressed in spherical coordinates. HOTPROC

digests this information and produces six files containing the circulation, the mass flow, the radial outflow angle, the swirl angle, the radial locations of the data points, and the velocity vector $\vec{v}$ in Cartesian room coordinates. The source listings of HOTPROC and HOTWIREV are contained in Appendix D, along with a more detailed account of their use.

Chapter 6

PERFORMANCE MEASUREMENTS

The thrust developed by the propeller, and also the torque required to drive it, are measured at a tunnel speed of approximately 29.5 m/s over an RPM range of 4,000-10,000. The drive motor is supported by a system of stainless steel flexures, shown in Figure 12. The D.C. motor (not pictured) bolts onto the mounting collar. The shaft to hold the propeller projects through the star-shaped opening. Two of the thrust flexures and two of the torque flexures are instrumented with four strain gauges each. The eight thrust flexure gauges, denoted a through dd, are arranged to form a Wheatstone bridge as shown at the top of Figure 13. A similar, but separate bridge exists for measuring torque. Either bridge may be connected to a Baldwin Lima Hamilton SR4 strain indicator box.

If the thrust (or torque) applied to the balance is not too large, it is directly proportional to the strain reading on the indicator box. We establish the constant of proportionality through direct calibration. Thrust and torque calibrations are given in the second section of Appendix E. The balance behaves quite linearly within the range of thrusts and torques encountered in the experiments.

We obtain a set of thrust and torque measurements in the following manner. The bridges are balanced to read zero, and the wind tunnel is brought up to a dynamic pressure of 2.5 inches of alcohol (about 29.5 m/s). We then operate the D.C. motor at a succession of speeds ranging from 4,000 to 10,000 RPM, usually in 1,000 RPM increments, and at each speed the thrust and torque, as indicated by the SR4 box, are recorded. We also write down the tunnel temperature at the beginning and end of each set.

Unfortunately, when we turn off the tunnel and motor at the end of the experiment, the SR4 box no longer reads zero for either of the strain gauge bridges. Sometimes the spurious readings exceed the low RPM measurements. If we wait about 15 minutes, the motor and the flexures cool off, and the bridges return to their original balanced state.

The zero drift is clearly a temperature dependent effect. If the flexure assemblies warp under the influence of heat, real strains will create an apparent zero drift. The Wheatstone bridges supposedly have temperature compensation, but they, too, are suspect. Refer to gauges b and aa in Figure 12. If the propeller exerts a positive thrust on the shaft, the flexure deforms into an "S" shape as shown, and the resistance of aa rises

while that of b falls. Thus, these gauges appear on adjacent legs of the bridge in Figure 13 (top) so that their signals add for thrust. Since they lie on opposite sides of a thin (1/16 inch) piece of steel, we don't expect them to experience very different temperatures. A shift in temperature may cause the gauge resistance to change, but if the gauges are well-matched the spurious temperature signals will cancel in the bridge because they have the same sign. We assume here that the resistance of a single strain gauge is a linear function, viz.

$$\frac{\Delta R}{R} \simeq C_\epsilon \Delta \epsilon_B + C_T \Delta T$$

where $\Delta \epsilon_B$ and ΔT are the flexure surface bending strain and the temperature shift. In the fourth part of Appendix A, we calculate the coefficients C_ϵ and C_T. Suppose ΔT = 75°C and $\Delta \epsilon_B = 1.5 \times 10^{-3}$ -- reasonable numbers in our work. The fractional change due solely to temperature (1.6×10^{-3}) exceeds half the change due to strain (3.1×10^{-3})! Therefore, if our temperature compensation has even a slight defect, considerable measurement errors could result.

Regardless of the cause of the drift, we make a simple correction by assuming that it is a linear function of time during the measurements, although this assumption may sometimes not work very well (see Appendix E, second section). We take the low RPM data at the beginning of

the test before the motor has heated up to avoid disproportionately large zero corrections.

Chapter 7

DISCUSSION OF THE RESULTS

7.1 Introduction to the Data Collection

Here we discuss the aerodynamic measurements, presented graphically in Figures 14 through 139. Figures 14 through 49 show cobra probe wake data, Figures 50 through 79, hot wire wake data, and Figures 80 through 139, performance data. In all graphs pertaining to the wake, the symbols represent calculations based on Munro's theory, while the continuous curves illustrate the corresponding experimental results. Exactly the opposite convention holds in the performance graphs.

Basically, we can measure three quantities in the wake: the velocity, the static pressure, and the total pressure, all circumferentially-averaged in our case. The hot wire only detects velocity, but the cobra probe yields the pressures as well. Given these basic physical quantities, one may compute the circulation from the tangential velocities, integrate the axial velocities to find the mass flow, and infer the velocity in the developed wake from the total pressure. As explained in Section 3.2, this last calculation loses its meaning if the propeller operates in front of a large nacelle.

A wake survey is made by traversing a probe along a line segment perpendicular to the propeller axis. The segment begins as close to the nacelle surface as possible, and ends outside the slipstream boundary. We low-pass filter the output of the probe. Because both the nacelle and the inflow to the propeller disc have axial symmetry, time-averages along the (fixed) radial line segments correspond to circumferential averages in a frame that rotates with the propeller. The axial location of the line varies between surveys. Cobra probe surveys are usually made 0.5R behind the disc plane, but distances of 0.11R and 1.22R are also used. Hot wire surveys are performed at 0.41R or 0.13R (R = tip radius of propeller).

We display each cobra probe survey in a series of two or three separate graphs. First we plot the circulation Γ versus the equivalent radius r_{eq}. The equivalent radius is the square root of the mass flow, normalized so that it becomes unity at the slipstream boundary. As explained in Section 3.2, this type of plot provides a mapping of the radial circulation distribution which, under our assumptions, should not vary with axial location even in the presence of the large nacelle. Predictions of Γ vs. r_{eq} are given along with the measurements. The second graph shows the static pressure p_s. The theory cannot provide an estimate of p_s. We plot it, mainly out of curiosity, versus r_{eq} for convenient comparison with

the circulation. Surveys with the minimum nacelle require a third graph comparing the predicted velocities in the developed wake to those indicated by the total pressure. Since the wake contracts somewhat, this plot has the reduced radius r_{red} as the horizontal coordinate. One obtains r_{red} by linearly scaling the actual radii in the wake such that $r_{red} = 1$ at the slipstream boundary.

In order to define r_{red} and r_{eq}, we must locate the boundary. We take as the edge of the slipstream that point in the survey where: 1) a sharp negative spike in static pressure occurs, and 2) the slope of the circulation curve has its largest negative value. These two things do happen at the same radius, as the cobra probe data shows. The spike marks the edges of the vortex sheets, which are beginning to roll up.

Every hot wire survey is displayed on three graphs. Again, the first one illustrates the theoretical and experimental circulation curves. Next, we plot the axial velocity as a function of either the reduced radius or the actual radius in motors. We use the actual radius in surveys at the 0.41R, 0.50R, and 1.22R axial locations with the symmetric nacelle. Otherwise, r_{red} is the abscissa. The theory can predict the axial velocities not only in the infinite wake, but also in the disc plane. Graphs of axial velocity for surveys made very close to

the propeller (at the 0.13R axial location) therefore show theoretical as well as measured values. The final graph gives the tangential (swirl) and radial velocities.

We present each performance measurement as a series of five separate figures: thrust coefficient C_T, power coefficient C_P, and efficiency η (or "performance parameter"), all versus the advance ratio λ, and the thrust T and torque Q, both versus RPM. The first three plots compose the traditional representation of propeller behavior. The thrust, as we usualy measure it, is simply the forward pull of the propeller on its shaft ("gross" thrust). In a few cases, we detach the front portion of the symmetric nacelle from the rear portion, and fasten it to the shaft housing instead. There exist positive static pressures behind the propeller, which then lower the measured thrust ("net" thrust). "Net" thrusts appear along with "gross" thrusts on certain plots. The term "performance parameter" applies to all cases with either of the large nacelles, which cause a radial variation in the inflow velocity and hence invalidate the usual simple expression for efficiency. Graphs of the "performance parameter" do not include theoretical values.

A uniformity of scales pervades the collection. Readers wishing to compare similar types of measurements

may do so by placing the graphs one behind the other before a strong light. Each figure also has a convenient list of experimental parameters. In the discussion that follows, we generally refer to the various figures simply by their numbers. The various quantities in the graphs are listed in Table VII. Tables VIII and IX index the wake surveys and performance measurements, respectively.

In Appendix E, we perform an error analysis on the hot wire and performance data. Tables III and IV contain the estimated errors in the time-averaged swirl velocity. Corresponding error bars appear on the graphs of circulation. In Table V, we list the error bars for the thrust and torque, but these do not appear in the figures because they are for the most part quite small. The reader will notice that the plots of measured efficiencies exhibit some scatter. This occurs partly because the efficiency, being computed from both the thrust and torque, involves twice as much experimental uncertainty as the other performance quantities. Furthermore, although the actual errors in torque are fractions of a newton-meter, the percentage errors become large at RPM below about 6000, where the torques (and thrusts) are small and sometimes even negative.

7.2 Wake Surveys

As a start, we happily observe that the circulation

distribution for the minimum nacelle cases, as measured by hot wire anemometry, agrees rather well with the theory (Figures 56, 59, 62, 74, 77). The Windsong propeller is designed specifically to shift the loading distribution inboard, and this objective has certainly been met. Notice, however, the odd little peak in the circulation of the Windsong at r_{eq} = 0.9 (Figures 71, 74), and also the higher than expected outboard loading. The same peak occurs in the Bruiser circulation (Figures 30, 34). The author cannot explain this quirk. We have tried to unload the tips of these two propellers. Evidently, the blades object. The Windsong propeller also exhibits a sharp step in swirl velocity at the 70% radius (Figures 74, 77). The 70% radius marks the beginning of a transition region between airfoil types. This region extends to the 80% radius, and is largely an artistic creation.

In the minimum nacelle cases, the comparison between the axial velocities at the 0.13R location and the theory in the disc plane achieves only moderate success, but this should not disappoint us too much (Figures 63, 75, 78). After all, the probe <u>is</u> a bit downstream. As the wake develops, it contracts and the axial velocities increase. This development probably occurs more rapidly at 10,000 RPM than at 7,000 RPM. Thus, we expect the theory to underestimate the velocities at 0.13R, and furthermore, the discrepancies at 10,000 RPM should

exceed those at 7,000 RPM. Indeed, we see exactly these trends.

The situation with the symmetric nacelle is more complicated. In all but one case, the circulation at the inboard sections, according to the hot wire, is considerably less than anticipated (Figures 50, 53, 65, 68, 71). The circulation toward the tip, while a little higher than predicted, doesn't seem to compensate for this; the wake indicates a diminished total thrust. Two pairs of cobra probe surveys shed some light on the matter (Figures 46, 48). Both these plots show the effect of axial location on circulation in the presence of the symmetric nacelle. Apparently, our special mapping doesn't quite work in these cases. The distributions imply that vorticity is not conserved, since the inboard circulation goes down as we move downstream, while the outboard values hardly change. We caution that the cobra probe may exaggerate this effect because of its inability to handle radial velocities properly.

One hot wire survey with the symmetric nacelle has the predicted inboard circulation, however (Figure 71). Another survey (Figure 53) unfortunately has a serious gain problem; this is the first hot wire measurement we made and it lacks all of the necessary speed calibration

information. The shapes of the theoretical and experimental curves agree. Both surveys are made very close to the propeller turning at 7,000 RPM. If we move downstream, again the inboard circulation decreases (Figure 68). Note that Figures 68 and 71 both pertain to the Windsong propeller operating under the same conditions. Only the axial location of the survey differs between these figures.

If we now turn the Windsong at 10,000 RPM, and measure close to the propeller (Figure 65), we no longer get the agreement of Figure 71. We conclude that the symmetric nacelle causes the circumferentially-averaged inboard circulation to decrease as we move downstream in the wake. Furthermore, the decrease is more rapid at 10,000 RPM than at 7,000 RPM. Quite possibly, the theory does as good a job at predicting the actual loading on the blade with the symmetric nacelle as without. Indeed, the performance measurements lend admirable support to this idea. Figures 123, 124 and Figures 133, 134 show the thrust and torque of the Windsong propeller operating in front of the symmetric and minimum nacelles, respectively. Also see Figures 83, 84 and 98, 99 and Figures 108, 109 and 118, 119 for similar comparisons with the Cessna and Bruiser propellers. The predictions work just as well with the symmetric nacelle as with the minimum nacelle.

The symmetric nacelle also has an unexpectedly large effect on the axial velocities (Figures 66, 72). Even in the case where the inboard circulation matches the theory (Figure 71), the inboard velocity is much lower than predicted (Figure 72). Once again, we point out that there surveys are made not in the disc plane, but 0.13R behind it. The radial velocities become fairly large as the wake flows around the nacelle, and, hence, the axial velocities must decrease. The nacelle forces the wake outward, as seen clearly in Figure 66. Incidentally, none of the surveys made at 0.13R with the symmetric nacelle cover the whole wake. The hot wire probe cannot get into the small space between the blade and the nacelle to measure at the innermost radii. In computing the mass flow for these cases, we assume the axial velocity has a constant value at these radii, equal to the value at the smallest possible measurement radius.

So far, we have said little about the cobra probe measurements. Recall that we anticipate some error in these measurements when the radial velocities are appreciable. Two of the minimum nacelle surveys show good agreement between the measured and predicted circulation (Figures 21, 27). In both of these surveys, the propeller either turns at 7,000 RPM, or has a reduced blade angle and turns at 10,000 RPM. Neither of them involves the Bruiser propeller. Observe the small dip

toward the tip in Figure 21. When we turn the propellers at 10,000 RPM, the radial inflow velocities increase, and large discrepancies between the theory and the experiments occur that did not occur with the hot wire. In particular, the small dip of Figure 21 turns into a huge dip in Figure 18, whereas the corresponding hot wire survey (Figure 56) shows excellent agreement. This type of distortion is even worse in the Bruiser surveys (Figures 34, 37) because the Bruiser produces more thrust than the other propellers, and, hence, its wake contracts more. The measurement of Figure 34 can't possibly be accurate, because the thrust (Figure 118) agrees reasonably well with the predictions.

The cobra probe has at least as much difficulty in the symmetric nacelle cases. Here, the theory always appears to greatly underestimate the circulation at the innermost sections (Figures 14, 16, 24, 30, 32, 40). The nacelle imposes an outward radial flow near its surface, as opposed to the inward flow caused by wake contraction in the minimum nacelle cases. Outward and inward flows seem to have opposite effects on the circulation measurements.

Measurements of total pressure, converted to the velocities in the developed wake, are plotted alongside the theory in Figures 20, 23, 26, 36, 39, 42 and 45. We

note good agreement for the Cessna at 7,000 RPM (Figure 23), moderately good agreement for the Cessna at 10,000 RPM (Figure 20), and only fair agreement for the other cases. As usual, the cobra probe has trouble with the Bruiser (Figures 36, 39). Two cobra probe measurements are made extremely close to the blade, both with the symmetric nacelle in place. The combined effects of radial velocity and unsteadiness render these surveys almost useless; only the total pressures survive. For Figures 26 and 42 we plot the velocities in the developed wake, interred from these pressures, against the theory. Strictly speaking, we shouldn't do this with the symmetric nacelle, but, in fact, the comparison of Figure 26 looks quite good at the outer radii, where the effect of the body is weak. The inner radii exhibit the expected blockage of flow.

Despite all the criticism the author has heaped upon the cobra probe, we do learn some interesting things from it. First of all, recall the small peak in the outboard circulation of the Windsong propeller. A similar sort of peak exists in the 10,000 RPM Bruiser data (Figures 30, 34), which shouldn't surprise us because the Bruiser has so much in common with the Windsong. The peak even seems to be mysteriously linked with the large dip in measured circulation of Figure 34.

The static pressure plots are also of interest. The negative spikes at r_{eq} = 1.0 indicate that the edges of the vortex sheets have at least started to roll up. The curled edges resemble miniature tornadoes. Since the pressure outside the wake is atmospheric, or nearly so, the pressure at the cores of these "tornadoes" must be less than atmospheric to balance the centritugal forces. Also, the size of these spikes follows a pattern. The spikes for the four 10,000 RPM nominal blade angle cases have nearly the same magnitude (Figures 15, 19, 31, 35) as do the spikes in the 7,000 RPM cases (Figures 17, 22, 33, 38). Even though the Bruiser produces more thrust than the Cessna, its pressure spikes are less than or equal to those of the Cessna. This probably occurs because the Bruiser carries proportionally less load at the outer radii, and thus creates vortex sheets with relatively weak edges. If we compare the Windsong and Cessna propellers (Figures 25, 28 and 41, 44), which produce very similar thrusts, we see the effect of the loading distribution more clearly.

Let us return to the hot wire surveys to point out some odd effects. The first effect involves the radial velocities in the minimum body cases (Figures 58, 61, 64, 76, 79.) Notice that the flow has an <u>outward</u> component at the inner portion of the wake. Suppose that the innermost part of the blade does little or no work on the

flow. The solidity is not very high, so air leaks through the center of the propeller without being "swirled." If somehow the wake imparts rotational velocity to this core, centrifugal forces will pull it outward radially. The manner in which the wake turns the core is not at all obvious. While the propeller does turn very quickly, the slipstream itself has tangential velocities on the order of 5 m/s, making viscous forces unlikely as the cause of appreciable core rotation. One might, however, imagine the vortex sheets acting as impeller blades. Munro [24] proves that the vortex sheets of a minimum induced loss propeller behave as though they were rigid. Since none of our propellers are truly minimum induced loss, the sheets deform as they move downstream, but the basic analogy between the slipstream of a propeller with a "leaky hub" and a centrifugal pump with two blades still holds.

The hubs of our propellers do indeed "leak." For one thing, the blades do not mount flush against the hubs. The gap between the innermost airfoil section and the hub is about 1/4 inch for our propellers. Furthermore, all the propellers are designed to operate in front of the symmetric nacelle, and thus have reduced attack angles at the inboard blade sections. The work done by these sections decreases when we use the minimum nacelle, and sometimes they even work against the flow.

Indeed, the total pressure (relative to the wind tunnel stagnation pressure) becomes negative at the inner radii in almost all of the minimum body surveys (Figures 20, 23, 29, 39, 45). Negative swirl appears in some cases (Figures 59, 62), and the hot wire shows axial velocities substantially less than the tunnel speed of approximately 29.5 m/s (Figures 57, 60, 63, 78). The theory occasionally predicts this negative work, or "windmilling," as well (Figures 27, 56, 59).

The "hub leakage" also explains another interesting effect. If the trailing edge of the blade ends, the vortex sheet also must end. The outside edge of the sheet curls up as already mentioned. Should not the inside edge roll up as well? Indeed it does! Most of the minimum body cases exhibit <u>two</u> downward spikes in static pressure -- one outboard, and one inboard (Figures 19, 28, 35, 38, 44). The inboard spike has nothing to do with the shaft boundary layer, which has a thickness on the order of 1/32 inch. The inner spikes undoubtedly exist in the symmetric nacelle cases. We just can't see them too well, either because the motor cooling flow has swallowed them, or because they diffuse as the wake wraps around the body. Remnants of these spikes linger in most of the graphs.

The flow in the vicinity of what we have called the

slipstream boundary exhibits several peculiar features. To begin with, the time-averaged radial velocities, measured with the hot wire at the 0.13R axial station, seem too small for the amount of wake contraction observed in the minimum nacelle cases. In Figure 11 we show a geometrical construction that illustrates this point, Intuitively, one would expect the rate of contraction per unit axial distance to vary monotonically with distance, so the purely hypothetical boundary in the figure is shown as a dotted line with the appropriate curvature. The angle β represents the time-averaged radial inflow angle at the edge of the slipstream, estimated from the hot wire data, and α results from the geometry. The angle α exceeds β.

For example, consider the Windsong propeller with a reduced blade angle turning at 10,000 RPM in front ot the minimum nacelle. We find $\alpha = 11.3^{o}$ from Table VIII, while $\beta = 7.7^{o}$ from Figures 75 and 76. We take as another example the Cessna propeller operating at 7,000 RPM, also with the minimum nacelle. Here $\alpha = 8.3^{o}$, but $\beta = 4.6^{o}$, from Figures 63 and 64. Notice also the small negative peak in the radial velocities just inside the wake boundaries. These are present in most of the hot wire surveys. The discrepancy between and may result from vortex sheet rollup, or perhaps from circumferential variations in the direction of the velocity vector. The

sheets might have higher inward radial velocities than the fluid between the sheets, and this would cause the slipstream boundary, as we have defined it, to shift inboard. This is pure conjecture, of course, because we have only time-averaged, fixed-probe measurements.

Another strange feature of the flow is the negative tangential velocity that is always present outside the wake. In Table VI we list these velocities for the hot wire surveys, with the corresponding swirl angles. The values given apply to the farthest outboard survey point in each case. Only the most lightly loaded propellers (Cessna, 7,000 RPM) show angles less than one degree. In six of the ten hot wire surveys, the measured tangential velocities outside the slipstream greatly exceed the estimated error (compare Tables IV and VI). Earlier we mentioned that small errors in alignment of the propeller axis with the free stream become magnified in the wake [12]. The author, suspecting a similar problem, subtracted the tangential velocities listed in Table VI from the measurements because, if he did not, the theoretical and experimental circulation curves diverged wildly. The radial and axial components, however, have not been adjusted in any way. Peter Dunbeck [36], who used the same facility as the author for propeller work, also measured swirl relative to the flow outside the slipstream boundary.

The axial velocity at the edge of the wake is less than the free stream value, and does not recover to the full value for quite some distance. All of the hot wire surveys exhibit this trait; the 10,000 RPM Windsong cases (Figures 66, 75) provide the best illustrations. Because this dip occurs with both the symmetric and minimum nacelles, simple curvature effects do not explain it.

In Table VIII we compare the predicted and measured total mass flows for all of the wake surveys. The experimental values depend on our definition of the slipstream boundary, which is apparently a somewhat nebulous object. Hence, the mild disagreements between the theoretical and experimental values in Table VIII should not surprise us. We cannot fully understand any of the phenomena associated with the boundary without time-dependent velocity measurements at several axial stations.

7.3 Performance Measurements

We now turn to the performance measurements. Although a few plots show spectacular agreement between the theory and the experiments (Figures 83, 88, 129, 138) systematic discrepancies mark most of the data. We consistently overestimate both the thrust and the torque; the thrust predictions usually look better. The best agreement for thrust tends to occur around an advance

ratio of λ = 0.17, which corresponds to 7,000 RPM at a tunnel speed of 29.5 m/s.

Many of the thrust and torque coefficients fall off much faster than anticipated with increasing advance ratio. This we loosely attribute to low Reynolds numbers. Here the Reynolds numbers are based on the chord c; $Re = \frac{Uc}{\nu}$, where U equals the speed of the airfoil relative to the fluid. As we increase λ, we decrease Re, and encourage the normally turbulent boundary layer to become laminar at the leading edge and separate. If this transition occurs, the section produces less lift, and we measure less thrust. Since the sections all make an appreciable angle with the propeller shaft, the torque will also go down, provided the decrease in the lift component outweighs the increased drag that results from separation. If a profile is on the verge of stalling, an increase in attack angle should worsen its performance. Thus, since the symmetric nacelle increases the relative attack angles at the inboard sections, we expect better agreement with the predictions for the minimum body cases than for the symmetric body cases. This effect can clearly be seen in the data for the Windsong and Bruiser. For some reason, the Cessna seems to suffer less from low Reynolds numbers with the symmetric body than without, and the author does not understand this (Figures 80, 95).

Recall that we make the Cessna predictions using section characteristics computed at the model Reynolds numbers, whereas we use section characteristics at full-scale Reynolds numbers in the Bruiser and Windsong calculations. The low RPM predictions for the Cessna are no better, and, in many cases, worse than those for the other two propellers. We conclude that the sections on the Windsong and Bruiser blades are superior in the sense that they suffer relatively less from low Reynolds number effects.

Chapter 8

CONCLUSION

8.1 Assessment of Theory

The theory does a fairly good job of predicting the performance and loading distribution of light aircraft propellers. Two features may be added to this theory that will probably improve the agreement with the experiments. The helical vortex sheet has two components of residual velocity. The more important component lies perpendicular to the geometrical direction ot motion ot the airfoil, and decreases the relative angle of attack. A small parallel component is also known [2], but unfortunately this was discovered after Munro and the author had finished most of their computations, and hence, has not been included. This component slightly decreases the speed of the airfoil relative to the fluid. Its effects on the predictions are to decrease both the thrusts and torques. The parallel component becomes only moderately important at low advance ratios, and vanishes at high advance ratios.

A second feature involves the Mach number correction to the airfoil characteristics. We have employed a simple Glauert rule, which strictly applies only to wings of infinite span. Prof. Larrabee [40] has suggested a semi-empirical correction, based on the Glauert rule, that

accounts for the finite blade radius. This so-called "effective Mach number" correction differs significantly from the Glauert rule only at the tip, where it decreases the lift. Thus, its primary effect is to lower the calculated thrusts at low advance ratios.

The author feels that our theory, whose primary purpose is to guide the practical design of small aviation propellers, does not warrant corrections any more elaborate than these. No matter how complete we try to be, aircraft manufacturers will still insist, with good reason, on testing their designs directly to "fine tune" them.

8.2 Comments on the Experiments

The only real disappointment in this project, as far as this author is concerned, is the behavior of the thrust and torque stand. Evidently, unless it receives better cooling, it will not provide the precision measurements for which it is designed. A more effective vacuum might improve the motor cooling, but it would definitely disturb the wake surveys and possibly alter the performance of the propeller. Perhaps a better solution is to leave the vacuum alone, and dribble in some liquid nitrogen at the cooling inlet. We could also add dummy strain gauges to the flexures for the exclusive purpose of temperature compensation. Each dummy (Figure 13, bottom), denoted by

primed letters, enters a bridge leg that opposes that of its partner. The dummies hardly respond at all to bending because of their orientation, but their temperature signals hopefully cancel their partners' temperature signals. The advantage of this arrangement over the present one is that the dummy gauges, being on the same surface as, and very close to, their partners, have an improved chance of experiencing the same temperature as their partners.

The author, however, distrusts strain gauge devices in temperature-varying environments, and recommends that all flexures be replaced by carefully made mechanical linkages that permit larger displacements. There are available today hydraulic piston cylinders with rolling diaphragm seals. These cylinders, intended for precision servomechanisms, have extremely low static friction and yet can support large loads. One could use these pistons to measure thrust as follows. Place one cylinder in the stand, interposed between the moving motor carriage and the fixed base. Place a second cylinder outside the tunnel with its axis vertical, and connect the two pistons with a pressure line. Introduce additional damping, if desired, with a valve in the line. Install a small platform on the outside cylinder to accept calibrated weights. The result is a dependable, operationally simple thrust detector that requires essentially no calibration

and involves no temperature-induced electrical problems. A similar scheme could give reliable torque measurements.

Hot wire wake surveys, while extremely informative, are difficult to make. Three-hole pressure probe measurements require much less effort and can provide adequate preliminary results. A cobra probe should not be used, however, because of its sensitivity to radial velocities. Experimenters wishing to perform traditional two-dimensional wake surveys are encouraged to look into the cylindrical yaw probe mentioned in Section 2.1 (Figure 1). Dean [41] states that in the presence of radial velocities, this type of probe can accurately measure swirl angles, but its pressure readings contain some error. One should perhaps obtain total pressure with a separate bell-mouthed single tube probe, which has little directional sensitivity.

Subsequent hot wire work might incorporate a more careful treatment of temperature. If the present alcohol thermometer in the wind tunnel were replaced by a device that could be read outside the tunnel, we could make better temperature calibrations and corrections. A strip chart recording of the temperature vs. time would be extremely useful.

The author realizes that the above remarks do not exhibit a great deal of cost consciousness. Their purpose

is to inspire future investigators who wish to further improve the experiments.

APPENDICES

Appendix A

MISCELLANEOUS CALCULATIONS

A.1 The Gradient $\vec{\nabla}Q$

We wish to find the gradient of the function

$$Q(|\vec{v}|,\Lambda,\Phi) = \sum_{i=1}^{4} (|\vec{v}|\sin\theta_i (a + b\varphi_i^2) - \omega_i)^2 .$$

Here the subscript i refers to the four wire rotations. The variables have already been defined in Section 5.4. In the spherical probe coordinates of Figure 10,

$$\vec{\nabla}Q = \hat{V}\frac{\partial Q}{\partial|\vec{v}|} + \hat{\Lambda}\frac{1}{|\vec{v}|}\frac{\partial Q}{\partial\Lambda} + \hat{\Phi}\frac{1}{|\vec{v}|\sin\Lambda}\frac{\partial Q}{\partial\Phi} \qquad \text{(A-1)}$$

Let

$$\delta_i \equiv |\vec{v}|\sin\theta_i (a + b\varphi_i^2) - \omega_i \qquad \text{(A-2)}$$

Then

$$\frac{\partial Q}{\partial|\vec{v}|} = \sum_{i=1}^{4} 2\delta_i \frac{\partial\delta_i}{\partial|\vec{v}|} \qquad \text{(A-3)}$$

$$\frac{\partial Q}{\partial\Lambda} = \sum_{i=1}^{4} 2\delta_i \frac{\partial\delta_i}{\partial\Lambda} \qquad \text{(A-4)}$$

$$\frac{\partial Q}{\partial\Phi} = \sum_{i=1}^{4} 2\delta_i \frac{\partial\delta_i}{\partial\Phi} \qquad \text{(A-5)}$$

where

$$\frac{\partial\delta_i}{\partial|\vec{v}|} = \sin\theta_i (a + b\varphi_i^2) \qquad \text{(A-6)}$$

$$\frac{\partial\delta_i}{\partial\Lambda} = |\vec{v}|\cos\theta_i \frac{\partial\theta_i}{\partial\Lambda}(a + b\varphi_i^2) + |\vec{v}|\sin\theta_i 2b\varphi_i \frac{\partial\varphi_i}{\partial\Lambda} \qquad \text{(A-7)}$$

$$\frac{\partial\delta_i}{\partial\Phi} = |\vec{v}|\cos\theta_i \frac{\partial\theta_i}{\partial\Phi}(a + b\varphi_i^2) + |\vec{v}|\sin\theta_i 2b\varphi_i \frac{\partial\varphi_i}{\partial\Phi} \qquad \text{(A-8)}$$

Now we need to express θ_1 and φ_i in terms of Λ and Φ. We do this by writing two representations of the same vector.

$$\frac{\vec{V}}{|\vec{V}|} = \hat{\imath}\sin\Lambda\cos\Phi + \hat{\jmath}\sin\Lambda\sin\Phi + \hat{k}\cos\Lambda$$

$$\frac{\vec{V}}{|\vec{V}|} = \hat{\imath}\sin\theta\sin\varphi + \hat{\jmath}(\cos\theta\cos\theta_o - \sin\theta\cos\varphi\sin\theta_o) + \hat{k}(\cos\theta\sin\theta_o + \sin\theta\cos\varphi\cos\theta_o)$$

Equating the coefficients of $\hat{\jmath}$ and $\hat{k}$ gives two equations. Multiply the $\hat{\jmath}$ equation through by $\cos\theta_o$, the $\hat{k}$ equation by $\sin\theta_o$, and add them to find (A-9) below. The $\hat{\imath}$ equation gives (A-10).

$$\cos\theta = \sin\theta_o\cos\Lambda + \cos\theta_o\sin\Lambda\sin\Phi \qquad \text{(A-9)}$$

$$\sin\theta\sin\varphi = \sin\Lambda\cos\Phi \qquad \text{(A-10)}$$

Now use implicit differentiation on (1) and (2), and rearrange:

$$\frac{\partial\theta_i}{\partial\Lambda} = (\sin\theta_o\sin\Lambda - \cos\theta_o\cos\Lambda\sin\Phi_i)/\sin\theta_i \qquad \text{(A-11)}$$

$$\frac{\partial\theta_i}{\partial\Phi} = -(\cos\theta_o\sin\Lambda\cos\Phi_i)/\sin\theta_i \qquad \text{(A-12)}$$

$$\frac{\partial\varphi_i}{\partial\Lambda} = (\cos\Lambda\cos\Phi_i - \cos\theta_i\sin\varphi_i\frac{\partial\theta_i}{\partial\Lambda})/\cos\varphi_i\sin\theta_i \qquad \text{(A-13)}$$

$$\frac{\partial\varphi_i}{\partial\Phi} = -(\sin\Lambda\sin\Phi_i + \cos\theta_i\frac{\partial\theta_i}{\partial\Phi}\sin\varphi_i)/\cos\varphi_i\sin\theta_i \qquad \text{(A-14)}$$

One first evaluates (A-11) through (A-14). The gradient $\vec{\nabla}Q$ is then found by back substitution with (A-8) through (A-1).

A.2 Coordinate Transformations

We require $\vec{\nabla}Q$ in Cartesian coordinates. Let

$$\vec{\nabla}Q = w_v\hat{v} + w_\Lambda\hat{\Lambda} + w_\Phi\hat{\Phi}$$
$$= w_x\hat{\imath} + w_y\hat{\jmath} + w_z\hat{k}$$

From Figure 10,

$$\begin{bmatrix} w_x \\ w_y \\ w_z \end{bmatrix} = \begin{bmatrix} \sin\Lambda\cos\Phi & \cos\Lambda\cos\Phi & -\sin\Phi \\ \sin\Lambda\sin\Phi & \cos\Lambda\sin\Phi & \cos\Phi \\ \cos\Lambda & -\sin\Lambda & 0 \end{bmatrix} \begin{bmatrix} w_v \\ w_\Lambda \\ w_\Phi \end{bmatrix}$$

Transformations from the coordinates $(|\vec{v}|, \Lambda, \Phi)$ to (v_x, v_y, v_z), and vice versa, are also needed in the computer programs.

$$\vec{v} = \hat{\imath}|\vec{v}|\sin\Lambda\cos\Phi + \hat{\jmath}|\vec{v}|\sin\Lambda\sin\Phi + \hat{k}|\vec{v}|\cos\Lambda$$
$$= \hat{\imath}v_x + \hat{\jmath}v_y + \hat{k}v_z$$

To go from (v_x, v_y, v_z) to $(|\vec{v}|, \Lambda, \Phi)$,

$$|\vec{v}| = v_x^2 + v_y^2 + v_z^2$$
$$\Lambda = \arccos(v_z/|\vec{v}|)$$
$$|\Phi| = \arccos(v_x/(|\vec{v}|\sin\Lambda))$$

If $v_y \geq 0$, $\Phi = |\Phi|$ If $v_y < 0$, $\Phi = -|\Phi|$

The computer programs skip the calculation of Φ if Λ is very small, and simply add $\frac{\pi\sqrt{5}}{3}$ to Φ.

Finally, we need a simple transformation relating the Cartesian probe coordinates to the room coordinates, because we tilt the probe axis with respect to the propeller axis by an angle β.

$$\vec{V} = \hat{\imath} V_x + \hat{\jmath} V_y + \hat{k} V_z$$
$$= \hat{\imath}_R V_x + \hat{\jmath}_R (V_y \cos\beta - V_z \sin\beta) + \hat{k}_R (V_y \sin\beta + V_z \cos\beta)$$

A.3 Analysis of Anemometer Drift

How does a change in the ambient temperature affect the linearized anemometer voltage? A complete answer to this question would involve an analysis of the electronics of both the anemometer and the linearizer. Here, we simply assume the instruments are ideal, and that King's law applies to the wire cooling. According to King's original paper [42], the heat loss H per unit time for large velocities is

$$H = K\theta_o + 2\theta_o\sqrt{\pi K s \sigma a}$$

where

K = thermal conductivity of fluid

θ_o = temperature of wire above ambient

= $T_{wire} - T_{ambient}$

a = wire radius

V = fluid velocity at ∞

S = specific heat at constant volume per unit mass

σ = fluid density

If the anemometer truly maintains the wire at a constant temperature, the wire resistance R_w will not change. An energy balance gives

$$H = I^2 R_w = E^2 C$$

where C = constant, E = anemometer voltage output. Suppose the actual ambient temperature T_1 differs from the temperature T_o, for which the instruments are adjusted. Denote the velocity indicated by the linearizer as v_L, let $\theta_1 \equiv T_{wire} - T_1$, and let $\Delta T = T_1 - T_o$.

$$v_L = [(E^2 C - K\theta_o)/2\theta_o\sqrt{\pi K s \sigma a}\,]^2$$

$$E^2 C = K\theta_1 + 2\theta_1\sqrt{\pi K s \sigma a}\; v^{1/2}$$

$$v_L = \left[\frac{\sqrt{K}}{2\theta_o\sqrt{\pi s \sigma a}}\right]^2 \Delta T^2 - \frac{\sqrt{K}}{\theta_o^2\sqrt{\pi s \sigma a}}\,\Delta T \cdot$$

$$\cdot(\theta_o - \Delta T)\, v^{1/2} + \left[\frac{\theta_o - \Delta T}{\theta_o}\right]^2 v$$

Notice the unfortunate square root dependence that creeps in. If $T_1 > T_o$, the sensitivity decreases. Our anemometer operates at an overheat ratio of 1.5, and the

tungsten wire has a length of 6×10^{-3}m and a radius of 1.27×10^{-5} m. We estimate θ_o from the relation $\theta_o \alpha = \frac{\Delta R}{R} = 1.5$, where α = temperature coefficient of resistance of tungsten = 0.0045/°C at room temperature. This yields $\theta_o \approx 330$°C. All of the other physical properties required to evaluate the coefficients in the expression for v_L may be found in handbooks. We obtain

$$v_L = v[1 - 6.1\times10^{-3}\Delta T + 9.2\times10^{-6}\Delta T^2]$$
$$+ v^{1/2}[-2.7\times10^{-3}\Delta T + 8.1\times10^{-6}\Delta T^2] + 1.8\times10^{-6}\Delta T^2$$

Taking v = 40 m/s and ΔT = 10°C as typical, we obtain for the three terms

$$v_L = 37.60 - 0.17 + 1.8\times10^{-4}$$

Thus, the drift in offset voltage is negligible, and the square root constitutes only 1/2% of the reading. Also, we may assume that the drift in the anemometer gain (the coefficient of v) depends linearly on temperature.

A.4 The Effect of Temperature on a Strain Gauge

The bridges are illustrated in Figure 13. The purpose of this analysis is to assess the relative importance of temperature in the output of a single gauge. A gauge consists of n parallel wire filaments connected in series. Let us analyze one filament, the resistance of which is given by

$$R = \frac{\rho L}{A}$$

where L = length, A = cross sectional area, and ρ = specific resistivity in ohm-meters. For small changes in ρ , L, and A,

$$\frac{\Delta R}{R} \cong \frac{\Delta \rho}{\rho} + \frac{\Delta L}{L} - \frac{\Delta A}{A} .$$

We write

$$\Delta \rho \cong \frac{\partial \rho}{\partial \epsilon} \Delta \epsilon' + \frac{\partial \rho}{\partial T} \Delta T$$

$$\Delta \epsilon' \cong \Delta \epsilon_B + (\beta - \alpha) \Delta T$$

$$\Delta L \cong L \Delta \epsilon_B + \beta \Delta T L$$

$$\Delta A \cong 2A[-\nu(\beta - \alpha)\Delta T - \nu \Delta \epsilon_B + \alpha \Delta T]$$

where α = temp. coefficient of expansion of filament material (cupro-nickel alloy), β = temp. coefficient of expansion of flexure material (stainless steel), ΔT = temperature rise, and $\Delta \epsilon_B$ = bending strain of flexure surface. Upon substitution into the equation for $\frac{\Delta R}{R}$, we find

$$\frac{\Delta R}{R} \cong \Delta \epsilon_B \left(\frac{1}{\rho} \frac{\partial \rho}{\partial \epsilon} + 1 + 2\nu\right)$$

$$+ \Delta T \left[(\beta - \alpha)\left(1 + 2\nu + \frac{1}{\rho} \frac{\partial \rho}{\partial \epsilon}\right) + \frac{1}{\rho} \frac{\partial \rho}{\partial T} - \alpha\right]$$

The ratio $\frac{\Delta R}{R}$ for the entire gauge does not depend on the number of filaments. The coefficient of $\Delta\epsilon_B$ is usually referred to as the "gauge factor." The quantities $\frac{1}{\rho}\frac{\partial\rho}{\partial\epsilon}$ and $\frac{1}{\rho}\frac{\partial\rho}{\partial T} - \alpha$ are the strain and temperature coefficients of resistivity. All the various constants have been found in a number of handbooks, and have the values $\nu = 0.3$, $\beta = 1.62 \times 10^{-5}$C, $\alpha = 1.08 \times 10^{-5}/^{o}$C, and $\frac{1}{\rho}\frac{\partial\rho}{\partial T} - \alpha = 1 \times 10^{-5}/^{o}$C. Our gauges have a "gauge factor" of 2.07. Inserting the numbers yields

$$\frac{\Delta R}{R} = (2.07)\Delta\epsilon_B + (2.12 \times 10^{-5}/^{\circ}C)\Delta T.$$

Appendix B

COBRA PROBE CALIBRATION

We show the cobra probe calibration setup in Figure B-1. The probe A is held in a jig (not shown) that permits one to rotate the probe about its axis and also read the flow angle θ. The axis is four inches from the mouth of the jet and perpendicular to the stream velocity. Each hole of the probe communicates with a strain gauge pressure transducer C via a tube B. These transducers contain diaphragms. While the "front" sides of the diaphragms feel the pressure from the tubes B, the "back" sides all feel the tunnel stagnation pressure p_o produced by a separate probe D and monitored by a manometer E. This arrangement mimics the setup used in the actual propeller experiments. The transducer voltages are read with a digital voltmeter.

The transducers themselves are calibrated with a hydraulic pressure device built by the author. We find that their output voltage is linear with pressure to within 1/4%. The transducer gains are different. They are

$$K_l = 7900 \text{ nt/m}^2\text{volt}$$

$$K_c = 9210 \text{ nt/m}^2\text{volt}$$

$$K_r = 6690 \text{ nt/m}^2\text{volt}$$

These values result from least squares fits to graphs of

transducer output as a function of pressure.

Since we're interested in three things (θ, v, p_s), the set of calibration curves must comprise three separate families. Let's consider them one at a time. We first investigate the angular behavior by rotating the probe about its axis while the tunnel speed remains constant. At each angle θ (-6^o, -4^o, -2^o....20^o) we record p_l, p_c, and p_r. This is done for several speeds ($1/2\rho v^2$ = 370, 570, 780, 950, 1150, 1350, 1550, 1750, 1950 pascals). At each tunnel speed we plot θ, which is known, versus the predicted angle, now called θ_T, which we obtain by plugging p_l, p_c, p_r into (5) of Section 4.2. In this way we produce a family of curves of θ vs. θ_T parameterized with respect to known speeds $1/2\rho v^2$. It turns out that our probe's angular behavior is practically independent of velocity, at least for the angles of interest, so that the angular "family" consists of the single curve shown in Figure B-2. It is essentially a straight line with the equation

$$\theta = \theta_T A + B$$

where

$$B = -1.03 \text{ degrees}, \quad A = 1.20.$$

This line represents the data to within 0.40^o.

Next we turn to the velocity calibration. Again we rotate the probe at various tunnel speeds, but this time we plot $1/2\ v_T^2$ versus 0_T^2 at each speed, where $1/2\ \rho\ v_T^2$ is gotten by substituting p_1, p_c, p_r into (6) of Section 4.2. Were the probe ideal, $1/2\ \rho\ v_T^2$ would be independent of θ_T and would equal $1/2\ \rho\ v^2$. In fact $1/2\ \rho\ v_T^2$ displays neither of these characteristics, as is evidenced by the curves presented in Figure B-3. This family of curves obeys the following empirical law:

$$\frac{1}{2}\rho v_T^2 = \begin{cases} A\left(\frac{1}{2}\rho v^2\right) + B, & \theta_T \leq 0.8 \text{ degrees} \\ A\left(\frac{1}{2}\rho v^2\right) + B + (\theta_T - 0.8)\left[C\sqrt[7]{\frac{1}{2}\rho v^2} + D\right], & \theta_T > 0.8 \text{ degrees} \end{cases}$$

where

$A = 1.48$, $B = 20.9$ pascals, $C = 41.1$ (pascals)$^{6/7}$/degree, $D = -88.0$ pascals/degree.

The calibration data obeys this law to within about 2%. Dynamic pressures rather than velocities have been used to make the calibration immune to changes in air density.

The third family of calibration curves pertains to the static pressure. Now we can easily vary θ and v, but we have no control over the ambient pressure of the room, which remains very nearly constant during the calibration. We may, however, put forth the following argument.

The Mach number of the flow is 0.2 at most, so that we can reasonably treat the problem as incompressible. The flow field around the probe may not obey our simple model, but we can still decompose the total pressure at a port into two parts, namely

$$p_{port} = p_{static} + p_{port\ dynamic}(\theta, v, \rho) - p_o.$$

$p_{port\ dynamic}$ is some complicated function that is affected by p_{static} only through changes in density ρ. Atmospheric pressure is about 10^5 pascals. Our measurements of p_{static} behind actual propellers never exceeded 600 pascals, so that we may ignore the effect of p_{static} on ρ. Thus, we calibrate for static pressure by finding an additive correction $f(\theta, v)$ defined as

$$f(\theta, v) \equiv p_s - p_{sT} = p_s - p_o - \left(\frac{p_L + p_R}{2}\right) + \frac{1}{4}\rho v^2$$

where p_s is merely atmospheric during calibration. Note that in the expression for p_{sT}, v rather than v_T has been used to reduce computation. $f(\theta, v)$ is non-zero because the flow doesn't obey the simple theory that led to the expression for p_{sT} ((7) of Section 4.2). $f(\theta, v)$ is shown in Figure B-4 and obeys another empirical law,

$$f(\theta, v) = \begin{cases} A + B\left(\frac{1}{2}\rho v^2\right), & \theta_T \leq 6 \text{ degrees} \\ A + B\left(\frac{1}{2}\rho v^2\right) + (\theta_T - 6.0)\left[C\ \frac{1}{2}\rho v^2 + D\right], & \theta_T > 6 \text{ degrees} \end{cases}$$

where

A=-2,06 pascals, B=0.187, C=12.37 (pascals) $^{6/7}$/degree, D= -25.0 pascals/degree.

The calibration data obeys this law to within about 5%. In the case of experimental measurements one calculates both $f(\theta, v)$ and p_{ST} from the port pressures to recover p_S.

Use of Calibration Curves

Given p_c, p_l, and p_r, how exactly do we use the calibration curves to find θ, v, and p_S? The procedure is as follows:

1) Calculate $\theta_{Texp} = 1/2 \arctan \left[\frac{p_R - p_L}{2p_c - p_L - p_R}\right]$

2) Use Figure B-2 to recover θ.

3) Compute $1/2\rho v^2_{Texp} = [2p_c - p_l - p_r] \cdot [1 + \tan^2 2\theta_T]^{1/2}$

4) Now go to Figure B-3 and draw a vertical line A-A through all the curves that intersects the horizontal axis at θ_{Texp}.

5) Each point where A-A intersects a curve has three pieces of information associated with it: θ_{texp} (the same for all the points), $1/2\,\rho\, v_T^2$ (the ordinate, measured along the vertical axis), and $1/2\,\rho\, v^2$ (the actual tunnel dynamic pressure corresponding to the curve).

6) The plot of step 5 will be nearly a straight line. Linearly interpolate to find the value of $1/2\,\rho\, v^2$ ($1/2\,\rho\, v^2_{actual}$) that corresponds to $1/2\,\rho\, v^2_{Texp}$.

7) Having found the actual dynamic pressure, convert it to velocity using the appropriate value for ρ. This varies a bit between experiments -- both tunnel temperature and atmospheric pressure were recorded for each wake survey.

8) Compute $p_{sT} = p_o + \frac{p_L + p_R}{2} - 1/4\,\rho\, v^2$.

9) Refer to Figure B-4. Draw a vertical line B-B through all the curves that intersects the horizontal axis at θ_{Texp}. Each point where B-B

intersects a curve has three pieces of information associated with it: θ_{Texp} (the same for all the points), $f(\theta, v)$ (the ordinate, measured along the vertical axis) and $1/2\rho v^2$. Plot $f(\theta, v)$ vs. $1/2\rho v^2$.

10) The plot in step 9 will again be nearly linear. Interpolate to find the value of $f(\theta, v)$ ($f_{actual}(\theta, v)$) that corresponds to $1/2\rho v^2_{actual}$.

11) Add $f_{actual}(\theta, v)$ to p_{sT}. This should give a good value for the static pressure p_s.

Needless to say, this reduction procedure is too laborious to be carried out for all of our wake data by hand. A FORTRAN computer program PREDUCE has been written that mimics the above steps.

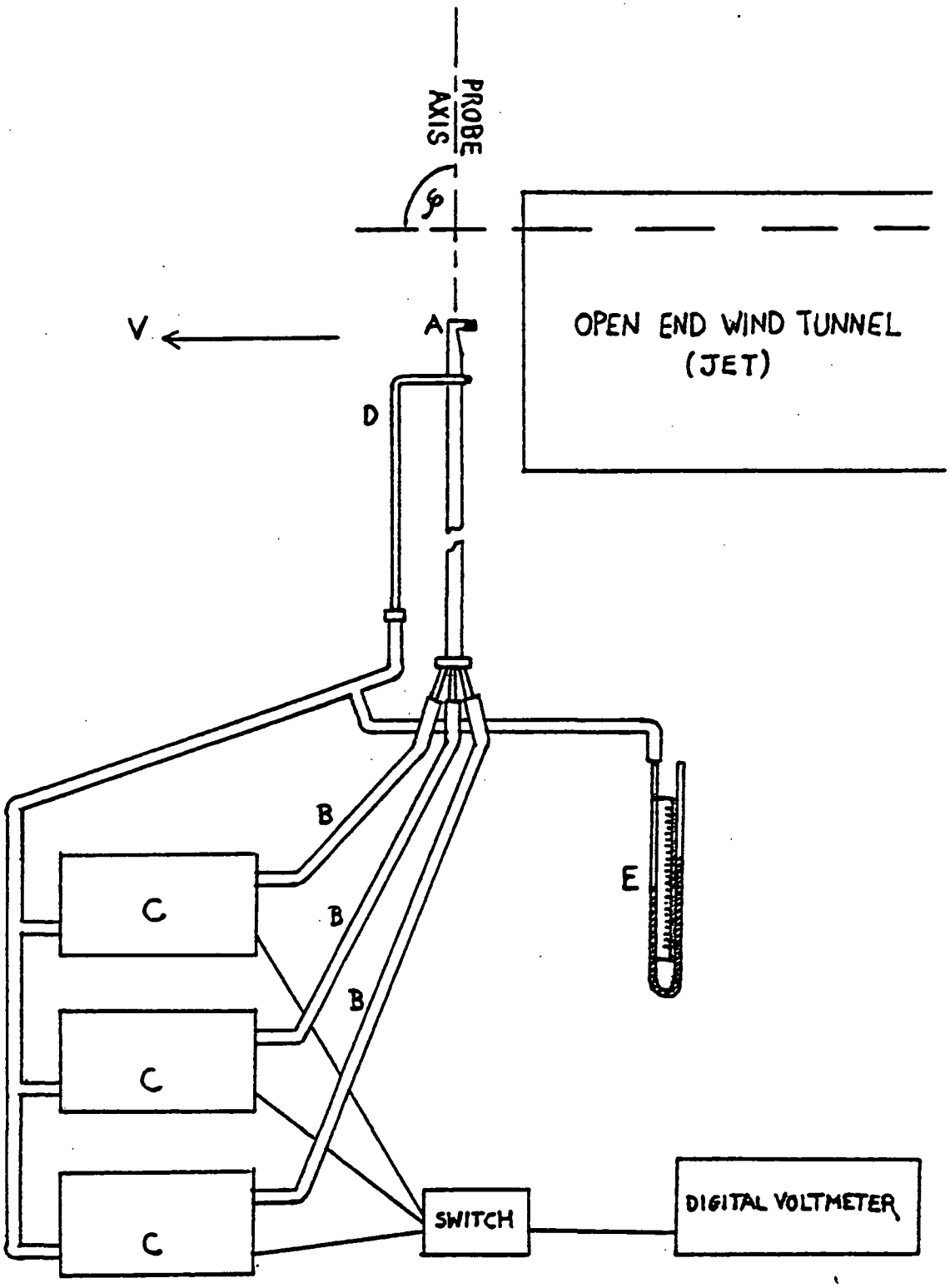

Fig. B - 1. Cobra probe calibration setup

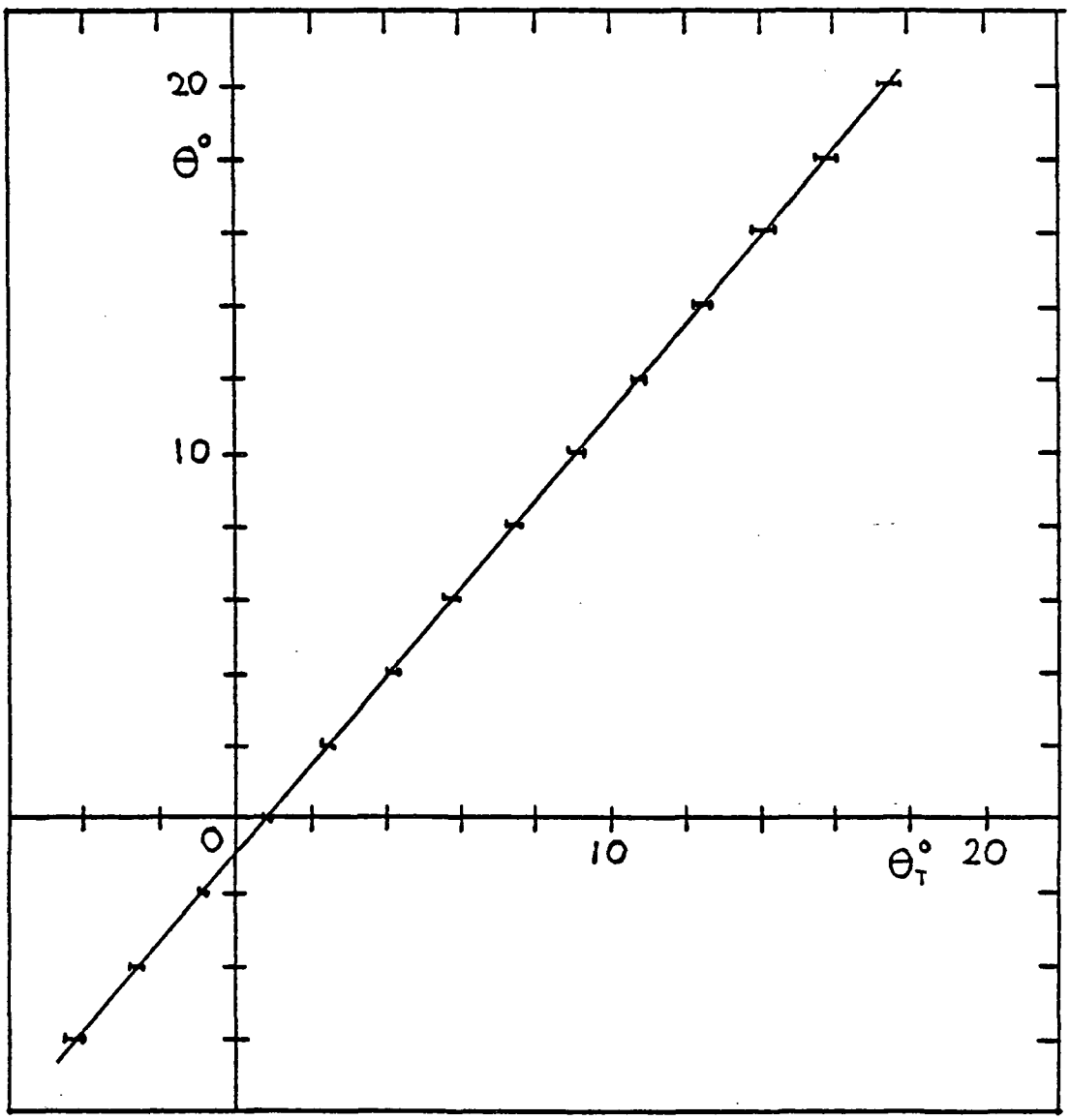

Fig. B - 2. Swirl angle calibration

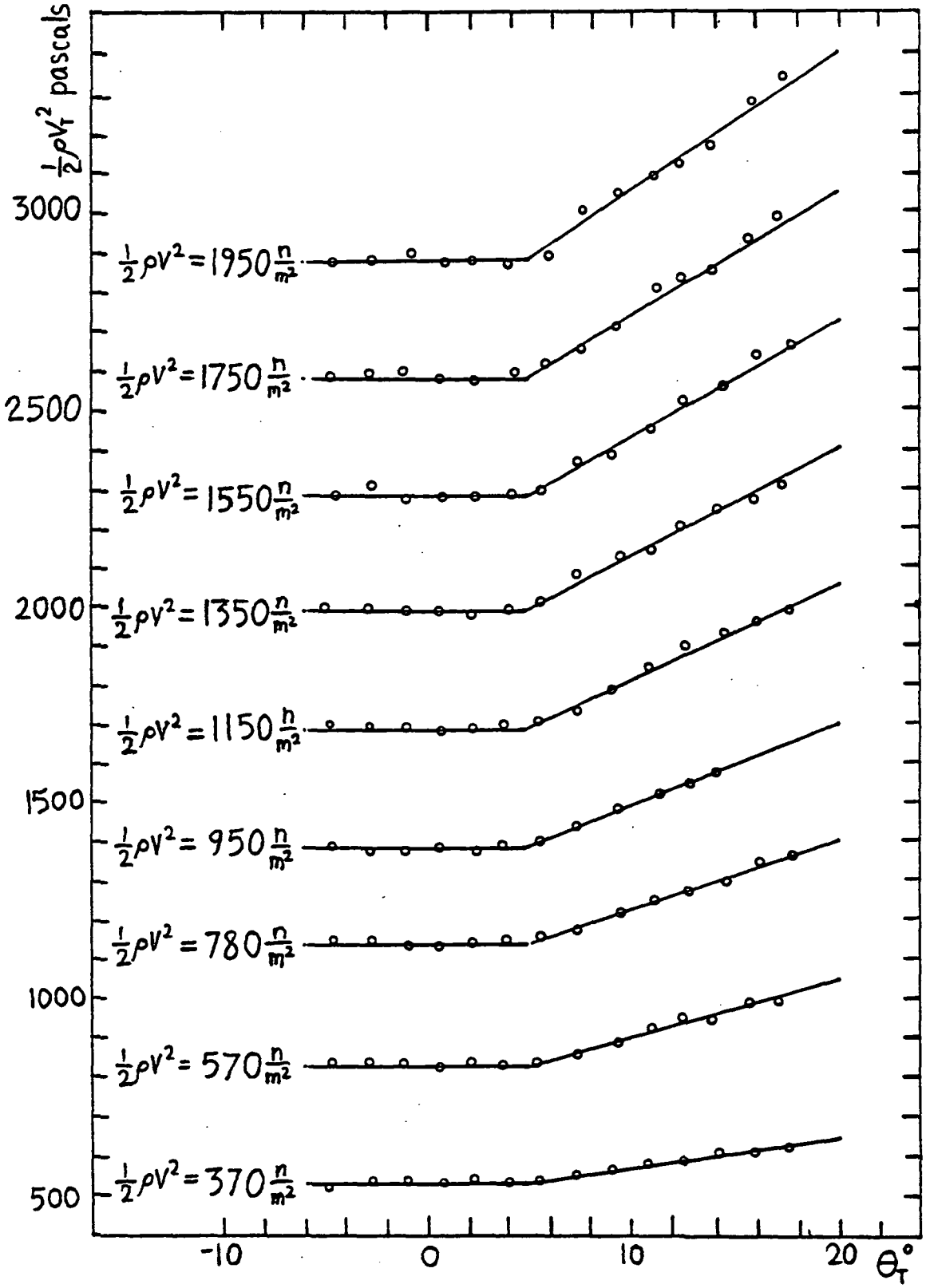

Fig. B - 3. Dynamic pressure calibration

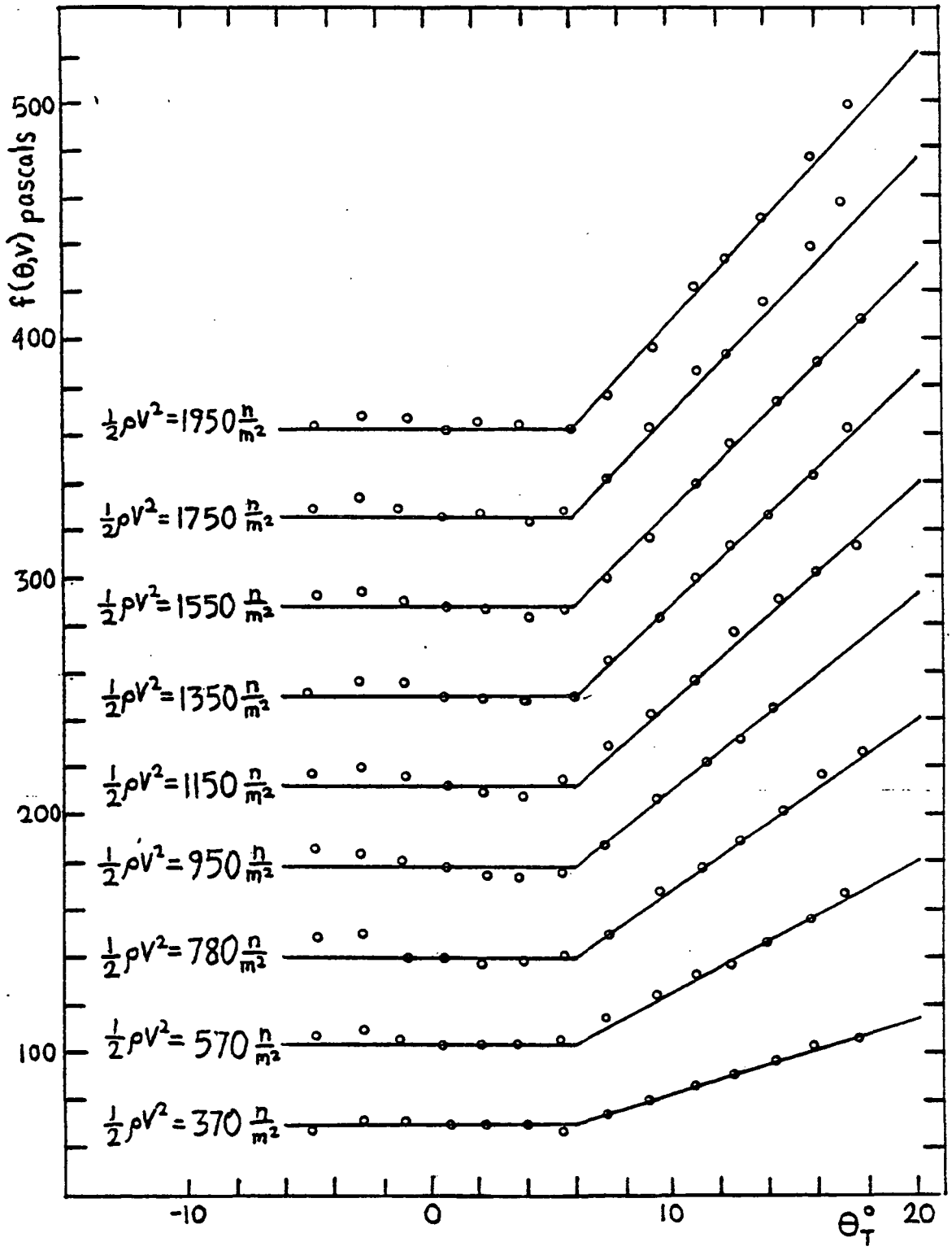

Fig. B - 4. Static pressure calibration

Appendix C

HOT WIRE CALIBRATION

The main purpose of this calibration is to find the directional dependence of the hot wire cooling, and express it in a convenient analytical form. We hold the probe in a jig, and mount it at the mouth of a low turbulence open jet tunnel as in the cobra probe calibration. The wire is rotated so that it makes various angles with the flow, and at each angle we write down the linearized anemometer voltage. The tunnel speed remains constant at 32 m/s during this process. Separate speed calibrations, in which we vary the tunnel speed with the wire oriented in the reference or "normal" position, (Section 5.4), establish the relationship between the wire cooling and the velocity magnitude in the absence of directional effects.

We assume that the directional characteristics do not vary with flow magnitude, so the expression for the linearized anemometer voltage is

$$V = A + B|\vec{v}|f(\theta, \varphi),$$

where f represents the directional dependence of the cooling, and A and B are constants obtained by speed calibration. The quantity $|\vec{v}|f$ is usually referred to as the "effective cooling velocity" in the literature. We

find f by performing four different types of probe rotations. Refer to Figure 9, and consider the probe orientation shown. For the first rotation, called A, we fix Φ at -90° and vary Λ between -45° and 45°. In rotations B and C, Φ is set at 180° and 225°, respectively, and Λ varies as before. In rotation D, we turn the probe about the wire axis, and hence φ varies between -45° and 45°.

If the wire were ideal, f would simply equal $\sin\theta$. We know, however, that the probe needles introduce some φ dependence. Hence, a first guess at the form of f is

$$f = \sin\theta\, g(\varphi)$$

where we use (27) of Section 5.4 with i = 1 to find θ, φ from Λ, Φ. Notice that only θ changes in rotation A, while only φ changes in D. Figure C-1 shows, for probe #2, the percent effective velocities F for rotations A and D, where

$$F \equiv \left(\frac{V-A}{B|\bar{v}|}\right)100$$

We are only interested in an angular calibration range of

$$15° < \theta < 95°, \quad -40° < \varphi < 40°.$$

In this range, g has the parabolic form

$$g(\varphi) = a + b\varphi^2$$

The values of a and b, found with the eyeball and calculator method, are approximately

$$a_2 = 0.786,\ b_2 = 0.2236\ \text{rad}^{-2}$$

for probe #2. As can be seen in the figure, $g(\phi)$ does a fair job of representing the behavior. It turns out that $\sin\theta$ works well for the θ dependence, provided that we take θ_o to be 35^o, rather than the measured wire angle of 34^o.

Figure C-2 shows the behavior for rotations B and C, in which θ and ϕ both vary. If f, in its present form, doesn't predict B and C properly, we have to modify f with some fancy cross terms. Fortunately, f does predict the directional dependence for these cases, as shown. We aren't terribly fussy about the accuracy of the curve fits because the symmetry of the "composite probe," and the redundancy of the effective velocities, cause directional calibration errors to partially cancel.

Probe #1 was used in only the first two of the ten surveys. Only two calibration rotations, A and B, exist for this probe. We suspect, however, that since the two probes have nominally identical geometries, we can use the same form for f as before. Inspection of Figure C-3 (left) yields $a = 0.736$, $\theta_o = 37^o$. Since we don't have a D rotation, we must deduce b from Figure C-3 (right) by

fitting $b\varphi^2$ to $-a + F/\sin\theta$. A comparison between $b\varphi^2$ and the actual values of $-a + F/\sin\theta$ is given in Figure C-4 (left). An annoying asymmetry is present, but since the parabolic correction is comparatively small, we don't model the asymmetry which could be due to crooked mounting in the jig. The fit for rotation B, where both φ and θ vary, is fair at best. Nonetheless, we take

$$a_1 = 0.736 \qquad b_1 = 0.1621 \text{ rad}^{-2}$$

for probe #1.

We show a calibration of the Flow Corporation linearized anemometer with probe #1 in Figure C-4. On the whole, the linearization is accurate to about 1%. However, the curvature of the plot will cause trouble if we calibrate at low speeds and try to extrapolate to high speeds. We attempt to mitigate this problem by finding the ratio between the slope of the least squares line and the local slope at $\mathcal{U} = 26.0$ m/s. This is done by fitting the function $\mathcal{U} = H(V) = A + BV^{1+\epsilon}$ to the actual linearizer output. H(V), with $\epsilon = 0.715$, A = 10.524 and B =1.497 fits the output extremely well, as shown in the figure. The slope of the least squares line is 8.277 m/s-volt. Since $\left.\frac{dH(V)}{dV}\right|_{\mathcal{U}=26.0} = 6.794$, the desired ratio α is approximately 1.22. The least squares line and H(V) cross about where $\mathcal{U} = 29.5$, so the linearizer curvature correction is

$$\omega = 29.5 + \frac{\alpha}{B+bt}(V - V_{MAX}), \text{ if } V > V_{MAX}$$

where V_{max} = (A + at) + (B + bt)29.5, t = temperature, and A, a, B, b are the speed constants discussed in Section 5.4.

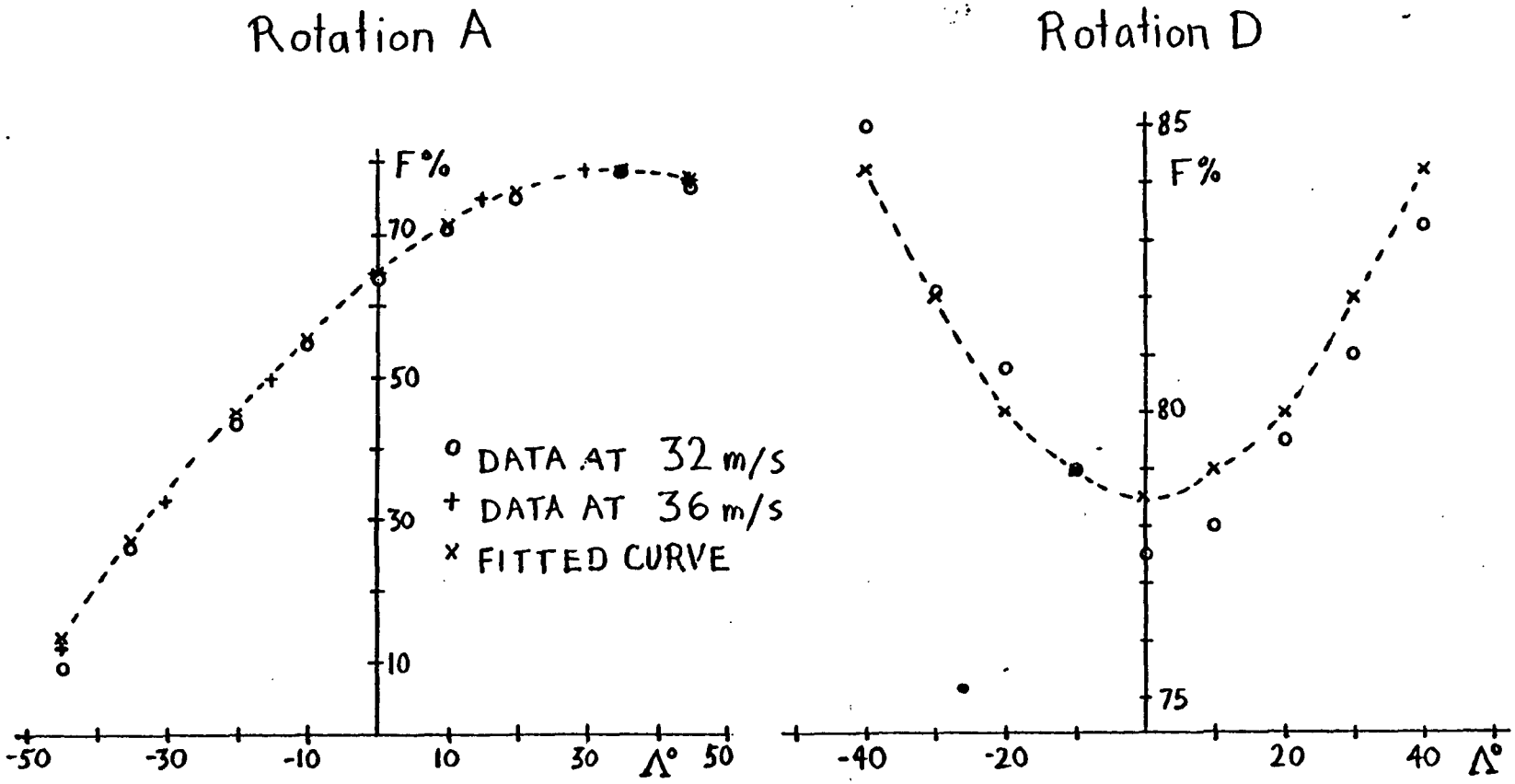

Fig. C - 1. Hot wire calibration, probe no. 2; rotations A and D

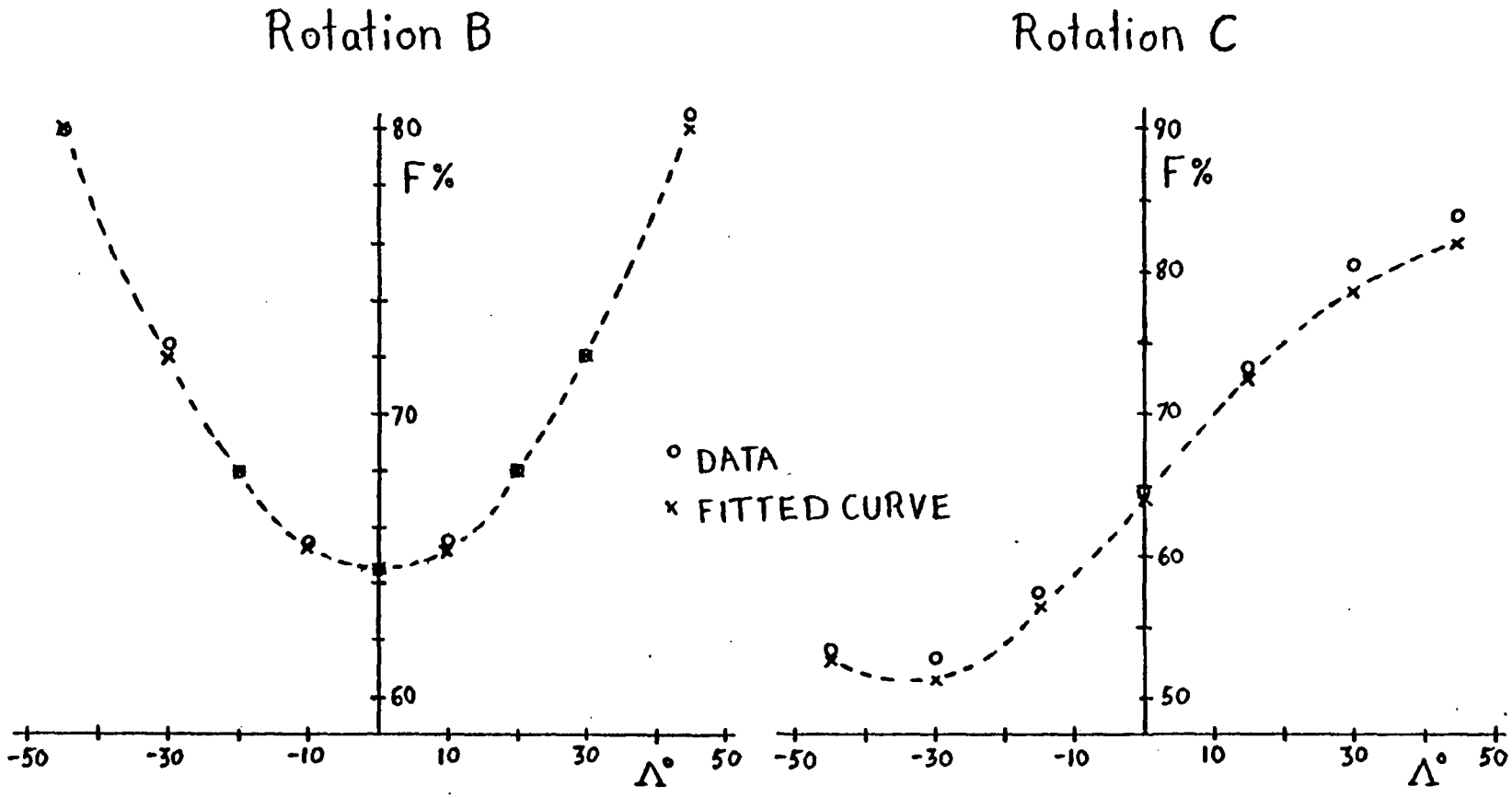

Fig. C - 2. Hot wire calibration, probe no. 2; rotations B and C

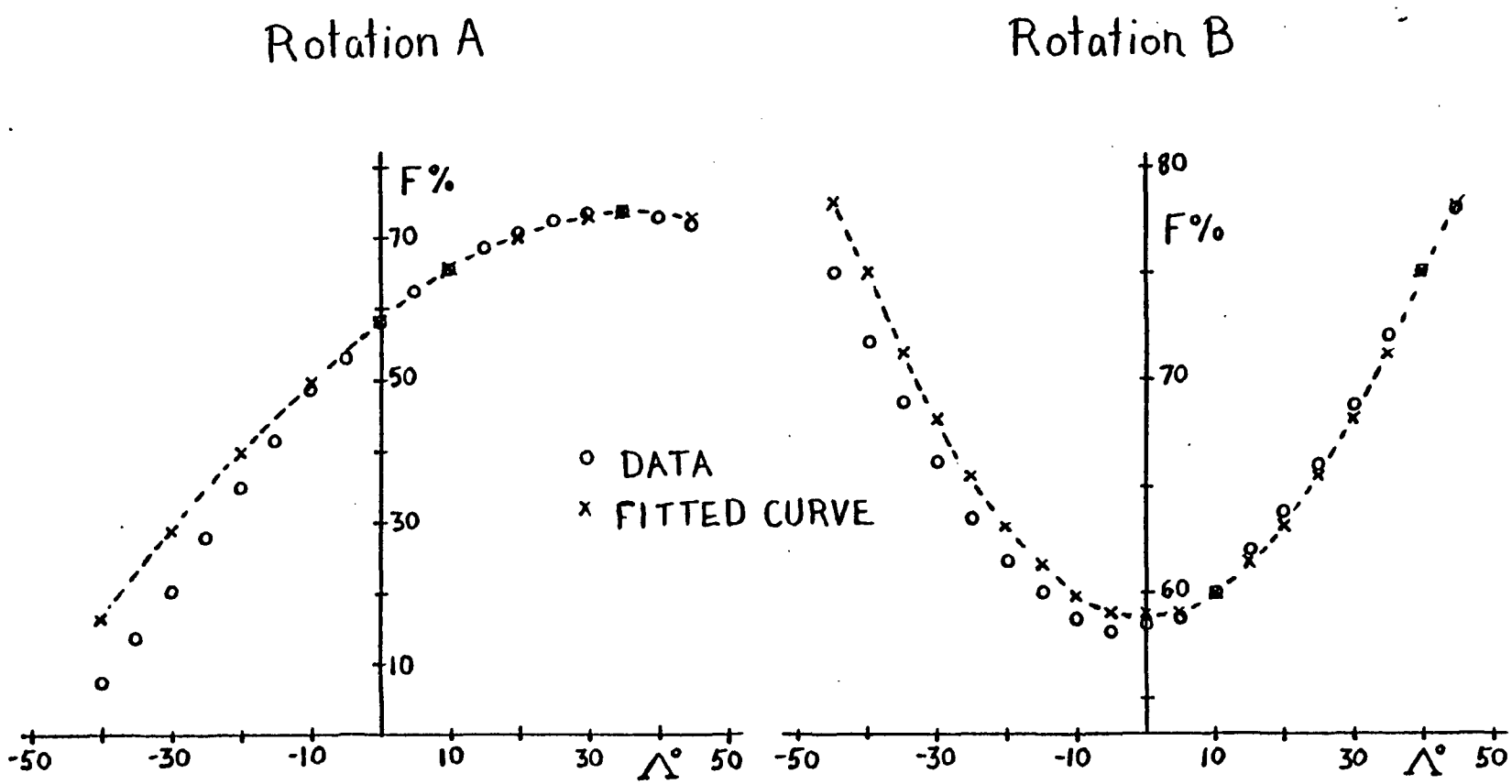

Fig. C - 3. Hot wire calibration, probe no. 1; rotations A and B

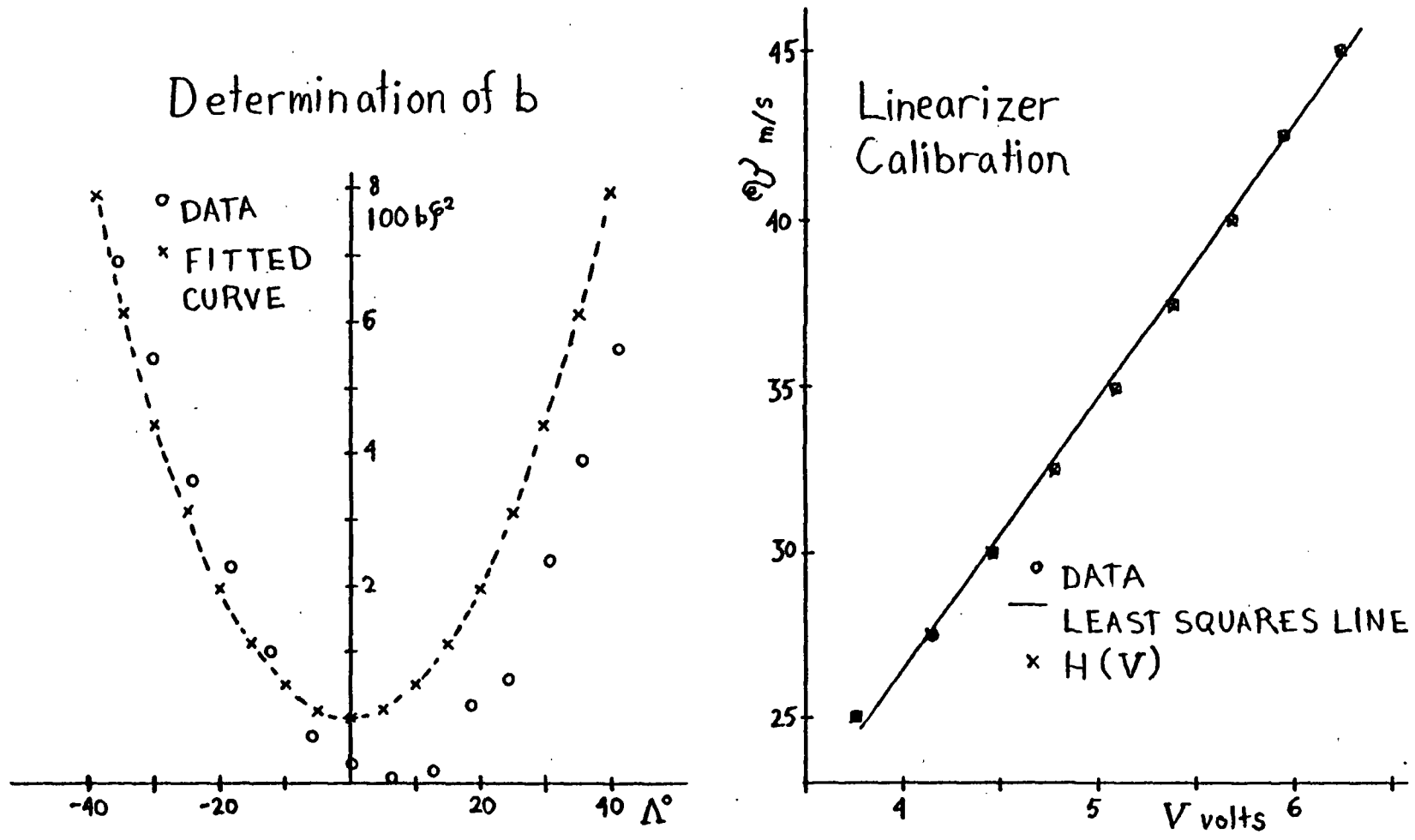

Fig. C - 4. Hot wire calibration, probe no. 1; rotation D and linearizer

Appendix D

COMPUTER PROGRAMS

D.1 PREDUCE

The FORTRAN listing for the cobra probe data reduction program, PREDUCE, appears below. PREDUCE asks the operator for the numbers:

RHO = air density

BORAD = nacelle radius at axial location of measurement

SURVEND = number of radial stations in survey.

In addition, the program requires the names of four files, which contain the transducer voltages corresponding to the left, center, and right ports of the probe. There are four files because, as explained in Section 4.4, the center pressures are recorded twice. PREDUCE reads the probe calibration data from separate files in steps 7200 to 8500. Here the matrices V and F contain the information displayed in Figures B-3 and B-4, respectively. The vector G represents the swirl calibration of Figure B-2. TU contains the tunnel stagnation pressures for the curves of Figures B-3 and B-4. The user must assign the appropriate logical units before running the program. PREDUCE writes the reduced data into several files in

steps 21,100 to 21,800. The quantities are:

RA = radial location of survey point

GRS = swirl angle, degrees

PSRS = static pressure referenced to the atmosphere

VAXS = axial velocity

VATS = tangential velocity

VAXFS = the axial velocity in the ultimate wake, deduced from the total pressure

CIRC = circulation

SMASS = mass flow

Again, the user must assign the indicated logical units prior to running.

D.2 HOTWIREV

The FORTRAN listing for the hot wire data reduction program, HOWIREV, appears below. HOTWIREV asks the user for quite a few numbers, defined below.

ISURVEND = number of radial stations in survey

AA = wire directional constant a

BB = wire directional constant b

T0 = wire angle θ_o

V0,L0,P0 = initial guesses for free stream velocity, in spherical coordinates $|\vec{v}|$,

Λ , Φ , with angles in degrees (steps 12,000 to 13,000)

ACC = accuracy parameter ϵ (step 25,100)

RMAX = operation parameter R_{max}

RMIN = operation parameter R_{min}

AS = initial step size for first survey point (step 26,000)

AS2 = initial step size for subsequent points (step 26,300)

The sixteen constants A(i), B(i), C(i), D(i), i = 1, 4 specify the behavior of the anemometer during the four traverses, and come directly from the anemometer equation (30) of Section 5.4:

$$A(i) = b(t_{2i} - t_{1i}) \qquad B(i) = B + bt_{1i}$$

$$C(i) = a(t_{2i} - t_{1i}) \qquad D(i) = A + at_{1i}$$

where t_{1i} is the tunnel temperature at the beginning of a traverse, and t_{2i} is the temperature at the end of a traverse. These constants may also be read from a separate file (step 13,200). As with PREDUCE, the operator must give the machine the names of four files (one for each traverse) that contains the linearizer voltages.

HOTWIREV computes the final values of the minimized

function Q, and writes Q for every tenth survey point into a file called ERRORS.DAT, along with the average value of Q for the entire survey.

Normally, when the computer asks, "Is this the first run?" the user answers "yes" by typing 1. In this case, the program requests the values of all the constants listed above. If the operator merely wishes to test the program, as described in Section 5.6, he answers "no" by typing 0 and the computer reads the various constants from files which were created during the previous run. The user may alter the operation parameters at step 23,600. Also, if large files of real data are being used for testing, the user can set IPREM to some integer less than ISURVEND. The computer will still read the data files completely, but it will only reduce the data for the first IPREM points. The number of iterations for each data point will be typed on the screen as the program works, if desired (step 3,500).

Certain important parameters are built into the program, but can be adjusted by editing. These are:

GMIN = minimum allowed value of $|\vec{\nabla}Q|$

LMIN = minimum allowed value of the coordinate Λ, in radians

NMAX = maximum number of iterations at a particular survey point.

If the number of iterations exceeds NMAX, the program issues a message, "BOMBOUT," writes any reduced data into a special file, and stops. In the usual case of normal termination, HOTWIREV writes the reduced data into a file called VELOC.DAT. The velocities in this file are in the spherical probe coordinates $|\vec{v}|$, Λ , and Φ .

If a future investigator wishes to use the author's hot wire technique, but has a probe with different directional behavior, he need make few changes as long as he adopts the author's coordinate systems. The empirical direction factor f enters only at steps 36,000 through 36,300, and at step 49,400. One may easily extend this program to deal with a larger number of wire rotations.

D.3 HOTPROC

HOTPROC, another FORTRAN program, "digests" the output of HOTWIREV by performing coordinate transformations, computing the mass flow, etc. The operator must assign the logical unit 1 to the appropriate VELOC file. HOTPROC requires some numbers like the other programs:

IPREM = number of survey points in VELOC

BETA = β = tilt angle of probe axis

BORAD = radius of nacelle at axial location of survey

BOMIN = minimum distance of probe from body surface

RHO = air density

At steps 7,200 and 7,600, the program offers to normalize the swirl angle, and asks for the number of averaging points ITAV. If the user invokes this feature, HOTPROC averages the swirl velocities over the first ITAV points of the survey (outside the slipstream), and subtracts this number from all the other swirl velocities in the wake. The program can also adjust the radial velocities so that the radial flow angle at the nacelle surface matches the known surface angle (STEPS 8,900, 9,300).

HOTPROC writes the processed data into several files at steps 12,300 through 14,000. The quantities are:

R = radial location of survey point

SMASS = mass flow

CIRCU = circulation

SWIRL = swirl angle

ANGRD = radial outflow angle

The user must assign the indicated logical units prior to running.

PROGRAM

PREDUCE

```
C     PROGRAM PREDUCE.
C     THIS PROGRAM CONVERTS THE RAW CCBRA PROBE DATA (FOUR
C     VOLTAGES PER SURVEY POINT) INTO VELOCITY,SWIRL ANGLE,
C     STATIC PRESSURE, CIRCULATION, MASS FLUX, AND VELOCITY
C     IN THE DEVELOPED WAKE (MINIMUM BODY ONLY).
C
        INTEGER*4 JSIZE,VERSION
        INTEGER*2 IDATA,IBUF
        CHARACTER NAME*6,LABEL*4,TABLE*8,EXPER*1,FILTYP*3,FRAC*2
     1  ,FNAM*16,BODY*1,BLADE*1,DATE*7,NAMP*1,SPCIAL*1,ANS*11
        DIMENSION IDATA(4,4096),param(7),ivzero(4),vnorm(4),begin(4),endit(4)
      DIMENSION V(11,13),F(11,13),G(13),TU(11),GRS(1024)
      DIMENSION PSRS(1024),VAXS(1024),VATS(1024),VAXFS(1024)
      DIMENSION CIRC(1024),SMASS(1024),RA(1024)
      DIMENSION VOL(1024),VOR(1024),VCC1(1024),VCC2(1024)
      INTEGER SURVEND
C
C     USER MUST GIVE MACHINE THE NAMES OF THE FOUR QUARTER
C     FILES IN PROPER ORDER (1,3,2,4).
C
        do 500, l=1,4
        type 100,l
100     format(' input filename ',i1)
        accept 110,name
110     format(a6)
        fnam=name//'.DT1'
C
C     READ FOUR FILES CONTAINING RAW DATA STORED AS INTEGERS.
C
        open (unit=11,name=fnam,recordsize=80,recordtype='fixed',TYPE='OLD')
        READ (11,155) name,date,nbook,npage,version,frac,exper,filtyp,
     1  blade,body,tangle,aangle,borien,(param(i),i=1,7),mike,namp,nasum
155     format(a6,a7,i1,i3,i1,a2,4a1,3F4.0,F5.0,2f5.1,F6.0,f5.3,f5.1,
     1  F4.0,F5.1,i1,a1,i3)
        READ(11,165)TRIG,ivz,ihz,vn,hn,begin,end,PROBE,AX
165     format(F6.2,2i4,2e10.2,2f7.2,A1,F6.1)
```

```
3700            IF(NAME(1:1).EQ.'A') N=4096
3800            IF (NAME(1:1).EQ.'H') N=2048
3900            IF(NAME(1:1).EQ.'C') N=1024
4000            ADUM=N/20
4100            K=JINT(ADUM)
4200            do 220 i=1,K
4300            READ (11,210)(idata(l,j+20*(i-1)),j=1,20)
4400    210     format(2014)
4500    220     continue
4600            m=mod(n,20)
4700            IF(M.EQ.0) go to 250
4800            READ (11,210)(idata(l,j+20*(i-1)),j=1,M)
4900    250     CLOSE(UNIT=11)
5000            IVZERO(L)=IVZ
5100            VNORM(L)=VN
5200            bgin(l)=begin
5300            endit(l)=end
5400    500     CONTINUE
5500    C
5600    C       LAKE SURVEY PARAMETERS
5700    C
5800            TYPE 410
5900    410     FORMAT(' INPUT RHO ')
6000            ACCEPT *,RHO
6100            TYPE 412



6200    412     FORMAT(' INPUT BORAD ')
6300            ACCEPT *,BORAD
6400            TYPE 414
6500    414     FORMAT(' INPUT SURVEND ')
6600            ACCEPT *,SURVEND
6700            NRAD=SURVEND
```

```
      NG=INT(NRAD/10.0)+1
C
C     READ CALIBRATION DATA FILES
C
      DO 65 I=1,11
      READ(3,66)(V(I,J),J=1,13)
66    FORMAT(13F7.1)
65    CONTINUE
      DO 67 I=1,11
      READ(4,68)(F(I,J),J=1,13)
68    FORMAT(13F6.1)
67    CONTINUE
      READ(8,70)(G(J),J=1,13)
70    FORMAT(13F5.1)
      DO 80 I=1,11
      READ(10,75)(TU(I))
75    FORMAT(F7.1)
80    CONTINUE
      do 998 jj=1,4
      if (ivzero(jj).gt.2047) ivzero(jj)=ivzero(jj)-4096
998   continue
      DO 1002 IRAD=1,SURVEND+10
C
C     CONVERT INTEGER DATA BACK TO ACTUAL VOLTAGES
C
      do 999 jj=1 , 4
      if (idata(jj,irad).gt.2047) idata(jj,irad)=idata(jj,irad)-4096
999   continue
      vel(irad)=(idata(1,irad)-ivzero(1))*vnorm(1)
      voc1(irad)=(idata(2,irad)-ivzero(2))*vnorm(2)
      vor(irad)=(idata(3,irad)-ivzero(3))*vnorm(3)
      voc2(irad)=(idata(4,irad)-ivzero(4))*vnorm(4)
1002  CONTINUE
C
C     FORCE TRANSDUCER ZEROS TO CONFORM TO KNOWN FREE
C     STREAM CONDITIONS.
```

```
10400   C
10500           VLZL=0
10600           DO 701 IE=1,10
10700           VLZL=VLZL+VOL(SURVEND-1+IE)
10800   701     CONTINUE
10900           VLZL=VLZL/10
11000           VLZR=0
11100           DO 702 IE=1,10
11200           VLZR=VLZR+VOR(SURVEND-1+IE)
11300   702     CONTINUE
11400           VLZR=VLZR/10
11500           VLZC1=0
11600           DO 703 IE=1,10
11700           VLZC1=VLZC1+VOC1(SURVEND-1+IE)
11800   703     CONTINUE
11900           VLZC1=VLZC1/10
12000           VLZC2=0
12100           DO 704 IE=1,10
12200           VLZC2=VLZC2+VOC2(SURVEND-1+IE)

12300   704     CONTINUE
12400           VLZC2=VLZC2/10
12500           ZEL=VLZL+0.047977
12600           ZER=VLZR+0.053042
12700           ZEC1=VLZC1+0.000543
12800           ZEC2=VLZC2+0.000543
12900   C
13000   C       DATA REDUCTION LOOP
13100   C
13200           DO 1001 IRAD=1,SURVEND
13300           PL=7902.32*(vol(irad)-ZEL)
13400           PC1=9217.87*(voc1(irad)-ZEC1)
```

```
13500           PC2=9207.87*(VOC2(irad)-ZEC2)
13600           PC=(PC1+PC2)/2
13700           PR=6692.75*(VOR(irad)-ZEP)
13800     C
13900     C     COMPUTE THEORETICAL SWIRL ANGLE,DYNAMIC PRESSURE.
14000     C
14100           IF(ABS(2*PC-PL-PR).LT.0.01) GO TO 301
14200           ARG=(PR-PL)/(2*PC-PL-PR)
14300           GAMT=28.6479*ATAN(ARG)
14400           VT=(2*PC-PL-PR)*SQRT(1+ARG*ARG)
14500           J=INT(GAMT/2)+3
14600           I=1
14700     5     IF(VT.LT.V(I,J)) GO TO 10
14800           I=I+1
14900           GO TO 5
15000     10    CONTINUE
15100           IF (I.EQ.1) GO TO 14
15200           K=I-1
15300           GO TO 15
15400     14    K=I
15500           I=I+1
15600     15    CONTINUE
15700           L=J+1
15800     C
15900     C     READ CALIBRATION CURVES,INTERPOLATE.
16000     C
16100           VL=V(K,J)+((GAMT/2)+3-J)*(V(K,L)-V(K,J))
16200           VH=V(I,J)+((GAMT/2)+3-J)*(V(I,L)-V(I,J))
16300           IF(ABS(VH-VL).LT.0.01) GO TO 301
16400           IF(ABS(TU(I)-TU(K)).LT.0.01) GO TO 301
16500           VR=TU(K)+(VT-VL)*(TU(I)-TU(K))/(VH-VL)
16600           GR=G(J)+((GAMT/2)+3-J)*(G(L)-G(J))
16700           FL=F(K,J)+((GAMT/2)+3-J)*(F(K,L)-F(K,J))
16800           FH=F(I,J)+((GAMT/2)+3-J)*(F(I,L)-F(I,J))
16900           FR=FL+(VR-TU(K))*(FH-FL)/(TU(I)-TU(K))
17000           PSF=521.4-0.5*VR+(PL+PR)/2+FR
```

```
17100    C
17200    C      CONVERT DYNAMIC PRESSURES INTO VELOCITIES.
17300    C
17400           VAX=SQRT(2*VR/RHO)*COS(0.0174533*GR)
17500           VAT=SQRT(2*VR/RHO)*SIN(0.0174533*GR)
17600           GO TO 302
17700    301    VAX=0.0
17800           VAT=0.0
17900           PSR=0.0
18000           GR=0.0
18100    302    CONTINUE
18200           VAXF=SQRT((PC+497.7)*2/RHO)
18300           GRS(IRAD)=GR

18400           PSRS(IRAD)=PSR
18500           VAXS(IRAD)=VAX
18600           VATS(IRAD)=VAT
18700           VAXFS(IRAD)=VAXF
18800           R=BORAD+0.000635*(IRAD-1)
18900           RA(IRAD)=R
19000    C
19100    C      COMPUTE CIRCULATION
19200    C
19300           CIRC(IRAD)=6.283185307*R*VATS(IRAD)
19400           IF(IRAD.EQ.1)GO TO 995
19500    C
19600    C      INTEGRATE TO FIND MASS FLUX
19700    C
19800           SMASS(IRAD)=SMASS(IRAD-1)+3.001994113*
19900          &(R-0.00.3175)*RHO*(VAXS(IRAD)+VAXS(IRAD-1))
20000           GO TO 996
20100    995    CONTINUE
```

```
20200           SMASS(IPAD)=0
20300    556    CONTINUE
20400    1001   CONTINUE
20500    C
20600    C      WRITE REDUCED DATA INTO FILES.
20700    C
20800           DO 1100 IQ=1,NG
20900           ML=10*IQ-9
21000           MH=10*IQ
21100           WRITE(12,104)(RA(MG),MG=ML,MH)
21200           WRITE(13,103)(GRS(MG),MG=ML,MH)
21300           WRITE(14,103)(PSPS(MG),MG=ML,MH)
21400           WRITE(15,103)(VAXS(MG),MG=ML,MH)
21500           WRITE(16,103)(VATS(MG),MG=ML,MH)
21600           WRITE(17,103)(VAXFS(MG),MG=ML,MH)
21700           WRITE(18,103)(CIRC(MG),MG=ML,MH)
21800           WRITE(19,104)(SMASS(MG),MG=ML,MH)
21900    103    FORMAT(10F8.2)
22000    104    FORMAT(10F8.4)
22100    1100   CONTINUE
22200           STOP
22300           END
```

PROGRAM

HOTWIREV

```
C
C
C     PROGRAM HOTWIREV.  THIS PROGRAM REDUCES SINGLE SENSOR
C     ROTATING HOT WIRE DATA INTO THREE VELOCITY COMPONENTS
C     IN SPHERICAL COORDINATES.
C
C
      REAL L,LMIN
      REAL LO,LO,LR,LRO
      INTEGER*4 JSIZE,VERSION
      INTEGER*2 IDATA,IBUF
      CHARACTER NAME*6,LABEL*4,TABLE*8,EXPER*1,FILTYP*3,
     6FRAC*2,FNAM*10,BODY*1,BLADE*1,DATE*7,MAPP*1,SPCIAL*1,ANS*11
      DIMENSION IDATA(4,4096),PARAM(7),IVZERO(4),VNORM(4),RGIN(4)
     6,ENDIT(4),VOL(1024),VOC1(1024),VOR(1024),VOC2(1024),
     6VCLT(500,4),A(4),B(4),C(4),D(4),FV(4),P(4),CP(4),SP(4),
     6CT(4),T(4),ST(4),SH(4),H(4),CH(4),DTDP(4),DTDL(4),DHDP(4),
     6DHDL(4),FV(4),DDV(4),DDL(4),DDP(4),DELTA(4),V(7),L(7),PT(7),
     6PTT(7),C(7),VR(500),LR(500),PR(500),VRO(500),LRO(500),
     6PRO(500),X(7),Y(7),Z(7)
      DIMENSION QE(51)
C
17    FORMAT(E13.6)
18    FORMAT(3F10.5)
19    FORMAT(4E13.6)
20    FORMAT(I4)
21    FORMAT(5F10.5)
22    FORMAT(3E13.6)
      TYPE 40
C
      TYPE 10
10    FORMAT(' IS THIS THE FIRST RUN? YES=1,NO=0')
      ACCEPT *,IANSW
      TYPE 11
11    FORMAT(' TYPE NUMBER OF ITERATIONS? YES=1,NO=0')
      ACCEPT *,NITER
```

```
3700          IF(IANSW.EQ.0) GO TO 50
3800    C
3900    C
4000          TYPE 245
4100    245   FORMAT(' INPUT ISURVEND')
4200          ACCEPT *,ISURVEND
4300          OPEN(UNIT=19,NAME='ISURVEND.DAT',TYPE='NEW')
4400          WRITE(19,20) ISURVEND
4500          CLOSE(UNIT=19,DISPOSE='SAVE')
4600    C
4700    C
4800    C     USER MUST GIVE MACHINE THE NAMES OF THE FOUR QUARTER
4900    C     FILES IN PROPER ORDER (1,3,2,4).
5000    C
5100            do 50, LY=1,4
5200            TYPE 100,LY
5300    100     format(' input filename ',i1)
5400            accept 110,name
5500    110     format(a6)
5600            fnam=name//'.DT1'
5700    C
5800    C
5900    C     READ FOUR FILES CONTAINING RAW DATA STORED AS INTEGERS.
6000    C
6100            open (unit=11,name=fnam,recordsize=64,recordtype='fixed',TYPE='OLD')




6200            READ (11,155) name,date,nbock,npage,version,frac,exper,filtyp,
6300          1 blace,body,bangle,aangle,terien,(param(i),i=1,7),mike,namp,nasum
6400    155     format(a6,a7,i1,i3,i1,a2,4a1,2F4.0,F5.0,2i5.1,F6.0,f5.3,f5.1,
6500          1 F4.0,F5.1,i1,a1,i3)
6600            READ(11,165)TRIG,ivz,ihz,vn,hn,begin,end,PROBE,AX
6700    165     format(F6.2,2i4,2e10.2,2i7.2,A1,F6.1)
```

```
6800            IF(NAME(1:1).EQ.'A') N=4096
6900            IF (NAME(1:1).EQ.'H') N=2048
7000            IF(NAME(1:1).EQ.'O') N=1024
7100            ADUM=N/20
7200            K=JINT(ADUM)
7300            do 220 i=1,K
7400            READ (11,210)(idata(LY,j+20*(i-1)),j=1,20)
7500    210     format(20i4)
7600    220     continue
7700            m=mod(n,20)
7800            IF(M.EQ.0) go to 250
7900            READ (11,210)(idata(LY,j+20*(i-1)),j=1,M)
8000    250     CLOSE(UNIT=11)
8100            IVZERO(LY)=IVZ
8200            VNORM(LY)=VN
8300            bgin(LY)=begin
8400            endit(LY)=end
8500    500     CONTINUE
8600    C
8700            DO 1002,IRAD=1,ISURVEND
8800    C
8900    C       CONVERT INTEGER DATA BACK TO ACTUAL VOLTAGES
9000    C
9100            do 999 jj=1 , 4
9200            if (idata(jj,irad).gt.2047) idata(jj,irad)=idata(jj,irad)-4096
9300    999     continue
9400            vol(irad)=(idata(1,irad)-ivzero(1))*vnorm(1)
9500            voc1(irad)=(idata(2,irad)-ivzero(2))*vnorm(2)
9600            vor(irad)=(idata(3,irad)-ivzero(3))*vnorm(3)
9700            voc2(irad)=(idata(4,irad)-ivzero(4))*vnorm(4)
9800    1002    CONTINUE
9900    C
10000   C       REVERSE ORDER OF VOLTAGES
10100   C
10200           DO 215 I=1,ISURVEND
10300           VOLT(I,1)=VOL(ISURVEND+1-I)
```

```
10400           VOLT(I,2)=VOC1(ISURVEND+1-I)
10500           VOLT(I,3)=VCR(ISURVEND+1-I)
10600           VOLT(I,4)=VOC2(ISURVEND+1-I)
10700     215   CONTINUE
10800     C
10900     C     REMEMBER VOLTAGES
11000     C
11100           OPEN(UNIT=13,NAME='VOLT.DAT',TYPE='NEW')
11200           DO 221 I=1,ISURVEND
11300           WRITE(13,19) (VOLT(I,J),J=1,4)
11400     221   CONTINUE
11500           CLOSE(UNIT=13,DISPOSE='SAVE')
11600     C
11700     C     INPUT TRIAL VELOCITY VECTOR IN SPHERICAL COORDINATES,
11800     C     ANGLES IN DEGREES
11900     C
12000           TYPE 15
12100     15    FORMAT(' INPUT GUESS FOR V')
12200           ACCEPT *,V0



12300           TYPE 26
12400     26    FORMAT(' INPUT GUESS FOR LAMBDA')
12500           ACCEPT *,L0
12600           L0=0.0174532925*L0
12700           TYPE 25
12800     25    FORMAT(' INPUT GUESS FOR PHI')
12900           ACCEPT *,P0
13000           P0=P0*0.0174532925
13100           TYPE 31
13200     31    FORMAT(' CONSTANTS ALREADY ON FILE? YES=1,NO=0')
13300           ACCEPT *,ICON
13400           IF(ICON.EQ.1) GO TO 32
```

```
C
C     INPUT ANEMOMETER CONSTANTS IN F FORMAT
C
      TYPE 30
30    FORMAT(' INPUT ESTIMATES OF A(1) THRU A(4).
     6  CR AFTER EACH ENTRY.')
      ACCEPT 17, A(1)
      ACCEPT 17, A(2)
      ACCEPT 17, A(3)
      ACCEPT 17, A(4)
      TYPE 35
35    FORMAT(' INPUT ESTIMATES OF B(1) THRU B(4)')
      ACCEPT 17, B(1)
      ACCEPT 17, B(2)
      ACCEPT 17, B(3)
      ACCEPT 17, B(4)
      TYPE 40
40    FORMAT(' INPUT ESTIMATES OF C(1) THRU C(4)')
      ACCEPT 17, C(1)
      ACCEPT 17, C(2)
      ACCEPT 17, C(3)
      ACCEPT 17, C(4)
      TYPE 45
45    FORMAT(' INPUT ESTIMATES OF D(1) THRU D(4)')
      ACCEPT 17, D(1)
      ACCEPT 17, D(2)
      ACCEPT 17, D(3)
      ACCEPT 17, D(4)
      GO TO 33
32    CONTINUE
      READ(41,19) (A(I),I=1,4)
      READ(41,19) (B(I),I=1,4)
      READ(41,19) (C(I),I=1,4)
      READ(41,19) (D(I),I=1,4)
33    CONTINUE
C
```

```
17100   C       INPUT WIRE CONSTANTS, SLANT ANGLE
17200   C
17300           TYPE 255
17400   255     FORMAT(' INPUT AA')
17500           ACCEPT *,AA
17600           TYPE 265
17700   265     FORMAT(' INPUT BB')
17800           ACCEPT *,BB
17900           TYPE 265
18000   265     FORMAT(' INPUT WIRE ANGLE')
18100           ACCEPT *,TO
18200           TO=TO*0.0174532925
18300   C
18400   C       REMEMBER ALL CONSTANTS
18500   C
18600           OPEN(UNIT=11,NAME='CONSTANTS.DAT',TYPE='NEW')
18700           WRITE(11,19) A(1),A(2),A(3),A(4)
18800           WRITE(11,19) B(1),B(2),B(3),B(4)
18900           WRITE(11,19) C(1),C(2),C(3),C(4)
19000           WRITE(11,19) D(1),D(2),D(3),D(4)
19100           CLOSE(UNIT=11,DISPOSE='SAVE')
19200           OPEN(UNIT=22,NAME='WIRE.DAT',TYPE='NEW')
19300           WRITE(22,22) AA,BB,TO
19400           CLOSE(UNIT=22,DISPOSE='SAVE')
19500   C
19600           GO TO 55
19700   C
19800   C
19900   50      CONTINUE
20000   C
20100   C       GATHER ALL NEEDED INFORMATION IF THIS IS A REPEAT RUN
```

```
C
      OPEN(UNIT=14,NAME='ISURVEND.DAT',TYPE='OLD')
      READ(14,20) ISURVEND
      CLOSE(UNIT=14)
      TYPE 421
420   FORMAT(' INPUT GUESS FOR V')
      ACCEPT *,V0
      TYPE 421
421   FORMAT(' INPUT GUESS FOR LAMBDA')
      ACCEPT *,L0
      L0=L0*0.0174532925
      TYPE 422
422   FORMAT(' INPUT GUESS FOR PHI')
      ACCEPT *,P0
      P0=P0*0.0174532925
      OPEN(UNIT=16,NAME='WIRE.DAT',TYPE='OLD')
      OPEN(UNIT=21,NAME='CONSTANTS.DAT',TYPE='OLD')
      READ(16,22) AA,BB,T0
      READ(21,19) A(1),A(2),A(3),A(4)
      READ(21,19) B(1),B(2),B(3),B(4)
      READ(21,19) C(1),C(2),C(3),C(4)
      READ(21,19) D(1),D(2),D(3),D(4)
      CLOSE(UNIT=16)
      CLOSE(UNIT=21)
      OPEN(UNIT=17,NAME='VOLT.DAT',TYPE='OLD')
C
C
      DO 225 I=1,ISURVEND
      READ(17,19) (VOLT(I,J),J=1,4)
225   CONTINUE
      CLOSE(UNIT=17)
C
C     CHANGE OPERATION PARAMETERS, IF DESIRED, FOR REPEAT RUN
C
      TYPE 251
251   FORMAT(' DO YOU WANT TO CHANGE OPERATION PARAMETERS?
```

```
23800         6  YES=1,NO=0')
23900          ACCEPT *,IANSW2
24000          IF(IANSW2.EQ.1) GO TO 55
24100          OPEN(UNIT=15,NAME='PARAM.DAT',TYPE='OLD')
24200          READ(15,21) ACC,RMAX,RMIN,AS,AS2
24300          CLOSE(UNIT=15)
24400          GO TO 84



24500    C
24600    55    CONTINUE
24700    C
24800    C     SET OPERATION PARAMETERS FOR FIRST RUN
24900    C
25000          TYPE 60
25100    60    FORMAT(' INPUT ACCURACY')
25200          ACCEPT *,ACC
25300          TYPE 70
25400    70    FORMAT(' INPUT RMAX')
25500          ACCEPT *,RMAX
25600          TYPE 75
25700    75    FORMAT(' INPUT RMIN')
25800          ACCEPT *,RMIN
25900          TYPE 80
26000    80    FORMAT(' INPUT FIRST AS')
26100          ACCEPT *,AS
26200          TYPE 81
26300    81    FORMAT(' INPUT SECOND AS')
26400          ACCEPT *,AS2
26500    C
26600    C     REMEMBER OPERATION PARAMETERS
26700    C
26800          OPEN(UNIT=20,NAME='PARAM.DAT',TYPE='NEW')
```

```
26900           WRITE(20,21) ACC,RMAX,RMIN,AS,AS2
27000           CLOSE(UNIT=20,DISPOSE='SAVE')
27100     84    CONTINUE
27200           CTO=COS(TO)
27300           STO=SIN(TO)
27400           NMAX=40
27500           GERR=0
27600           IRAD=1
27700           TYPE 758
27800     C
27900     C     INPUT SMALLER NUMBER OF POINTS. IPREM.LE.ISURVEND
28000     C
28100     758   FORMAT(' INPUT IPREM')
28200           ACCEPT *,IPREM
28300           GMIN=0.00000001
28400           LMIN=0.0045
28500     C
28600           DO 300 I=1,ISURVEND
28700           VR(I)=0
28800           LR(I)=0
28900           FR(I)=0
29000     300   CONTINUE
29100     C
29200     C     MAIN COMPUTATIONAL LOOP
29300     C
29400     85    CONTINUE
29500     C
29600     C     COMPUTE EFFECTIVE VELOCITIES FROM VOLTAGES
29700     C
29800           DO 240 J=1,4
29900           VOLTMAX=D(J)+C(J)*(ISURVEND+1-IRAD)/ISURVEND
30000          6+(A(J)*(ISURVEND+1-IRAD)/ISURVEND+B(J))*29.5
30100           IF(VOLT(IRAD,J).GE.VOLTMAX) GO TO 196
30200           FV(J)=(VOLT(IRAD,J)-C(J)*((ISURVEND+1-IRAD)/ISURVEND)-D(J))/
30300          6(A(J)*((ISURVEND+1-IRAD)/ISURVEND)+B(J))
30400           GO TO 197
```

```
30500   106   CONTINUE



30600   C
30700   C     LINEARIZER CURVATURE CORRECTION
30800   C
30900         EV(J)=29.5+(VOLT(IRAD,J)-VOLTMAX)*1.22/
31000        6(A(J)*(ISURVEND+1-IRAD)/ISURVEND+B(J))
31100   107   CONTINUE
31200   240   CONTINUE
31300   C
31400         N=0
31500   C
31600   C     INNER COMPUTATIONAL LOOP. ITERATE TO FIND VECTOR
31700   C
31800   90    CONTINUE
31900   C
32000   C
32100         N=N+1
32200   C
32300   C
32400         SL=SIN(LO)
32500         CL=COS(LO)
32600   C
32700   C     FIND SPHERICAL ROOM COORDINATES OF TRIAL VECTOR FOR THE
32800   C     FOUR WIRE ROTATIONS
32900   C
33000         DO 95 I=1,4
33100         P(I)=PO-(I-1)*1.570796327
33200         PZ=P(I)
33300         CP(I)=COS(PZ)
33400         SP(I)=SIN(PZ)
33500   95    CONTINUE
```

```
33600    C
33700    C      TRANSFORM TO AUXILLIARY COORDINATES
33800    C
33900           DO 101 I=1,4
34000           CT(I)=STO*CL+CTO*SL*SP(I)
34100           T(I)=ACOS(CT(I))
34200           ST(I)=SIN(T(I))
34300           SH(I)=SL*CP(I)/ST(I)
34400           H(I)=ASIN(SH(I))
34500           CH(I)=COS(H(I))
34600    101    CONTINUE
34700    C
34800    C      COMPUTE ANGULAR DERIVATIVES
34900    C
35000           DO 105 I=1,4
35100           DTDP(I)=-CTO*SL*CP(I)/ST(I)
35200           DTDL(I)=(STO*SL-CTO*CL*SP(I))/ST(I)
35300           DHDP(I)=-(SL*SP(I)+SH(I)*CT(I)*DTDP(I))/(CH(I)*ST(I))
35400           DHDL(I)=(CL*CP(I)-SH(I)*CT(I)*DTDL(I))/(CH(I)*ST(I))
35500    105    CONTINUE
35600    C
35700    C      COMPUTE DELTA DERIVATIVES
35800    C
35900           DO 111 I=1,4
36000           FV(I)=VO*(AA+BB*H(I)*H(I))
36100           DCV(I)=(AA+BB*H(I)*H(I))*ST(I)
36200           DDL(I)=VO*ST(I)*2*BB*H(I)*DHDL(I)+FV(I)*CT(I)*DTDL(I)
36300           DDP(I)=VO*ST(I)*2*BB*H(I)*DHDP(I)+FV(I)*CT(I)*DTDP(I)
36400           DELTA(I)=FV(I)*ST(I)-EV(I)
36500    111    CONTINUE
36600    C
```

```
C
      DGV=0
      DGL=0
      DGP=0
C
C     COMPUTE DERIVATIVES OF G
C
      DO 115 I=1,4
      DGV=DGV+2*(DELTA(I)*DDV(I))
      DGL=DGL+2*(DELTA(I)*DDL(I))
      DGP=DGP+2*(DELTA(I)*DDP(I))
115   CONTINUE
C
C
      CGL=DGL/V0
      CGP=DGP/(VC*SL)
C
C     FIND MAGNITUDE OF GRADIENT
C
      GMAG=SQRT(DGV**2+CGL**2+CGP**2)
C
C     IF GRADIENT VERY SMALL, GO TO NEXT POINT IN SURVEY
C
      IF(GMAG.LT.GMIN) GO TO 120
C
C     COMPONENTS OF GRADIENT OF G, NORMALIZED
C
      GRV=DGV/GMAG
      GRL=CGL/GMAG
      GRP=CGP/GMAG
C
C     GRADIENT TRANSFORMED TO CARTESIAN COORDINATES
C
      GRZN=GRV*CL-GRL*SL
      GRXN=GRV*SL*CP(1)+GRL*CL*CP(1)-GRP*SP(1)
      GRYN=GRV*SL*SP(1)+GRL*CL*SP(1)+GRP*CP(1)
```

```
40300   C
40400           IF(N.EQ.1) GO TO 230
40500   C
40600   C       FIND Z (ZQ), AND ADJUST STEPSIZE (AS)
40700   C
40800           ZX=(GRXN-GRXO)/2
40900           ZY=(GRYN-GRYO)/2
41000           ZZ=(GRZN-GRZO)/2
41100           ZG=SQRT(ZX**2+ZY**2+ZZ**2)
41200           R=ZQ*(RMAX-RMIN)+RMIN
41300           AS=AS/R
41400   C
41500   230     CONTINUE
41600   C
41700           GRXO=GRXN
41800           GRYO=GRYN
41900           GRZO=GRZN
42000   C
42100   C
42200   C
42300   C       VARIOUS CALCULATIONS FOR ACCURACY TEST, INCLUDING ANTI-
42400   C       CRASH PRECAUTIONS AND TRANSFORMATION OF TRIAL VECTOR TO
42500   C       CARTESIAN COORDINATES
42600   C
42700           XNEW=VO*CP(1)*SL-GRXN*AS

42800           YNEW=VO*SP(1)*SL-GRYN*AS
42900           ZNEW=VO*CL-GRZN*AS
43000           RNEW=SQRT(XNEW**2+YNEW**2+ZNEW**2)
43100           LO=ACOS(ZNEW/RNEW)
43200           ITESTL=
43300           IF(LO.LT.LMIN) ITESTL=1
```

```
      IF(ITESTL.EQ.1) PO=PO+2.34160491
      IF(ITESTL.EQ.1) LO=LMIN
      IF(ITESTL.EQ.1) GO TO 121
      SNLO=SIN(LO)
      CHECK=XNEW/(RNEW*SNLO)
      IF(CHECK.GT.0.999999) APO=0.002
      IF(CHECK.GT.0.999999) GO TO 1005
      APO=ACOS(XNEW/(RNEW*SNLO))
1005  CONTINUE
      IF(YNEW.GE.0) PO=APO
      IF(YNEW.LT.0) PO=-APO
121   CONTINUE
      VO=RNEW
C
C
C
C     ACCURACY TEST
C
      CRIT=SQRT((GRXN*AS)**2+(GRYN*AS)**2+(GRZN*AS)**2)/RNEW
      IF(CRIT.LE.ACC) GO TO 120
C
C     STOP IF TOO MANY ITERATIONS
C
      IF(N.GE.NMAX) GO TO 205
C
C     RETURN TO BEGINNING OF ITERATION LOOP IF NOT ACCURATE
C     ENOUGH
C
      GO TO 9
C
C
120   CONTINUE
      IF (NITER.EQ.1) THEN
      TYPE 123,N
123   FORMAT(' NUMBER OF ITERATIONS= ',I3)
      ENDIF
```

```
47000    C
47100    C      FIND ACTUAL VALUE OF G AT THE MINIMUM
47200    C
47300    C
47400           I=1
47500           V(I)=V0
47600           L(I)=L0
47700           PT(I)=P0
47800    C
47900           G(I)=0
48000    C
48100           SL=SIN(L(I))
48200           CL=COS(L(I))
48300           DO 135 J=1,4
48400           PTT(J)=PT(I)-(J-1)*1.570796327
48500           CP(J)=COS(PTT(J))
48600           SP(J)=SIN(PTT(J))
48700    135    CONTINUE
48800    C
```



```
48900    C
49000           DO 140 J=1,4
49100           T(J)=ACOS(ST0*CL*CT0*SL*SP(J))
49200           ST(J)=SIN(T(J))
49300           H(J)=ASIN(SL*CP(J)/ST(J))
49400           DELTA(J)=V(I)*(AA+BB*H(J)*H(J))*ST(J)-EV(J)
49500    140    CONTINUE
49600    C
49700    C
49800           DO 145 J=1,4
49900           G(I)=G(I)+(DELTA(J))**2
50000    145    CONTINUE
```

```
C
C
      VR(IRAD)=VC
      LR(IRAD)=LC
      PR(IRAD)=PC
C
C
      GERR=GERR+G(1)
      IGE=INT(IRAD/10.0+0.05)
      IF(ABS(IRAD/10.0-IGE). T.0I02) GE(IGE)=G(1)
C
      IRAD=IRAD+1
C
C     RETURN TO BEGINNING OF MAIN LOOP TO WORK ON NEXT SURVEY
C     POINT, IF ANY. RESET STEP SIZE. USE VELOCITY VECTOR
C     JUST COMPUTED AS THE BEGINNING TRIAL VECTOR FOR NEW
C     ITERATION
C
      IF(IRAD.LE.ISURVEND) AS=AS2
      IF(IRAD.GE.IPREM+1) GO TO 756
      IF(IRAD.LE.ISURVEND) GO TO 85
756   CONTINUE
C
C
      TYPE 180
180   FORMAT(' NORMAL TERMINATION. VECTOR (V,L,P) IS IN
     6 VELOC.DAT WITH FORMAT 3F10.5.')
C
C
      AGERR=GERR/IPREM
C
C     WRITE ERRORS (VALUES OF G EVERY 10 SURVEY POINTS) INTO
C     FILE
C
      OPEN(UNIT=12,NAME='ERRORS.DAT',TYPE='NEW')
      WRITE(12,19) AVERV,AVERL,AVERP,AGERR
```

```
      IGEMAX=INT(IPREM/10.0+0.05)
      NG=INT(IGEMAX/6.0+0.05)
910   FORMAT(6E13.6)
      DO 915 IG=1,NG
      ML=6*IG-5
      MH=6*IG
      WRITE(12,910) (QE(MQ),MQ=ML,MH)
915   CONTINUE
      IF(NG*6.EQ.IGEMAX) GO TO 920
      WRITE(12,910) (QE(MQ),MQ=NG*6+1,IGEMAX)
920   CONTINUE
      CLOSE(UNIT=12,DISPOSE='SAVE')
C
```

```
C     WRITE FINAL RESULTS FOR SURVEY INTO VELOCITY FILE
C
      OPEN(UNIT=10,NAME='VELOC.DAT',TYPE='NEW')
      DO 195 I=1,ISURVEND
      LR(I)=LR(I)*57.29577951
      PR(I)=PR(I)*57.29577951
      WRITE(10,18) VR(I),LR(I),PR(I)
195   CONTINUE
      CLOSE(UNIT=10,DISPOSE='SAVE')
C
C
      GO TO 210
C
C
250   CONTINUE
C
C     ISSUE RUNBOUT MESSAGE. RECORD ANY RESULTS
C
```

```
56800          TYPE 211
56900    211   FORMAT(' BOMBCUT.  N HAS EXCEEDED NMAX.  VELOCITIES
57000         6 (IF ANY) ARE WRITTEN IN A FILE CALLED VFAIL.DAT.
57100         6  THE FORMAT OF EACH LINE IS 3F10.5.')
57200          OPEN(UNIT=23,NAME='VFAIL.DAT',TYPE='NEW')
57300          DO 305 I=1,ISURVEND
57400          WRITE(23,18) VR(I),LR(I),PR(I)
57500    305   CONTINUE
57600          CLOSE(UNIT=23,DISPOSE='SAVE')
57700    C
57800    C
57900    200   CONTINUE
58000    C
58100    C
58200          STOP
58300          END
```

```
C
C
C     PROGRAM HOTPROC.  THIS PROGRAM PROCESSES THE OUTPUT OF
C     HOTWIREV.  ITS OUTPUTS ARE THE CARTESIAN VELOCITY COM-
C     PONENTS, THE RADIAL POSITIONS OF THE DATA POINTS, THE
C     MASS FLOW, CIRCULATION, AND THE SWIRL AND RADIAL OUTFLOW
C     ANGLES IN DEGREES.
C
C
      DIMENSION VELOCV(500),VELOCL(500),VELOCP(500),
     &ELOCV(500),ELOCL(500),ELOCP(500),V(500,3)
      DIMENSION R(500),SMASS(500),CIRCU(500),SWIRL(500),
     &ANGRD(500)
C
C
      TYPE 10
10    FORMAT(' INPUT IPREM')
      ACCEPT *,IPREM
C
      TYPE 15
15    FORMAT(' INPUT BETA IN DEGREES')
      ACCEPT *,BETA
      BETA=BETA*0.0174532925
C
      TYPE 20
20    FORMAT(' INPUT BORAD')
      ACCEPT *,BORAD
C
      TYPE 25
25    FORMAT(' INPUT MINIMUM DISTANCE FROM BODY')
      ACCEPT *,BOMIN
C
      TYPE 51
51    FORMAT(' INPUT RHO')
      ACCEPT *,RHO
C
```

Preceding page blank

```
      35    FORMAT(3F10.5)
            DO 30 I=1,IPREM
            READ(1,35) VELOCV(I),VELOCL(I),VELOCP(I)
            VELOCL(I)=VELOCL(I)*0.0174532925
            VELOCP(I)=VELOCP(I)*0.0174532925
      30    CONTINUE
C
C     REVERSE ORDER OF RADIAL STATIONS SO THAT FIRST
C     STATION IS NEAREST THE NACELLE
C
            DO 40 I=1,IPREM
            ELOCV(I)=VELOCV(IPREM+1-I)
            ELOCL(I)=VELOCL(IPREM+1-I)
            ELOCP(I)=VELOCP(IPREM+1-I)
      40    CONTINUE
C
            CB=COS(BETA)
            SB=SIN(BETA)
C
C     TRANSFORM TO CARTESIAN COORDINATES
C
            DO 45 I=1,IPREM
            SL=SIN(ELOCL(I))
            V1=ELOCV(I)*SL*COS(ELOCP(I))
            V2=ELOCV(I)*SL*SIN(ELOCP(I))



            V3=ELOCV(I)*COS(ELOCL(I))
            V(I,1)=V1
            V(I,2)=V3*SB-V2*CB
            V(I,3)=V2*SB+V3*CB
            R(I)=BGRAD+BOMIN+(I-1)*0.000635
            IF(I.EQ.1) GO TO 5
```

```
5805    C
5810    C       FIND MASS FLOW BY TRAPEZOIDAL INTEGRATION
5815    C
5900            SMASS(I)=SMASS(I-1)+3.0019949113*RHO*
6000           6(R(I)-0.0003175)*(V(I,3)+V(I-1,3))
6100            GO TO 55
6200    50      CONTINUE
6205    C
6210    C       MASS FLOW AT FIRST RADIAL STATION ASSUMES UNIFORM
6215    C       VELOCITY FROM BODY SURFACE TO FIRST STATION.
6220    C       VALUE OF VELOCITY IS THAT AT FIRST STATION.
6225    C
6300            SMASS(I)=3.141592654*((BORAD+BCMIN)**2-BORAD**2)
6400           6*V(I,3)
6500    C
6600    55      CONTINUE
6700    C
6800    C
6900    45      CONTINUE
7000    C
7005    C       OPTIONAL NORMALIZATION OF SWIRL AND RADIAL COMPONENTS
7010    C
7100            TYPE 100
7200    100     FORMAT(' NORMALIZE SWIRL ANGLE? YES=1,NO=0')
7300            ACCEPT *,IANS3
7400            IF(IANS3.EQ.0) GO TO 105
7500            TYPE 110
7600    110     FORMAT(' INPUT NUMBER OF POINTS FOR AVERAGE')
7700            ACCEPT *,ITAV
7800            VISUM=0
7900            DO 115 I=1,ITAV
8000            VISUM=VISUM+V(IPREM-ITAV+I,1)
8100    115     CONTINUE
8200            VISUM=VISUM/ITAV
8300            DO 120 I=1,IPREM
8400            V(I,1)=V(I,1)-VISUM
```

```
 8500    120   CONTINUE
 8600    105   CONTINUE
 8700    C
 8800          TYPE 125
 8900    125   FORMAT(' NORMALIZE RADIAL ANGLE? YES=1,NO=0')
 9000          ACCEPT *,IANS4
 9100          IF(IANS4.EQ.0) GO TO 130
 9200          TYPE 135
 9300    135   FORMAT(' INPUT BODY SURFACE ANGLE')
 9400          ACCEPT *,BANGL
 9500          V2FORC=TAN(0.0174532925*BANGL)*V(1,3)
 9600          V2CORR=V2FORC-V(1,2)
 9700          DO 140 I=1,IPREM
 9800          V(I,2)=V(I,2)+V2CORR
 9900    140   CONTINUE
10000    130   CONTINUE
10100    C
10105    C     COMPUTE CIRCULATION, SWIRL AND RADIAL OUTFLOW ANGLES
10110    C
```



```
10200          DO 46 I=1,IPREM
10300          CIRCU(I)=6.28318530?*R(I)*V(I,1)
10400          SWIRL(I)=57.2957795?*ATAN(V(I,1)/V(I,3))
10500          ANGRD(I)=57.2957795?*ATAN(V(I,2)/V(I,3))
10600    46    CONTINUE
10700    C
10800    61    FORMAT(8F10.5)
10900    65    FORMAT(6F10.5)
11000    C
11005    C     WRITE PROCESSED DATA INTO FILES. V=VELOCITY VECTOR
11010    C     (TANGENTIAL,RADIAL,AXIAL).  SMASS=MASS FLOW.
11015    C     CIRCU=CIRCULATION.  SWIRL=SWIRL ANGLE,DEGREES.
```

```
11020    C      ANGRD=RADIAL OUTFLOW ANGLE,DEGREES.
11025    C
11100           NG=INT(IPREM/8.0+0.05)
11200           NR=INT(IPREM/2.0+0.05)
11300    C
11400           DO 70 IR=1,NR
11500           WRITE(2,65) V(IR*2-1,1),V(IR*2-1,2),V(IR*2-1,3),
11600          6V(IR*2,1),V(IR*2,2),V(IR*2,3)
11700    70     CONTINUE
11800           IF(NR*2.EQ.IPREM) GO TO 75
11900           WRITE(2,65) V(IPREM,1),V(IPREM,2),V(IPREM,3)
12000    75     CONTINUE
12100    C
12200    C
12300           DO 80 IG=1,NG
12400           ML=8*IG-7
12500           MH=8*IG
12600           WRITE(3,60) (R(MG),MG=ML,MH)
12700           WRITE(4,60) (SMASS(MG),MG=ML,MH)
12800           WRITE(5,60) (CIRCU(MG),MG=ML,MH)
12900           WRITE(6,60) (SWIRL(MG),MG=ML,MH)
13000           WRITE(7,60) (ANGRD(MG),MG=ML,MH)
13100    80     CONTINUE
13200    C
13300    C
13400           IF(NG*8.EQ.IPREM) GO TO 85
13500           WRITE(3,60) (R(MG),MG=NG*8+1,IPREM)
13600           WRITE(4,60) (SMASS(MG),MG=NG*8+1,IPREM)
13700           WRITE(5,60) (CIRCU(MG),MG=NG*8+1,IPREM)
13800           WRITE(6,60) (SWIRL(MG),MG=NG*8+1,IPREM)
13900           WRITE(7,60) (ANGRD(MG),MG=NG*8+1,IPREM)
14000    85     CONTINUE
14100    C
14200    C
14300           STOP
14400           END
```

Appendix E

ERROR ANALYSIS

Here we perform a simple error analysis to get a rough idea of the reliability of the data. We don't have repeated experiments, so we cannot use a rigorous statistical approach. Instead, we add up the estimated errors from various sources. The author cannot offer an intelligent assessment of the uncertainty in the cobra probe data, and therefore does not consider this data here.

D.1 Hot Wire Data

Several types of error are present in the rotating hot wire data:

1) Speed calibration inaccuracies

2) Imperfect linearization

3) Directional calibration error

4) Incorrect time averaging

5) Nonlinear dependence of tunnel temperature on time.

We cannot, unfortunately, estimate the errors from all of these sources directly. The speed calibrations contain

three uncertainties: voltage reading, tunnel speed, and temperature reading errors. Only the first of these is known. The linearized anemometer voltages may be read to within at least 1/2%. The linearizer, whose output we show in Figure C-4, produces a signal that deviates less than 1% from the least squares line. The directional calibration error consists mainly of the difference between the actual wire behavior and the function we fit to the directional calibration data. While we do know this difference, no simple correlation exists between it and the errors in the reduced wake survey data. The time-averaged effective velocities do not quite pertain to the true time-averaged velocities because the wire cooling is a nonlinear function of angle. Finally, we correct the linearizer for changes in ambient temperature by assuming the temperature of the tunnel rises linearly with time, but we do not really know the time dependence.

Recall that we have redundant data for the hot wire surveys (four effective velocities to determine three velocities at each field point), and that we find the velocity vector $\vec{v}$ by minimizing a sum of squares of errors, Q ((29) of Section 5.4). The last four types of uncertainty listed above manifest themselves, at least in part, as a positive minimum value of Q. Errors in speed calibration alone, even if they are large, cannot affect Q because they influence the four effective velocities in

exactly the same linear way. The magnitude of the apparent velocity $\vec{v}$ is affected, but its direction is not and the redundant voltages remain compatible. Thus, we use Q to assess the error in the direction of $\vec{v}$, and add to this error the 1 1/2% uncertainty in speed. We also add the error in time averaging, although it does have some effect on Q because the time history of the wire cooling differs for the four wire orientations.

We study the dependence of Q on errors in the effective velocities through a sensitivity analysis. The function Q has the form

$$Q = \sum_{i=1}^{4} \left(\mathcal{U}_i - f_i\left(\frac{\vec{v}}{|\vec{v}|}\right)|\vec{v}| \right)^2 ,$$

where $\mathcal{U}_i$ is the effective velocity and $f_i(\frac{\vec{v}}{|\vec{v}|})$ is the directional cooling factor, a known analytic function fitted to the calibration data. Suppose the $\mathcal{U}_i$'s contain errors $\nu \epsilon_i |\vec{v}_a|$, viz:

$$\mathcal{U}_i = f_i\left(\frac{\vec{v}_a}{|\vec{v}_a|}\right)|\vec{v}_a| + \nu \epsilon_i |\vec{v}_a| ,$$

where variables with the subscript a represent actual quantities. Q now becomes

$$Q = \sum_{i=1}^{4} \left(f_{i_a}|\vec{v}_a| + \nu \epsilon_i |\vec{v}_a| - f_i|\vec{v}| \right)^2$$

One may nondimensionalize Q, such that

$$Q^* = Q/|\vec{v}_a|^2 = \sum_{i=1}^{4} \left(f_{i_a} + \nu \epsilon_i - f_i|\vec{v}|/|\vec{v}_a| \right)^2 .$$

The numbers ϵ_i are components of a four-dimensional effective velocity error vector $\vec{\epsilon} = \epsilon_1\hat{e}_1 + \epsilon_2\hat{e}_2 + \epsilon_3\hat{e}_3 + \epsilon_4\hat{e}_4$, $|\vec{\epsilon}| = 1$. When Q is minimized, $\vec{v}$ does not equal the true vector $\vec{v}_a$ if $\nu \neq 0$.

In a general sensitivity analysis, we compute f_i for particular direction of v_a, introduce various ν and $\vec{\epsilon}$, minimize Q* by adjusting $\vec{v}$, and compare $\vec{v}$ to $\vec{v}_a$. We do this for all directions of $\vec{v}_a$ that occur in the data. The difference between $\vec{v}$ and $\vec{v}_a$ depends on ν and $\vec{\epsilon}$, neither of which we know in a real situation. Suppose, however, that we think of $\vec{v} - \vec{v}_a$ as a function of Q*. The function differs for each direction of $\vec{\epsilon}$. Find the absolute values of the three components of $\vec{v} - \vec{v}_a$ as functions of Q* for many $\vec{\epsilon}$, and consider all directions of $\vec{\epsilon}$ to be equally probable. Now pick a particular value of Q*, and average the magnitude of the components over all $\vec{\epsilon}$. Do this for many values of Q*. The result is the most likely error in the components as a function of Q*.

A complete sensitivity analysis is beyond the scope of this thesis. However, the author has undertaken an analysis that strongly resembles the one just described, but is "incomplete" in that it utilizes only a few carefully chosen directions of $\vec{\epsilon}$, and only one direction of $\vec{v}_a$. We choose as a typical direction of $\vec{v}_a$ in the slipstream $\Lambda = 10^\circ$ and $\Phi = 45^\circ$ in our usual spherical

probe coordinates. The magnitude of $\vec{v}_a$ stays fixed at unity in light of the nondimensionalization. Let there be nine vectors $\vec{\epsilon}$:

$$\vec{\epsilon}_1 = 0.9962\hat{e}_1 + 0.0872\hat{e}_2$$
$$\vec{\epsilon}_2 = 0.9962\hat{e}_2 + 0.0872\hat{e}_3$$
$$\vec{\epsilon}_3 = 0.9962\hat{e}_4 + 0.0872\hat{e}_1$$
$$\vec{\epsilon}_4 = 0.7042\hat{e}_1 + 0.09\hat{e}_2 + 0.7042\hat{e}_3$$
$$\vec{\epsilon}_5 = 0.7042\hat{e}_2 + 0.09\hat{e}_3 + 0.7042\hat{e}_4$$
$$\vec{\epsilon}_6 = 0.7042\hat{e}_1 + 0.7042\hat{e}_2 + 0.09\hat{e}_3$$
$$\vec{\epsilon}_7 = 0.7042\hat{e}_1 + 0.09\hat{e}_2 - 0.7042\hat{e}_3$$
$$\vec{\epsilon}_8 = 0.7042\hat{e}_2 + 0.09\hat{e}_3 - 0.7042\hat{3}_4$$
$$\vec{\epsilon}_9 = 0.7042\hat{e}_1 - 0.7042\hat{e}_2 + 0.09\hat{e}_3$$

The relative size of the error, ν , takes on the five values 0.006, 0.024, 0.054, 0.096, and 0.15. Nine vectors compose a very sparse collection of directions in four-dimensional space, but we have tried to make the assortment diverse.

Define the percent error in the swirl component of velocity as

$$E_{sw} = \left| \frac{(\vec{v}_a - \vec{v}) \cdot \hat{i}}{\vec{v}_a \cdot \hat{i}} \right| 100 ,$$

where $\hat{i}$ is the unit vector in the tangential direction. In Figure E-1 we plot $\log_{10} E_{sw}$ against $\log_{10} Q^*$ for the 45 combinations of $\vec{\epsilon}$ and ν . Interestingly, for a given $\vec{\epsilon}$, the points nearly lie along a straight line. The least

squares fit lines are shown for each of the nine $\vec{\epsilon}$ and numbered accordingly. We average the slopes and y-intercepts ot the lines to arrive at an approximation for the most likely percentage error in swirl velocity as a function of Q:

$$\log_{10} E_{sw} = 2.77 + 0.483 \log_{10}(Q/|\vec{v}_a|^2).$$

We generalize the results by replacing Q* with $Q/|\vec{v}_a|^2$. Because of our choice of direction of $\vec{v}_a$, this relationship also holds for the radial component of velocity.

Note that in arriving at the above expression, we have averaged the logarithm of E_{sw} rather than E_{sw} itself. This is because the lines are more uniformly distributed on a logarithmic plot than would be the corresponding curves on a linear plot. As we'll see below, the real data involves values of ν no larger than about 0.02, for which the sensitivity analysis gives negligible errors in the axial component.

The FORTRAN program HOTWIREV outputs the value of Q at every tenth radial location in the wake surveys. We graph $\log_{10}Q$ versus the number of the location in Figures E-3, E-4, for all ten surveys, which are identified with the alphanumeric code explained at the bottom of Table VIII. In order to compute Q* for the actual data, we

approximate $|\vec{v}_a|$ by $|\vec{v}|$. For selected points in the survey, indicated by the small arrows in Figures E-3, E-4, we find E_{sw}.

The error in time averaging is estimated by introducing sinusoidal fluctuations into the ideal linearized law of cooling for a hot wire. We take as the mean direction $\Lambda = 0$, $\Phi = 90^\circ$. The wire angle is 35°.

$$\mathcal{U} = |\vec{v}|\sin\theta \qquad \theta = \theta_s + \theta_f \sin\omega t$$

$$|\vec{v}| = A + a\sin\omega t \qquad \theta_s = 55^\circ$$

Here θ_f and a are the sizes of the angle and magnitude fluctuations. Expand $\sin\theta$ as a Taylor series about 55° and retain terms to fourth order in θ_f. Find $\langle\mathcal{U}\rangle_t$, and subtract from it the true mean effective velocity $A\sin\theta_s$ to find the averaging error. Take as the peak fluctuation amplitude $\mathcal{U}\big|_{\omega t=\frac{\pi}{2}} - \mathcal{U}\big|_{\omega t=0}$. Nondimensionalize the expressions for peak amplitude F and fractional error E to find

$$F = (1+\tfrac{a}{A})\sin(\theta_s+\theta_f) - \sin\theta_0$$

$$E = -\frac{\sin\theta_0}{4}\theta_f^2 + \frac{\sin\theta_s}{48}\theta_f^4 + \frac{a}{A}\left(\frac{1}{2}\right)\theta_f\cos\theta_s - \frac{a}{A}\left(\frac{1}{12}\right)\theta_f^3\cos\theta_s$$

Both F and E represent fractions of the steady velocity A.

Recall that we tape recorded the unfiltered output of

the linearizer during the hot wire wake surveys. The largest fluctuations in voltage are observed with the Windsong propeller operating at 10,000 RPM in front of the symmetric nacelle. For this case, the amplitude of the voltage fluctuations, expressed as a fraction of the mean, is 7% or less out to the 75% radius, 12% or less out to the 95% radius, and 23% in the shear layer. The corresponding maximum averaging errors, gotten by maximizing E for F fixed at 0.07, 0.12, and 0.23, are 0.4%, 1.4%, and 6.6%. Since our error analysis has concentrated on the middle portion of the blade, we take the lowest figure as representative, and add it to our error estimate.

The errors in swirl velocity outside the wake are also of interest. We assess them with a procedure similar to the one used to find E_{sw}, but with two changes. First, we take $\vec{v}_a$ to be $\Lambda = 1/4^o$, $\Phi = 0^o$. Second, since the swirl velocity outside the slipstream should be zero (or very small), we can't consider percentage errors in swirl. Instead, we define a dimensionless quantity

$$\Delta V_{sw}^* = \frac{\Delta V_{sw}}{|\vec{V}_a|}$$

where Δv_{sw} is the magnitude of the swirl component of $\vec{v}_a - \vec{v}$. In Figure E-2 we plot $\log_{10} \Delta v_{sw}^*$ as a function of $\log_{10} Q^*$ for the same 45 combinations of $\vec{\epsilon}$ and ν as before. The most typical line relating Δv_{sw}^* and Q^* is

$$\log_{10}\Delta V_{sw}^{*} = 0.0246 + 0.472\log_{10}Q^{*},$$

where again we must approximate $\vec{v}_a$ by $\vec{v}$ in order to apply this result.

In summary, the error in the axial component of velocity is about 2%. The uncertainty in the other two components, in the wake, is 2% plus E_{sw}, which varies between surveys. Outside the wake, the uncertainty in the swirl velocity is ΔV_{sw}. Appropriate error bars, based on these figures, appear on all the hot wire circulation curves except the one for the case CS7 (0.41R). We omit the bars in this case because, as mentioned previously, the speed calibration data is incomplete. The error estimates for the swirl velocities also appear in Tables III and IV.

D.2 Performance Data

Only two important errors enter the performance data:

1) Changes in the sensitivities of the thrust and torque balances with temperature

2) Inaccurate correction for temperature-induced zero drift

We may assess both these errors directly and then add

them. The first we estimate by calibrating the balance when it is hot and when it is cold. In Figure E-5 we show the cold thrust and torque calibrations. The slopes of the least squares lines are

$$b_{Tcold} = 0.05824 \text{ n/SR4 box unit}$$

$$b_{Qcold} = 0.05711 \text{ n-m/SR4 box unit}$$

for the thrust and torque, respectively. The slopes for the hot calibrations are

$$b_{Thot} = 0.05959 \text{ n/SR4 box unit}$$

$$b_{Qhot} = 0.005846 \text{ n-m/SR4 box unit.}$$

We use the hot values to reduce the data. Hence, we might overestimate both the thrust and torque by as much as two percent.

The two front thrust flexures (Figure 12) are normally used, but the rear flexures also have strain gauge instrumentation. We compare four sets of thrust readings for the same experiment in Figure E-6. The points marked 1 and 2 are the readings from the front and back flexures, uncorrected for zero drift. The points marked 1' and 2' are corrected by assuming that the total zero drift observed at the end of the experiment accumulates linearly with time. Apparently, this linear assumption doesn't quite fit the real situation. The

symmetry of the spread of points at each RPM suggests that the true values of thrust lie in the middle of each cluster. Hence, at 7,000 RPM, the error is about half the size of the zero correction, which in turn is 7/11 of the total zero drift, which we know for each experiment. The drift can be of either sign. Thus, at 7,000 RPM, the error bar extends downward by 2% of the measurement, and its ends are lengthened by 7/22 times the total zero drift. We tabulate these bars for all the performance measurements in Table V, but we do not try to draw them on the graphs because they are too small for the most part.

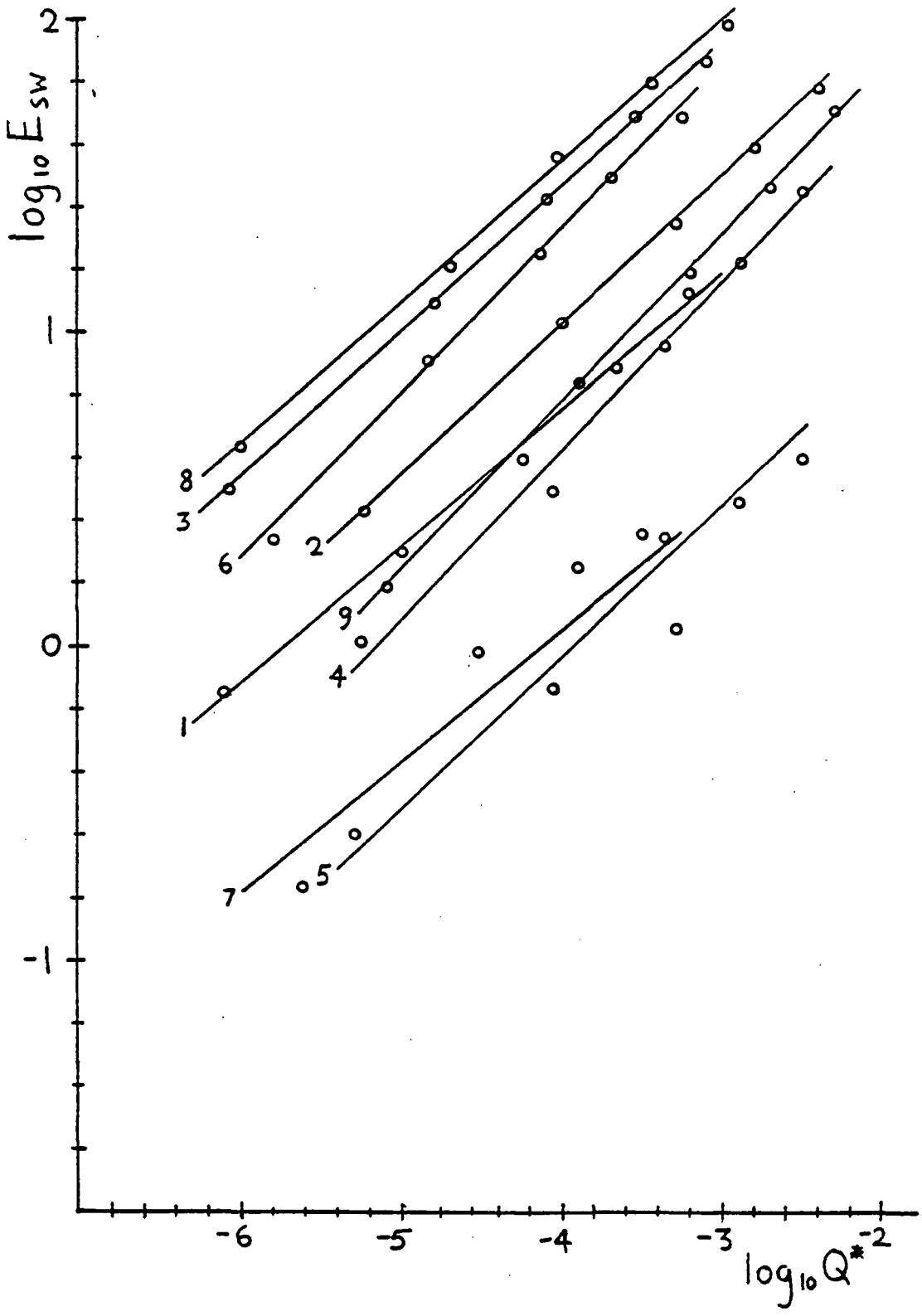

Fig. E - 1. Swirl error in wake

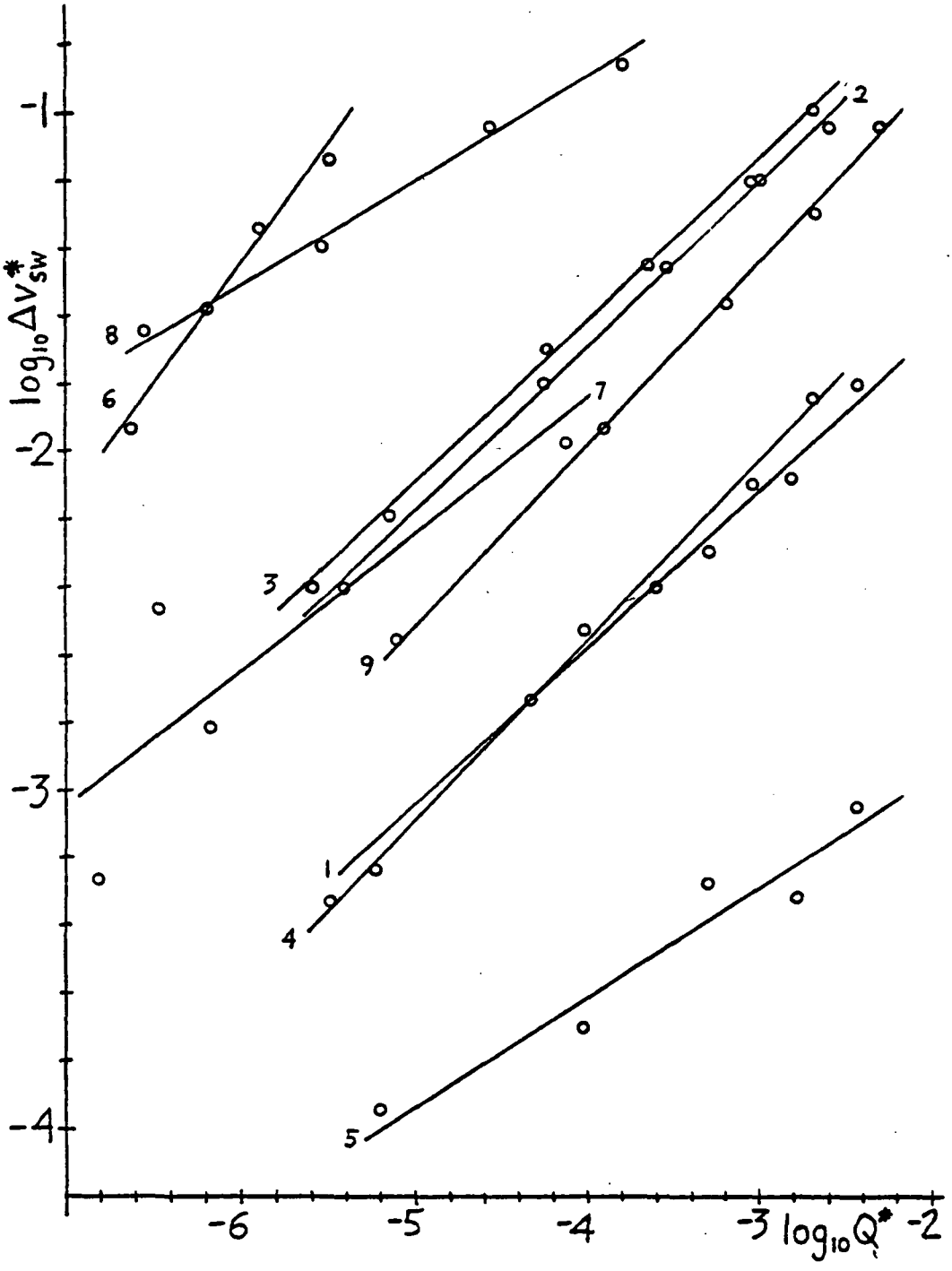

Fig. E - 2. Swirl error outside wake

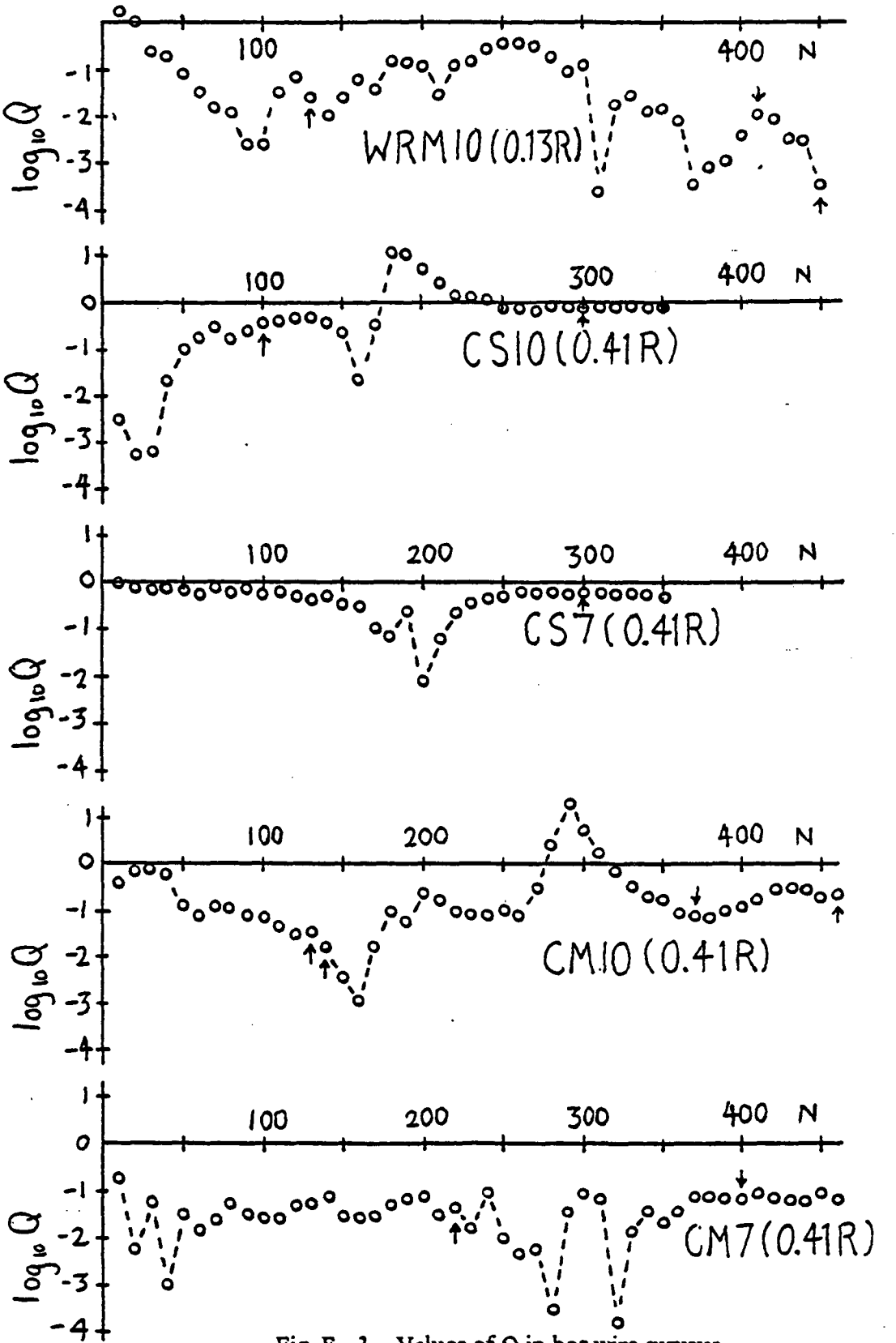

Fig. E - 3. Values of Q in hot wire surveys

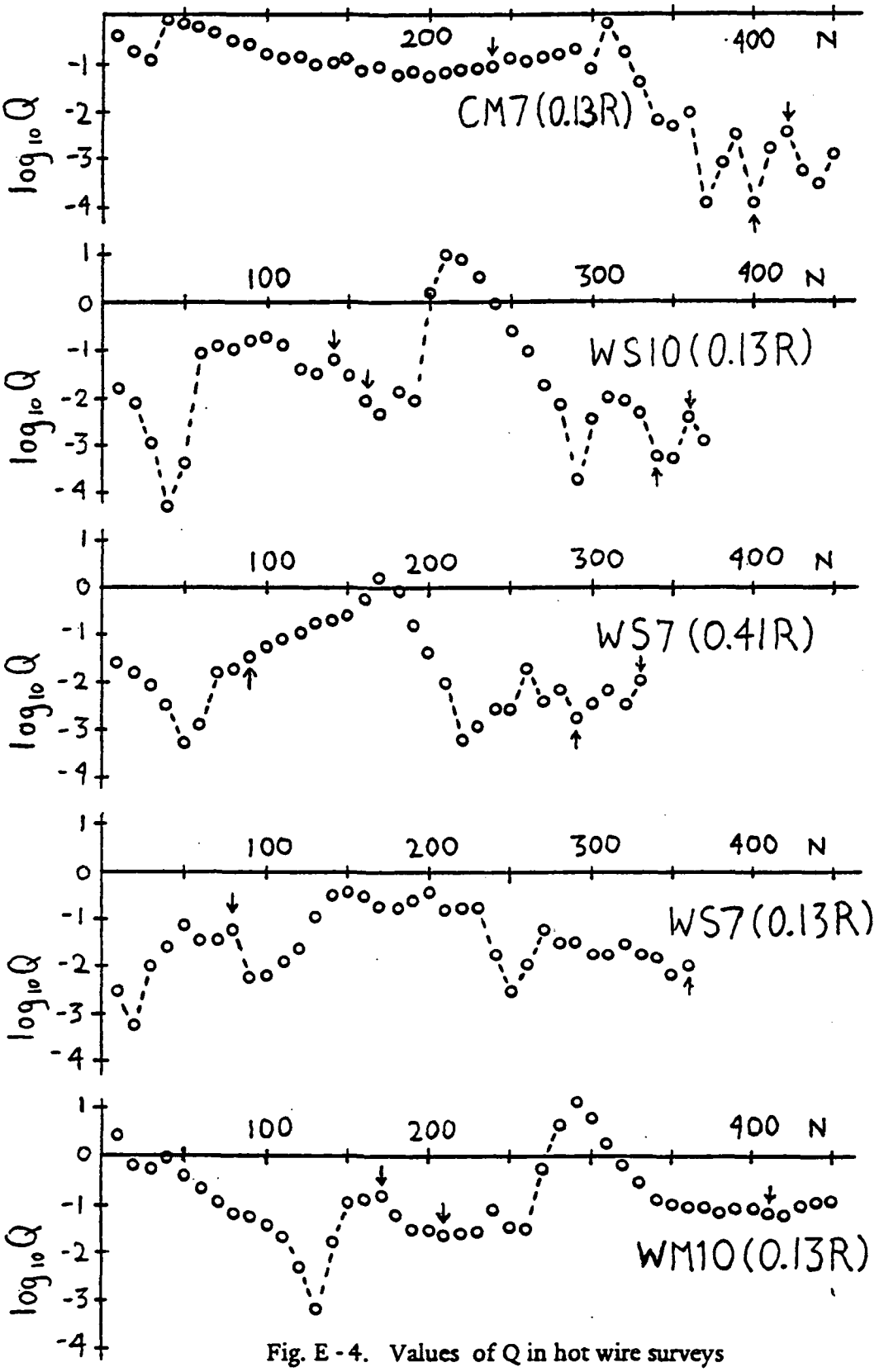

Fig. E - 4. Values of Q in hot wire surveys

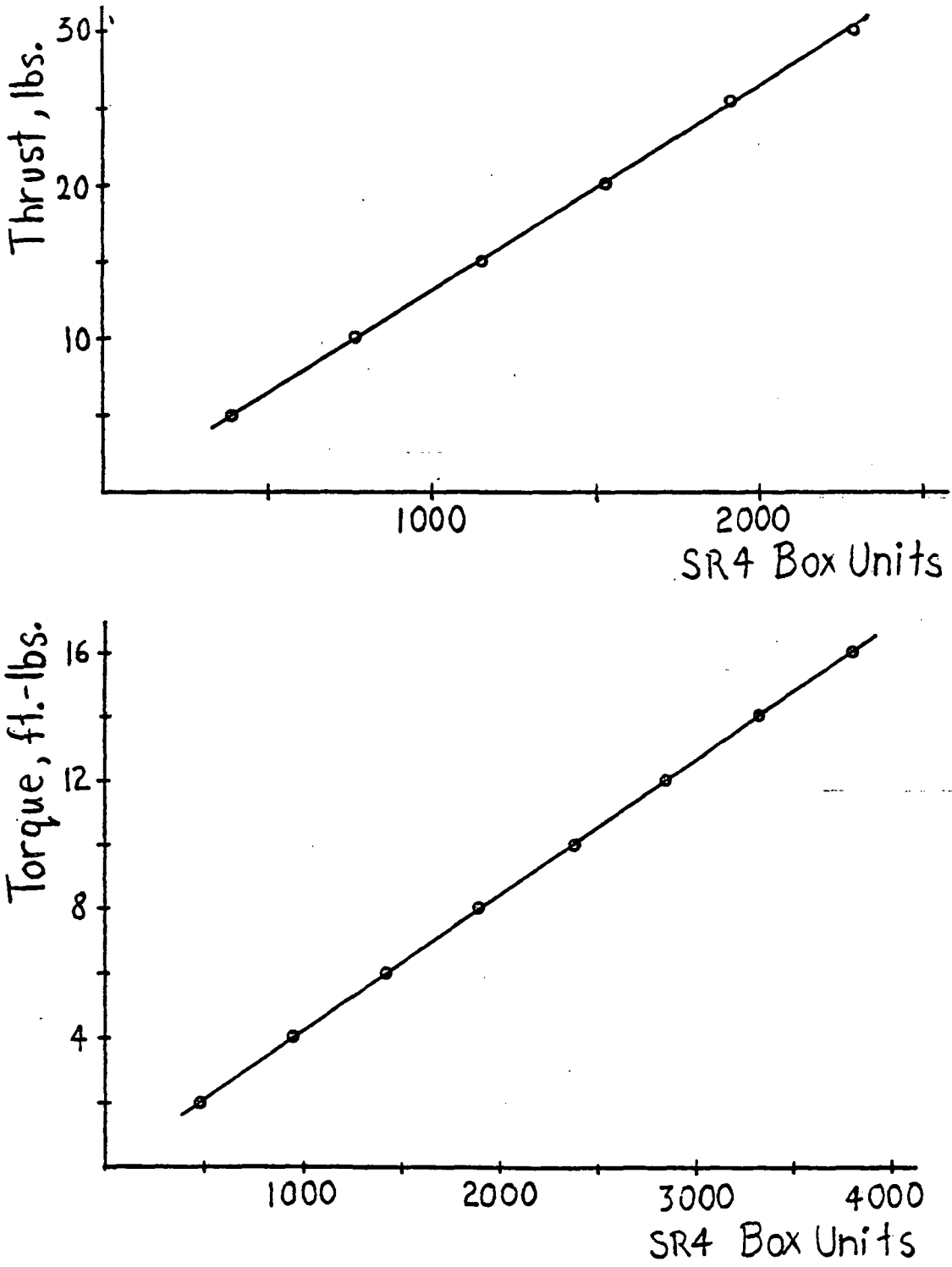

Fig. E - 5. Cold thrust and torque calibrations

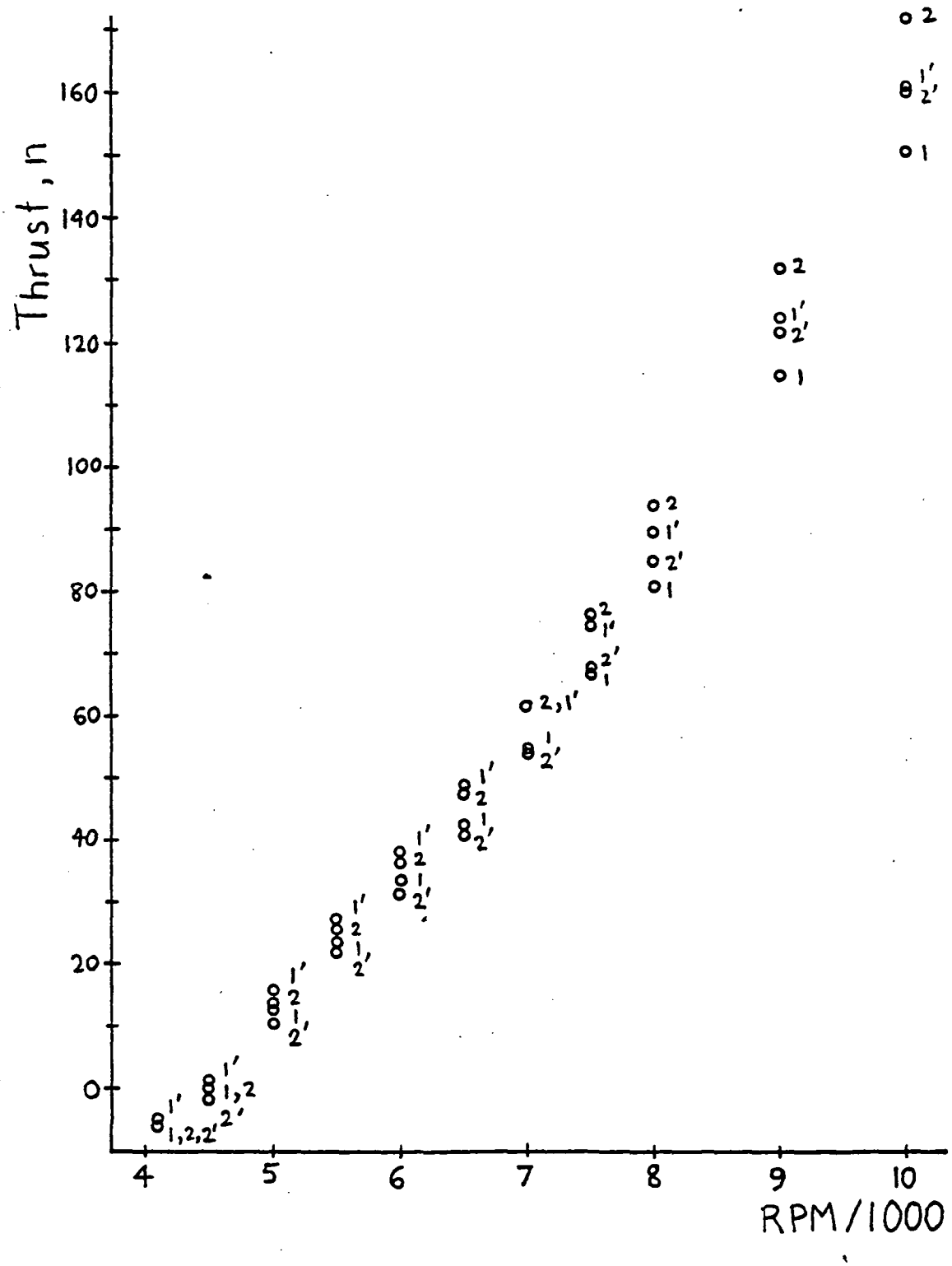

Fig. E - 6. Comparison of both sets of thrust flexures

References

1. E. E. Larrabee, "Practical Design of Minimum Induced Loss Propellers," Transactions, 1979 SAE Business Aircraft Meeting

2. D. Munro, "The Production of Sound by Moving Objects," Doctoral Dissertation, Department of Physics, M.I.T., 1980

3. W. F. Durand, E. P. Lesley, "Experimental Research on Air Propellers," NACA Report 141, 1922

4. J. W. Crowley, Jr., "Investigation of Slipstream Velocity," NACA Report 194, 1924

5. E. P. Lesley, "Experiments With a Counter-Propeller," NACA Technical Note 453, 1933

6. E. G. Reid, "Wake Studies of Eight Model Propellers," NACA Technical Note 1040, 1946

7. H. Glauert, "Airplane Propellers," in Aerodynamic Theory, Vol. IV, Division L, Durand, W-Ed., Julius Springer, Berlin, 1935

8. J. C. Roberts, P. F. Yaggy, "A Survey of the Flow at the Plane of the Propeller of a Twin-Engine Airplane," NACA Technical Note 2192, 1950

9. L. Salters, Jr., "Velocity Distributions Measured in the Slipstream of Eight-Blade and Six-Blade Dual-Rotating Propellers at Zero Advance," NACA RML55D21

10. M. Panetti, "Experimental Apparatus for the Study of Propellers," NACA Technical Memorandum 819, 1937

11. C. Ferrari, "Some Experiments on the Slipstream Effect," NACA Technical Memorandum 820, 1937

12. R. E. Pendley, "Effect of Propeller Axis Angle of Attack on Thrust Distribution Over the Propeller Disk in Relation to Wake Survey Measurement of Thrust," NACA WRL-517

13. H. C. McLemore, M. D. Cannon, "Aerodynamic Investigation of a Four-Blade Propeller Operating Through an Angle-of-Attack Range from 0^{o} to 180^{o}," NACA Technical Note 3228, 1954

14. D. Favier, "Determination des vitesses induites a l'aval d'une helice quadripale a l'aide d'un anemometre a film chaud et a temperature constante," C. R. Acad. Sc. Paris, Serie A, p. 39, 1974

15. D. Favier and N. Pellerin, "Measurement of all three mean velocity components by a single hot film anemometer," Rev. Sci. Instrum., Vol. 47, p. 368, 1976

16. J. Valensi, "Notes on the vortex lines behind an airscrew and their utilisation for measuring the circulation along the blades and checking the airscrew theory," A.R.C. Report 8274 A. P. 478, 1944

17. A. Betz, "Schraubenpropeller mit geringstem Emergieverlust;" also Prandtl, L., Appendix for the above, Göttinger Nachrichten, 1919

18. S. Goldstein, "On the Vortex Theory of Screw Propellers," Proceedings of the Royal Society (A) 123, p. 440, 1929

19. T. Theodorsen, "The Theory of Propellers," NACA Reports 775 through 778, 1947

20. N. Poliakhov, "The Minimum Energy Loss Propeller," NACA Technical Memorandum 1067, 1944

21. F. Losch, "Calculation of the Induced Efficiency of Heavily Loaded Propellers Having Infinite Number of Blades," NACA Technical Memorandum 884, 1939

22. K. Kramer, "The Induced Efficiency of Optimum Propellers Having a Finite Number of Blades," NACA Technical Memorandum 884, 1939

23. A. Betz, "The Theory of Contra-Vanes Applied to the Propeller," NACA Technical Memorandum 909, 1938

24. D. Munro, "A General Formulation of the Minimum Induced Loss Problem," (unpublished), 1979

25. G. de Bothezat, "The General Theory of Blade Screws," NACA Report 29, 1918

26. T. Bienen, "Calculating Thrust Distribution and Efficiency of Air Propellers," NACA Technical Memorandum 444, 1927

27. H. Reissner, "On the Vortex Theory of the Screw Propeller," Journal of the Aeronautical Sciences, Vol. 5, p. 1, 1937

28. T. Moriya, Selected Scientific and Technical Papers, Dept. of Aeronautics, Univ. of Tokyo, Tokyo, Japan, 1959

29. G. Hough, "A Numerical Study of the Fluctuating Flowfield of a Uniformly Loaded Propeller," Journal of Aircraft, Vol. 4, p. 36, 1967

30. P. Freymuth, "A Bibliography of Thermal Anemometry," TSI Incorporated, St. Paul, MN 55164, 1978

31. H. Fujita, L. S. G. Kovasznay, "Measurement of Reynolds Stress by a Single Rotated Hot Wire Anemometer," Rev. Sci. Instrum., Vol. 39, p. 1351, 1968

32. C. E. Whitfield, J. C. Kelly, B. Barry, "A Three-Dimensional Analysis of Rotor Wakes," Aeronautical Quarterly, Nov. 1972, p. 285

33. D. P. Schmidt, T. H. Okiishi, "Multistage Axial-Flow Turbomachine Wake Production, Transport and Interaction," AIAA Journal, Vol. 15, p. 1138, 1977

34. B. Lakshminarayana and R. Davino, "Mean Velocity and Decay Characteristics of the Guidevane and Stator Blade Wake of an Axial Flow Compressor," ASME Paper 79-GT-9, 1979

35. K. Korkan, et al, "Two Dimensional Aerodynamic Analysis of Nine Propeller Sections," Ohio State University, GA/ADAC TDR 78-04, 1978

36. P. Dunbeck, "Performance of Light Aircraft Propellers," Masters Thesis, Dept. of Aero. and Astro., M.I.T., 1979

37. P. Bauer, S. Widnall, "The Development of a Wind Tunnel Facility for the Study of V/STOL Noise," FTL Report R-72-6,1972

38. A. S. Iberall, "Attenuation of Oscillatory Pressures in Instrument Lines," Journal of Research of the National Bureau of Standards, Vol. 45, p. 85, 1950

39. H. Weyer, "The Determination of Time-Weighted Average Pressures in Strongly Fluctuating Flows, Especially in Turbomachines," Translation of DLR-FB 74-34, Institut für Luftstrahlantriebe, Porz-Wahn, W. Germany, 1974

40. E. Larrabee, W. Stalnaker, "Approximate Analytic Theory for the Design and Performance Estimation of Propellers and Windmills," (unpublished), 1977

41. R. C. Dean, Jr., "Aerodynamic Measurements," Gas Turbine Laboratory, M.I.T., 1953

42. L. V. King, "On the Convection of Heat from Small Cylinders in a Stream of Fluid; Determination of the Convection Constants of Small Platinum Wires with Applications to Hot Wire Anemometry," Royal Society of London, Philo. Trans., Vol. A214, p. 373, 1914